TÉCNICO LISBOA

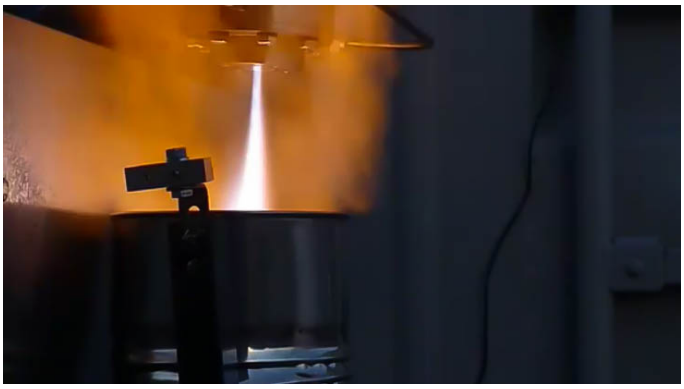

Small Liquid Propellant Rocket Engine

Mariana Peralta Páscoa Martinho Marques

Thesis to obtain the Master of Science Degree in

Aerospace Engineering

Supervisor(s): Prof. Aires José Pinto dos Santos
Prof. Edgar Caetano Fernandes

Examination Committee

Chairperson: Prof. Fernando José Parracho Lau
Supervisor: Prof. Edgar Caetano Fernandes
Member of the Committee: Prof. Jorge Manuel Martins Barata

December 2016

To my parents, for everything.
To my grandmother, who did not live
long enough to see me become an engineer.

Acknowledgments

In order to express my gratitude to the people that surround me I would like to start this section with a quote, from Antoine Saint-Exupéry, that says: “Those who pass by us do not go alone, and do not leave us alone; they leave a bit of themselves, and take a little of us.”

I must recognize that I have a long list of people who I should be thanking, and I apologize for the long acknowledgment section.

First of all, I would like to thank everyone directly involved in this project. I want to thank all the staff of Omnidea Lda. for taking me in as one of their own. A special word to Horàcio Moreira, for all the patience, for sharing his knowledge with me and for guiding me through the process. Thank you for spending all this time teaching me, for reviewing my work and for helping me. I would also like to thank Rei Fernandes, for all the good talks during this time, Renato Salles for the help, Ricardo Pereira for spending so much time building pieces for the test stand and to Filipa Lourenço, who always had a kind word. To Tiago Pardal, owner of Omnidea, I would like to thank him for giving me this opportunity.

To Edgar Fernandes and Aires dos Santos, my supervisors, an enormous thank you for being there for me during this time and for guiding me in the right direction, in every step of this work. Most of all, thank you for teaching me patiently and persistently.

For those who made it possible without being directly involved.

To my parents, who thought me unconditional love and support, who pushed me to be better, stronger and to fly high. I am sorry for the bad mood in the difficult hours. This thesis is for you, because no one else in the world has supported and loved me like you do.

To my brother, who pushed me to overcome myself and be an example to him.

To my aunts: Isabel that is a second mother to me, that has the kindest heart and biggest patience; and Claudia, like an older sister and one of my best friends, who I can talk to and always has an advice to give me. Thank you for being there, for believing in me. To my uncle, Nuno, for the example that he is, for taking me down his wing and showing me that I can do more.

To João, for his love and support, for being proud of me and make me laugh.

To all my friends, that were also a part of this. A special word for Sarah Saint-Maxent, Sara Velasco, Carolina Smet, Andreia Ferreira, António Fayad and Telma Oliveira. Thank you for putting up with my difficult personality and for supporting me.

To my grandmother, Maria do Carmo, who once told me she would be very proud if her granddaughter one day became an engineer.

Resumo

Esta tese de mestrado insere-se no projecto S-SHE da empresa Omnidea Lda. Ambicionando iniciar-se no âmbito dos lançadores, a Omnidea pretende posicionar-se com um conceito inovador na área da pressurização dos tanques de reagentes.

O trabalho desenvolvido visa projectar, construir e testar um protótipo. O sistema desenvolvido é flexível o suficiente para permitir que o estudo seja faseado. Inicialmente usa-se pressurização externa para provar a estabilidade e o comportamento do motor e, após esta fase, haverá um estudo do conceito da autopressurização através de arrefecimento regenerativo.

Este protótipo será capaz de produzir uma força da ordem de 25N e foi desenhado para uma pressão de 15bar na câmara. O objectivo inicial não passa por maximizar a eficiência do protótipo, mas por ter um sistema que cujo funcionamento seja estável.

O trabalho desenvolvido pode ser dividido em quatro fases: projecto preliminar, projecto detalhado, construção da bancada e testes. A primeira fase inclui todo o dimensionamento da câmara de combustão, bem como a análise da queima - recorrendo a um *software* disponível. Uma parte significativa do trabalho versou também sobre o estudo da transferência de calor e arrefecimento da câmara. A análise térmica permitiu escolher o material adequado e o combustível que permite ir de encontro ao objectivo de autopressurização. O projecto detalhado foca os pormenores do sistema e o desenho de algumas peças. O plano de testes esteve também incluído no trabalho desenvolvido.

A campanha de testes foi o culminar deste projecto e todo o seu plano e tratamento de dados faz parte deste trabalho.

Palavras-chave: motor de foguete com reagentes líquidos, autopressurização, arrefecimento regenerativo, injeção gasosa, ignição repetível.

Abstract

This master thesis is a part of S-SHE project of the company Omnidea Lda. The company aims to enter the rocket market with a different concept of pressurization of the reactants tanks.

In this framework the scope was to design, build and test a prototype. The developed system is flexible enough to allow a phased study. Initially external pressurization is used to prove the engine's stability and understand its behaviour. After this phase the study of self-pressurization using regenerative cooling is conducted.

The prototype should be able to produce a thrust of 25N with a chamber pressure of 15bar. At this stage of the project there, maximizing the efficiency was not the main concern.

The work can be divided in four stages: preliminary project, detailed project, construction and tests. The first phase includes the sizing and the burn analysis - using available software. An important part of the work has to do with the heat transfer analysis. This study allows to choose the material and the fuel that meets the project requirements. The test plan is also a part of the work.

The test campaign and the data analysis are the final part of the work.

Keywords: small liquid propellant rocket engine, self-pressurization, regenerative cooling, gaseous injection, repeatable ignition.

Contents

List of Tables

List of Figures

Nomenclature

Roman symbols

A Area.

A^* Sonic throat area.

B Swirl position.

c^* Characteristic exhaust velocity.

C_d Coefficient of drag.

c_p Heat capacity.

C_{sf} Surface-fluid coefficient.

D Diameter.

f Darcy friction factor.

F Thrust force.

g Gravitational acceleration.

G_g Specific gravity.

h Convection coefficient or enthalpy.

I_{sp} Specific impulse.

l Length.

L^* Characteristic length.

m Mass.

M Molecular weight.

$\dot{m}$ Mass flow rate.

Ma Mach number.

N_2 Unity correction factor.

Nu Nusselt number.

p Pressure.

P Pressure.

$P(0)$ Initial pressure.

P_{jet} Engine's power.

Pr Prandlt number.

q'' Heat flux.

$\dot{Q}$ Heat transfer rate.

r Radius.

R Gas constant.

s Slant height of a truncated cone.

S Entropy.

Sw Swirl number.

T Temperature.

u Internal energy.

U Heat transfer coefficient.

V Velocity.

Vol Volume.

x Quality of the mixture.

X Position.

Greek symbols

α Conic nozzle divergent angle.

β Conic nozzle convergent angle.

γ Specific heat coefficient.

δ Thickness.

ϑ Ration between angular and axial velocities.

κ Thermal conductivity coefficient.

λ Correction factor.

μ Viscosity coefficient.

ν Specific volume.

ρ Density.

σ Surface tension.

σ_{Boltz} Stefan-Boltzmann constant.

ϕ Blade inclination.

ω Radial velocity.

Subscripts

$()_0$ Stagnation.

$()_1$ Combustor inlet.

$()_2$ Combustor.

$()_\infty$ Upward properties.

$()_{aw}$ Inner wall.

$()_c$ Chamber.

$()_{cri}$ Critical value.

$()_e$ Exit.

$()_{ext}$ Exterior.

$()_f$ Fuel.

$()_{fg}$ Phase change.

$()_g$ Saturated gas phase.

$()_{inj}$ Injector.

$()_{int}$ Interior.

$()_l$ Saturated liquid phase.

$()_{LDF}$ Leindenfrost point.

$()_{max}$ Maximum value.

$()_{min}$ Minimum value.

$()_{ox}$ Oxidizer.

$()_s$ Surface.

$()_{sat}$ Saturated.

$()_t$ Throat.

$()_T$ Tank.

$()_v$ Vaporizer.

$()_{wh}$ Outer wall.

Glossary

CEA Chemical Equilibrium with Applications. Is a software developed by NASA that allows to calculate chemical equilibrium in complex mixtures. The solution can be estimated with several application, as rocket performance, shock-tube parameters for incident and reflective shocks, Chapman-Jouguet detonations and thermodynamic states.

CHF Critical Heat Flux. It is the point from where the efficiency of heat exchange decreases abruptly.

CJ Chapman–Jouguet is a theory to predict the behaviour in detonations or deflagrations in gases.

CNSA China National Space Agency.

ESA European Space Agency.

FEM Finite Element Method, is a numerical method to estimate the solutions of problems involving partial differential equations.

JAXA Japan Aerospace Exploration Agency

NASA National Aeronautics and Space Administration.

OF Oxidizer-fuel ratio. It is the ratio between the oxidizer and fuel mass flow.

ROSCOSMOS Russia's federal space agency.

TEOS Tetraethyl orthosilicate, which chemical formula is $Si(OC_2H_5)_4$. It is also known as ethyl silicate. Its main use is to link silicone polymers and as a precursor to silicon dioxide in semiconductors.

Chapter 1

Introduction

The purpose of the work developed in this master thesis is to design, build and test a small liquid rocket engine following some specific objectives. This document reflects the approach that was taken to solve the problem, the results and a detailed discussion.

1.1 Motivation

This master thesis was proposed to me two years after my summer internship at Omnidea. Since the beginning of space exploration there is a need to make systems lighter and less complicated. For rockets this issue is crucial and that is why the idea of a simple pressurization system arose. Conventional pressurization systems are complex and usually involve a significant amount of extra weight, therefore minimizing their complexity is an important advantage in aerospace industry. The proposed project revolves around self-pressurization. The interest on revisiting this concept comes from the belief that it can simplify the pressurization mechanism.

1.2 Objectives

The objectives of this master thesis are to design, produce and test a small rocket in the class of 25N of thrust. Oxygen in gaseous phase will be used as the oxidizer. It is also required to verify the feasibility - and assess the constrains - of the following points:

- Injection should be performed in gaseous phase;
- The ignition system must be initiated several times, making the system re-startable;
- Study the feasibility of the system's ability to achieve fuel pressurization without using turbo-pumps or auxiliary pressurized gases - self pressurization.

1.3 Overview

As is was mentioned before, commercial engines rely on feed systems that significantly increase the engine's mass. The current work aims to study the feasibility of an engine that is self pressurized, with a gaseous injection. The first approach to the problem is to identify the different components needed for this engine, which are illustrated in figure 1.1.

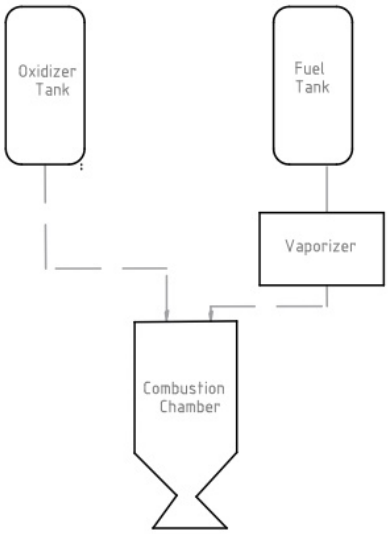

Figure 1.1: Basic system schematic.

The strategy to achieve the objectives of this work can be understood by the workflow through the flow chart in figure 1.2. However, it is necessary to understand the self pressurization concept.

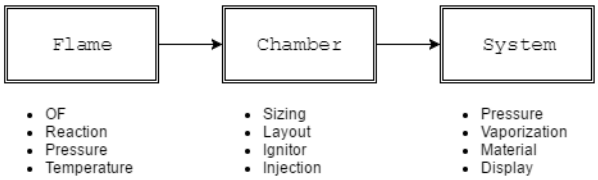

Figure 1.2: Work flow.

Today's feed systems use turbo-pumps or helium-pressurized blowdown systems that increase the system's mass. The intention is to find a suitable alternative. As it will be explained further, cooling of the combustion chamber is crucial to ensure material integrity. The idea is to use the heat from the chamber to evaporate the fuel, through regenerative cooling. The flame temperature in the combustion chamber is influenced by the OF [1] - its dependency can be observed in figure 1.3. The ideal operation is near the stoichiometric point. The base premise of the idea is that it is self stable, because an alteration in the OF should trigger a sequence of reactions that will drive the system to correct the deviation. This correction sequence is based on the following mechanism: when the pressure in the fuel tank decreases, the OF will increase, because the fuel entering the chamber will be less. Figure 1.3, which gives the evolution

[1] The OF is the ratio between oxidizer and fuel's mass flow

of temperature with OF for the case where ammonia is used as fuel, shows that the increase of OF will lead to a hotter flame, raising the heat transfer and, therefore, the fuel pressure, and decrease the OF. The ideal operation is between 0.5 and 1.2.

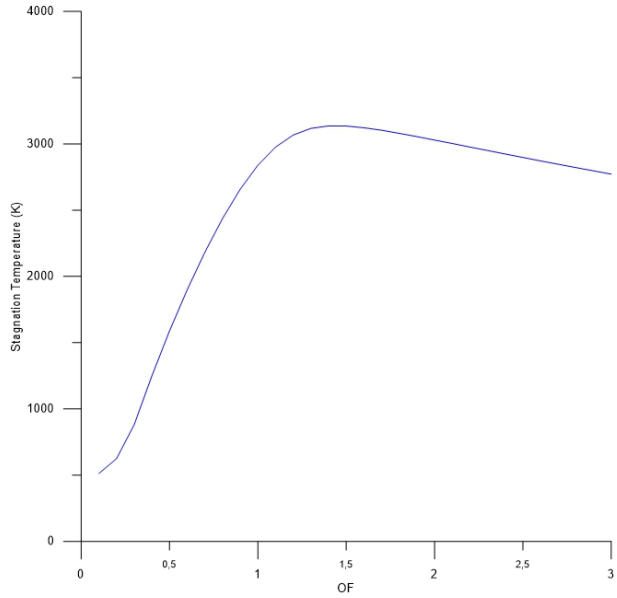

Figure 1.3: Stagnation temperature as function of OF.

1.4 Thesis Outline

The present work is organized as follows:

Chapter 2

In the chapter 2 there is a summary of the literature research. There was a concern to divide the fundamentals of liquid rocket engines - an important part to understand the operation of this type of engines - from the presentation of the state of art.

Chapter 3

In this chapter the mathematical modelling of the problem is presented. As the burn characteristics are computed using an existing software - it was decided that the mathematical model should focus on the study of the auto-pressurization mechanism. This chapter shows the problem formulation and the equations used to solve it. The model is used to study the stability of the engine and to compare the variables - pressure, temperature and thrust - with those that were obtained experimentally.

Chapter 4

The fourth chapter is where the most relevant part of the design work is presented. The experimental part includes the design of the chamber: sizing, choice of material and heat transfer analysis.

Chapter 5

This chapter comprises the description of the test stand, the test plan and the test results. All the information regarding the tests is exposed and developed in this section.

Chapter 6

A discussion of the results that were obtained in this project is presented in this chapter. Both mathematical and experimental results are analysed and compared.

Chapter 7

Finally the conclusions that arose from the project discussion are presented. In the work plan that was created in the beginning of this project there was the requirement that some ideas for the further work should be presented. Those ideas are explained in this section.

Chapter 2

Background

The relevant part of the literature research that was conducted in the beginning of this project is exposed in this chapter as a way to ease the understanding of the problem and the path taken to its solution.

2.1 Liquid Rocket Engine Basics

Rocket propulsion is based on Newton's third law, as figure B.1 shows. The mission requirements define the necessary conditions of the engine as, for example, the burn profile and total impulse. On the rockets produced to the present date we find that they have several stages to operate in the different phases of the flight. It is common practice that the several stages incorporate different types of rocket motors, in order to fulfil the requirements of the mission at each step.

Figure 2.1: Rocket action reaction illustration.

There are three types of rockets motors: solid, liquid and hybrid. Their designations are based in the physical state of the propellants involved. There are also mono-propellants and bi-propellants engines. The first ones are made of a single substance and their use relies on their exothermal decomposition by a catalyst - for example, hydrogen peroxide or hydrazine. In the second case, there are two reactants that are stored apart. In this particular project we are dealing with a bi-propellant liquid rocket engine. When compared to a solid motor, both have advantages and disadvantages. The liquid propellant engines are usually more efficient in terms of specific impulse - I_{sp}, can be shut down and may be throttleable and

re-startable if necessary [1]. The system of a liquid engine can be divided into five main parts:

- Thrust chamber - which contains the nozzle, injector and the combustion chamber;
- Tanks - for the reactants;
- Feed mechanism - either using pumps or pressurant gases. In some cases both mechanisms are combined;
- Piping;
- Control systems.

The thrust chamber is the main part, where the reaction occurs. Its design must consider the sizing so there is enough space to allow an effective reaction, atomization and mixture of the reactants. The gases produced are accelerated and ejected through the nozzle at high speed. There are three significant shapes of chambers: spherical, near-spherical and cylindrical. The spherical and near-spherical chambers were used in early European rockets, the cylindrical were mostly used by USA [2]. The advantages of the first two types is linked to the lighter structure for the same weight and less cooling surface area. A cylindrical chamber is far easier to manufacture, which decreases engine costs, and it is the most widely used, since it offers a fair length for the reaction to develop. Usually, the characteristic chamber length corresponds to the length that the chamber would have if it were a straight tube with the same volume [1]

$$L^* = \frac{Vol_c}{A_t} \tag{2.1}$$

The characteristic length values vary between 0.8 and 3 meters in the engines described in the literature.

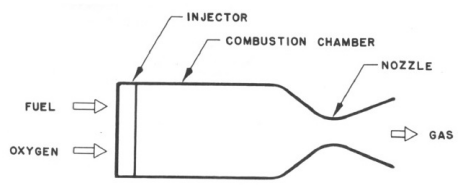

Figure 2.2: Current rocket thrust chamber layout [3].

The nozzle is the component where gases are expanded to match the outer pressure. There are several types of nozzle shapes: conic, bell and spike. The divergent part of the nozzle is crucial to rocket performance, since only convergent-divergent nozzles allow expansion to supersonic velocities. The expansion ratio - ratio between exit and throat area - is an engine parameter that depends on the chamber geometry. Its optimal value depends on engine parameters such as the chamber pressure, reactants, etc. Knowing the throat area, the exit area can be estimated for a certain atmosphere pressure in order to avoid a normal shock in the diffuser.

The nozzle should be as short as possible, minimizing the mass, the friction and cooling requirements; there should be minimum separation and turbulence losses; the gas flow should be uniform, and

strictly axial in order to achieve the maximum propulsive efficiency; and, at last, because costs are very important, it should be cheap to manufacture.

The conical nozzle, in figure 2.3 is the simplest considered. The angles of the convergent section - β - vary between 20 and 45 degrees, and for the divergent section - α - range from 12 to 18 degrees. Even though it is easy to produce, there are some performance losses due to the radial component of the exhaust gas velocity in the exit section. When the angle of the divergent part decreases, the efficiency increases, due to the drop of the radial component of the velocity. For high α angles, the radial component is significant, which means that the axial velocity will be smaller, minimizing the efficiency.

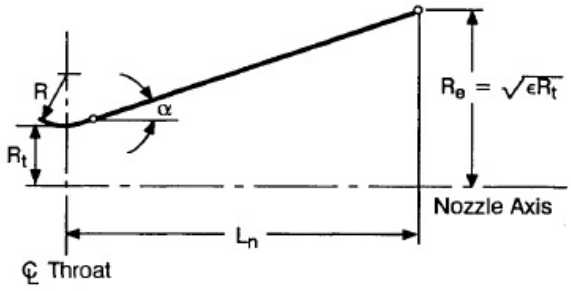

Figure 2.3: Conic nozzle layout [2].

A correction factor for the calculation of exhaust gas momentum exists for this type of nozzles. It is a ratio between the exhaust gas momentum and the ideal nozzle - which has uniform, parallel and axial flow. This correction factor is given by

$$\lambda = \frac{1}{2}(1 + \cos\alpha) \tag{2.2}$$

The bell nozzle was developed to achieve higher performance. From figure 2.4 it is possible to understand that in the beginning of the divergent region there is a fast-expansion section that provides a uniform, axial flow. The smoothness of the nozzle avoids the oblique shocks. Its design can be made using the method of characteristics.

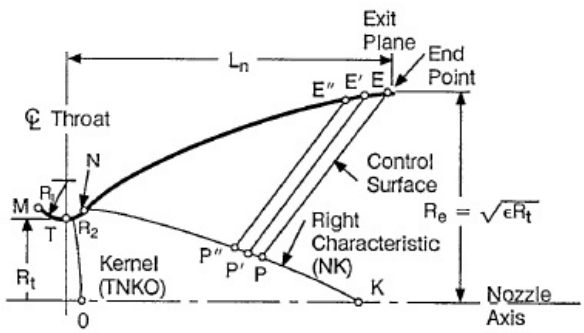

Figure 2.4: Bell nozzle layout [2].

The spike nozzle is a type of annular nozzle. These nozzles avoid over-expansion, which occurs when the exit pressure is lower than the external pressure, reducing thrust. A particular advanced spike nozzle is the aerodynamic spike, that introduces a secondary flow into the nozzle base. The

primary flow is the biggest contributor to the produced thrust and expands beyond the nozzle surface, enclosing a subsonic recirculating flow region. The free jet boundary acts like a self-adjusting wall that compensates changes in atmospheric pressure. On the opposite side there is a free-jet boundary. This type of nozzle improves performance, nevertheless it has high cooling requirements and is heavier and harder to manufacture.

For the nozzle sizing it is current practice to apply isentropic expansion relations. The exit area - A_e - is given by the relation between the exit and the throat area - A_t -, for a sonic throat.

$$\frac{A_e}{A_t} = \frac{1}{Ma_e}\left(\frac{1+\frac{\gamma-1}{2}Ma_e^2}{(\gamma+1)/2}\right)^{\frac{\gamma+1}{2(\gamma-1)}} \tag{2.3}$$

Where M_e corresponds to the Mach number at the exit and γ is the heat capacity ratio. The throat area is computed using the sonic throat assumption. Equation 2.4 can be manipulated in order to solve it for the maximum accepted area to have sonic conditions, given by A^*, from the drag coefficient - C_d -, mass flow rate - $\dot{m}$ -, density - ρ_{gt} and pressure - P_t.

$$\dot{m} = C_d A^* \sqrt{2\rho_t P_t \left(\frac{2}{\gamma+1}\right)^{\frac{\gamma+1}{\gamma-1}}} \tag{2.4}$$

The material should also be carefully analysed. Some materials are not compatible with some propellants, for example, ammonia deteriorates copper. It is also desirable to have a material with strong mechanical properties to ensure that the chamber is capable of withstanding both pressure and temperature conditions. The temperatures in the chamber during the combustion are higher than the service temperature of most of the materials, whereby the need for chamber cooling must be considered during the design to avoid damage. This is paramount for calculating wall thickness and choosing the right material. The heat transfer is a crucial part of the design. Chamber heat is mostly transferred by convection from the hot gases to the wall, and then conducted through the wall. Figure 2.5 shows presented the typical axial heat transfer distribution. There is a significant increase of the heat transfer in the throat, which means that the cooling must be exceptionally effective in this area to avoid significant damage.

When the chamber overheats, exceeding the material service temperature or its melting point, common damage types can occur. One of them is the burn-through, which results in damaged walls that compromise the system's integrity. Peeling can also occur, resulting in less resistant structures. When the melting point is surpassed, the chamber's material can melt. As it was mentioned above, the throat region is critical, and it is likely to have throat abrasion. Finally, in extreme circumstances, the chamber can burst.

Cooling can be done mainly by a combination of five different methods:

- Regenerative cooling - It is the most used method. One or both propellants pass trough conduits in the chamber's outer wall in order to cool it before being injected.
- Film cooling - In this case, as its name indicates, the wall surface is protected from excessive heat by a thin film of a coolant or propellant, that is introduced in the chamber around the injector or through orifices in the chamber wall. It can be used in combination with regenerative cooling.

- Transpiration cooling - It is similar to film cooling. In this case the walls in the chamber are porous. A coolant is introduced through them at a rate that allows the a desired temperature to be maintained.

- Ablative cooling - This method was mainly used in solid motors, although it is also suitable to liquid engines of short duration and low chamber pressure. For this method the wall material is a thermal insulator, resulting in a poor heat transmission to the outside. In the inner chamber wall the material suffers melting, vaporization, and chemical changes to dissipate heat.

- Radiation cooling - The heat is radiated from the surface to the outer wall of the chamber. This type of cooling is preferable in regions with low heat flux as, for example, nozzle extensions.

There are also uncooled rocket motors. Those are meant to operate for a short period and their chamber's wall must act as a heat sink. In this case the engine should stop before the exposed walls reach critical temperatures.

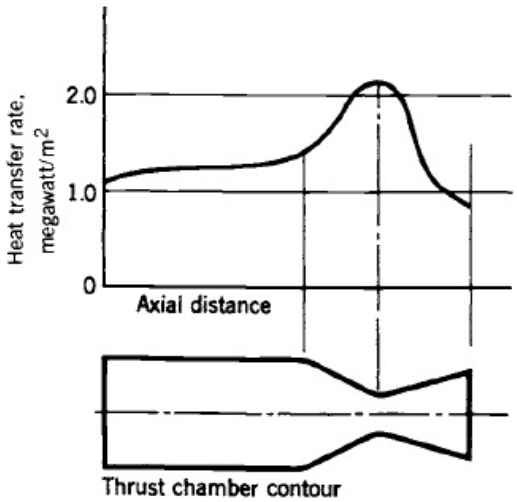

Figure 2.5: Typical heat transfer profile in the chamber [3].

The most relevant performance parameter is the specific impulse - I_{sp} - which SI unit is $\frac{N \cdot s}{kg}$. It depends on a wide range of factors such as chamber pressure and propellants ratio. It is given by the ratio between the engine's thrust - F - and the total mass flow rate - $\dot{m}$ [3]:

$$I_{sp} = \frac{F}{\dot{m}} \tag{2.5}$$

As the chamber pressure increases, so does the specific impulse, until a point where it nearly stabilizes. However, having high pressures in the chamber denotes that there will be a significant amount of inert mass in the tanks, when no pumps are used - resulting in extra weight - and also an increase in heat transfer to the chamber and nozzle wall, which is not always desirable and may also the lifetime of the system [4]. Regarding the OF, having a lean or rich mixture is determinant to the combustion efficiency. This ratio can be calculated from the stoichiometric combination of the fuel and the oxidizer.

For instance, when combining ammonia with oxygen the reaction is:

$$4NH_3 + 3O_2 \rightarrow 2N_2 + 6H_2O \tag{2.6}$$

As the molecular mass of the oxygen is 32g/mol and ammonia's 17g/mol, the stoichiometric OF is about 1.4. It is desirable to work near the stoichiometric value, however the most efficient ratio - in terms of I_{sp} - is observed for a slightly rich mixture. This happens because the specific impulse depends on both the burn and the expansion. The burn will be more efficient at the stoichiometric point, but the expansion is more effective when low-molecular-mass gases are formed as a result of the combustion. In fact, when running CEA [1] for a mixture of ethanol and gaseous oxygen - which has a stoichiometric OF of 2 - for three different OF values it was notorious the difference in the formed species (table 2.1). As it was expected, at low OF lighter molecules are formed as a consequence of the formation of H_2 and CO, instead of heavier H_2O and CO_2.

Table 2.1: Different species formed at different ratios.

OF=0.6		OF=1		OF=2	
CH_4 - 0.11%	H_2O - 10.776%	H - 0.649%	H_2O - 31.359%	H - 2.546%	H_2O - 40.518%
CO - 36%	CO_2 - 3.919%	CO - 33.95%	CO_2 - 5.881%	CO - 17.418%	CO2 - 16.804%
H_2 - 49.136%		H_2 - 27.97%	O - 0.0003%	H_2 - 5.294%	O - 2.244%
		OH - 0.185%	O_2 - 0.001%	OH - 8.486%	O_2 - 6.678%
				H_2O_2 - 40.518%	HO_2 - 0.011%
$I_{sp_{Exit}}$ - 2177	$I_{sp_{Throat}}$ - 1140	$I_{sp_{Exit}}$ - 2471	$I_{sp_{Throat}}$ - 1232	$I_{sp_{Exit}}$ - 2322	$I_{sp_{Throat}}$ - 1118

The choice of propellants is a trade off between some relevant factors such as their availability, cost, performance - specific impulse, etc. -, hazards, desirable characteristics, ignition and combustion requirements, property variations, specifications and additives. In the following section there is a table of several fuels and oxidizers commonly used.

The injector is the component responsible for introducing the reactants into the combustion chamber. Usually the propellants are in liquid state when injected. Therefore the injector must be capable of breaking down the stream into small droplets in order to maximize the mixing and achieve an effective burn. There is a pressure drop in the injector that must be considered when designing the system. It can be estimated by the non-saturated throat equation, obtained from the mass conservation equation.

$$\dot{m} = C_d A_{inj} \sqrt{2\rho P \left(\frac{\gamma}{\gamma - 1}\right) \left(\left(\frac{P_c}{P}\right)^{\frac{2}{\gamma}} - \left(\frac{P_c}{P}\right)^{\frac{\gamma+1}{\gamma}}\right)} \tag{2.7}$$

There is a lot of research about injectors and their influence in the engine behaviour, regarding the orifice pattern, angles on injection, etc. Although it is a field with a considerable complexity, the goal of this project was to design a simple injector. Having a good mixture is the key factor to achieve an efficiency near the expected.

During the operation time the tanks will lose pressure despite the high pressure burned gases in the chamber. To ensure that the propellants keep entering the chamber, a feed system is required. This can

[1] Chemical Equilibrium with Applications

be achieved by either using turbopumps or pressurized gas systems. The main engine cycles are [1]:

- Pressure-fed cycle - in this type of cycle the propellants come from pressurised tanks, using inert gases (figure 2.6 a). These tanks are heavy and their optimal pressure is low, which will limit engine's power. However, all the fuel is burned, increasing efficiency.

- Gas-generator cycle - a turbopump is powered by the burn of a small part of the propellants or an auxiliary propellant. Combustion products are usually expelled by the main nozzle, or a secondary one. These pump turbines are large enough to allow high pressure chambers, and therefore high power engine (figure 2.6 b).

- Expander cycle - the cooling of walls and nozzle is made by circulating cryogenic fuel, vaporizing and expanding it. The fuel is then used to drive the turbopumps before entering the combustion chamber. It is important to notice that the heat available is limited, which will lead to restrictions on the engine power. However, this type of cycle usually results in high efficiency and high power turbopumps, (figure 2.6 c).

- Staged combustion cycle - a lean or rich mixture is burned in a pre-chamber and expanded in a turbine in order to power the turbopump (figure 2.6 d). The resulting gas from the combustion is injected directly in the main chamber, where it undergoes a new combustion process with the desired OF ratio. This cycle allows very high chamber pressure and overall efficiency.

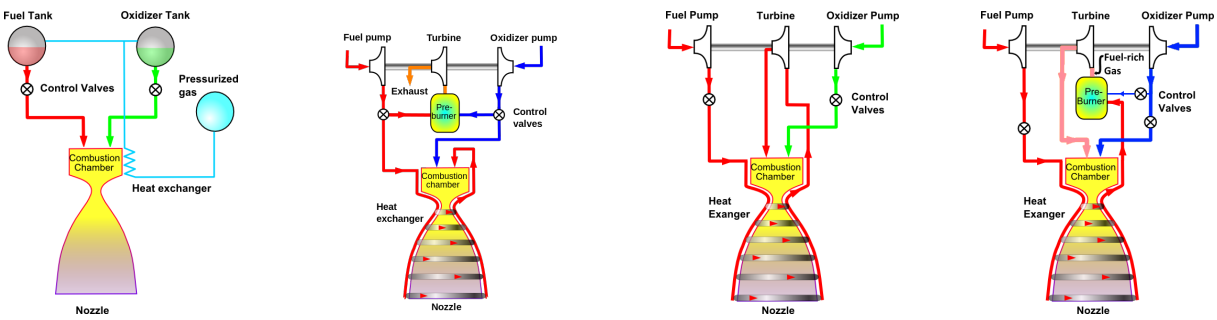

(a) Pressure-fed cycle diagram [5].

(b) Gas generator cycle diagram [6].

(c) Expander cycle diagram [7].

(d) Staged combustion cycle diagram [8].

Figure 2.6: Illustration of engine cycles.

To predict the engine performance and the combustion characteristics, software is available from NASA - CEA [9] [10] - that is capable to compute these parameters. This software, called Chemical Equilibrium with Applications, was developed to calculate chemical equilibrium and properties of complex mixtures. It has specific functionalities for rocket problems, and was used during this project. In the consulted literature [11] an analytical model was also found for computing engine's parameters. In figure 2.7, the flowchart indicates the steps to parameters prediction. This flowchart was an important departure for implementing the mathematical model, leading to understand which properties were needed in the iteration.

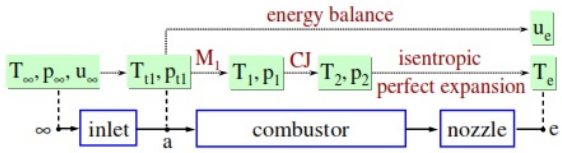

Figure 2.7: Flowchart to performance prediction [11].

In the flowchart, CJ stands for Chapman–Jouguet, which is a one-dimension model to predict properties in a detonation. The other variables, have the usual meaning: M is the Mach number, T is the temperature, P is the pressure and u the velocity.

2.2 State of Art

The present section resumes the state of art of the involved technology. It was important to the project developed to take advantage of conventional solutions whenever applicable, since the time to build the prototype wasn't much and the budget was low.

There are currently five main organizations leading the space exploration [12]: NASA from the United States of America, ROSCOSMOS from Russia, ESA from Europe, JAXA from Japan and CNSA from China.

Currently the number of launchers in use is very high, therefore it was decided to approach the most used and successful launchers from the present-days. Reference [13] shows that those can be resumed to: Ariane 5 and Vega, from ESA; Falcon 9 - which belongs to the Falcon family, previous owned by NASA, and now belongs to the private company SpaceX; Atlas V and Delta IV, from NASA; Long March (also known as CZ), from CNSA; H-II from JAXA; and finally Soyuz and Proton M from Russia. Soyuz is currently the main vehicle to transport astronauts into space.

(a) Ariane 5 [13] (b) Delta IV [13] (c) Falcon 9 [13] (d) Proton [13] (e) Soyuz [14]

Figure 2.8: Launchers.

These vehicles have several stages, some of them have liquid engines and their technology is presented in this section.

Propellants combination

When considering bi-propellant engines there are some combinations that are more commonly used and can be seen in table 2.2. The information about specific impulse values was found on reference [15].

Table 2.2: Common combinations and their specific impulse for an expansion from 68bar to 1bar.

Oxidizer	Fuel	I_{sp} [N· s/kg] (sea level)	I_{sp} [N· s/kg] (vacuum)	Engines
LOx	H_2	3816	4462	RS-25 (Space Shuttle), Vulcain (Ariane)
LOx	RP-1 (Kerosene)	2941	3510	Merlin (Falcon 9), RD-107 (Soyuz)
N_2O_4	Hydrazine	2862	3369	RD-275 (Proton), YF-20 (C23)

In the first steps of the project the idea was to use Ethanol as fuel. The research indicates that there will be an increase of rocket boosters with hydrocarbon fuels [16]. In fact some work is being conducted in order to develop a reusable rocket-plane with an ethanol propulsion system [4]. Ethanol is safe for the environment and was regularly used between the decades of 30 and 50 however, it is not the highest performance fuel, so it fell into disuse by the mainstream industry, which was mainly driven towards high performance during and after the cold war.

Chamber cooling/Heat transfer

As it was explained in section 2.1, it is necessary that the combustion chamber and the nozzle are cooled in order to preserve the integrity of the materials in use. Heat flux is highly influenced by the type of injectors chosen [4]. The use of a simple injector is one of the objectives of this work. As the time is also limited and the project is globally in its early stage, the refinement of heat transfer characteristics is beyond the scope of the present work. However, there is a lot of ongoing research in this field [17] [16].

It is crucial to ensure two things when regarding heat transfer and cooling:

- On the hot gas side, it is desirable to keep the most heat as possible. Usually, the goal is to avoid the formation of deposits. The use of some hydrocarbon fuels potentiates the formation of small particles that inhibit heat transfer [16]. However, in some specific cases found in the literature [18], it is desirable to have these deposits in order to protect the chamber wall. In the mentioned literature, it is explained that the use of TEOS results in the formation of deposits that minimize heat transfer to the wall. TEOS stands for tetraethyl orthosilicate, it is a colorless liquid used in the production of aerogel. It can be added to the fuel and when burned forms a layer of silicon oxide deposit that limits the heat transfer.

- On the coolant side a fluid with proper cooling capabilities - given by specific and latent heat - should be used. In some cases, in small scale test stands, water is chosen, rather than the fuel [3]. It has a very satisfactory heat absorption capability. The liquid flows inside cooling jackets (figure 2.9) - steady flow - and rapidly enough to avoid boiling. Boiling can result in instabilities that will deteriorate the heat transfer characteristics. When considering this option is it crucial to design the engine carefully so it operates within the nucleate boiling region. This can be difficult to achieve due to the high values of heat fluxes because, when there is transition to film boiling, a gas film

is formed near the outer wall, severely reducing the heat transfer. Since in rockets it is desirable to minimize the weight of the system, meaning that a separate water-based cooling mechanism that would make the system heavier. That is why regenerative cooling is a viable option. This mechanism of cooling, as it was previously explained, is based on the circulation of one of the propellants before the injection - usually the fuel. When working with ethanol a problem arises, because ethanol has low heat-absorption capability when compared to water, although it is still better than hydrocarbons [19] [20].

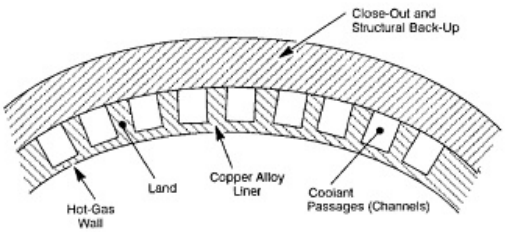

Figure 2.9: Typical cooler jacket layout [2].

Nevertheless, for this project, the aim is to evaporate the fuel in order to guarantee a gaseous injection of both propellants. The system includes a vaporizer which performs similarly to a boiler. The problem with the boiling process is the regime of boiling in which the vaporizer operates. There is nucleate boiling, film boiling and the transition stage in between them. Film boiling will drastically decrease the heat transfer and may result in the chamber deterioration. This problem will be discussed in detail in the section 4.2. However, NASA conducted some research to experimentally determine the critical heat flux of ethanol - when the transition occurs. They concluded that CHF [2] may not be the limit for the admissible heat flux, once there was not material damage [19].

Injector

Injectors are determinant to heat transfer and efficiency. Their shape and performance will influence the mixing of the reactants and, therefore, the combustion parameters.

The most used rocket injector is the shower injector, which - as the name suggests - is similar to shower heads (figure 2.10). However,several disadvantages may be identified, namely: high manufacturing cost due to its complexity. In addition, there are some instabilities issues regarding this type of injectors.

[2]Critical Heat Flux

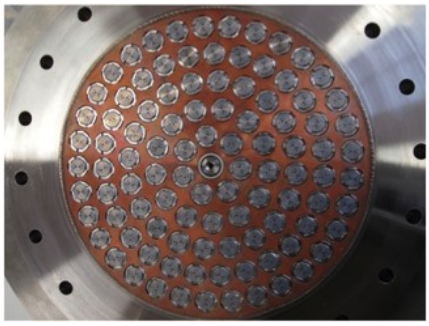

Figure 2.10: Example of shower injector from an experimental engine from JAXA [4].

These injectors introduce both propellants into the chamber without pre-mixing them. The number of holes for the oxidizer and fuel is a parameter that should be defined during the design phase, as well as their slope angle and diameter.

As it was mentioned above, the goal is to design a simple injector that can be easily manufactured. To fulfil this requirements the Pintle Injector is a strong candidate [21]. This injector consists of two coaxial tubes where propellants flow. It is a combination of a purely radial flow with an axial flow, which maximizes the mixture and improves efficiency. The radial injection of fuel at creates a recirculation bubble. Its importance will be clarified in section 4.2.

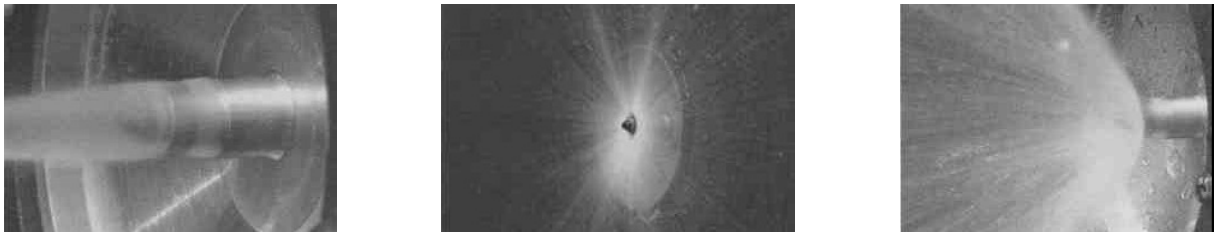

(a) Outer flow - Axial. (b) Inner flow - Radial. (c) Combined flows.

Figure 2.11: Illustration of flows in Pintle Injection [21].

Another possibility of injection is to use a rotating flow like is done in the jets engines. Swirl flows increase the engine performance, as the length travelled by the species is bigger than in flows without tangent velocity, providing a more efficient mixture of the components.

Both cases have a highly desirable characteristic in common: a recirculation zone. In fact, research shows that this effect is very similar in both cases [22].

Feed System

There are two main types of feed systems: turbo-pumps and blow-down systems.

In the engines where turbo-pumps are used there is no need for an auxiliary gas, and the pumps are responsible for driving the propellants into the combustion chamber. However, these systems require other elements such as turbines and its power sources, speed reduction gear transmissions, lubrication systems, accessory drivers, propellant inlets and discharge ducts and turbo-pumps mounts [2]

The gas-pressurized feed systems work as a blow-down system, where an inert gas at high temper-

ature is responsible to push propellants into the combustion chamber.

Engines

To sum up all the technology used nowadays some engines are presented, being possible to understand the most used and the combination of technologies. It is important to keep in mind that, just as for launchers, engines are also categorized i families. Each family has similar characteristics and there is a constant evolution. It is possible to find contemporary engines from the same family, used in different vehicles. It is a very conservative field of research and technology from the past decades is still used. The list of engines that follows consists mainly on cryogenic engines. Figure 2.12 shows schematically how this type of engine works.

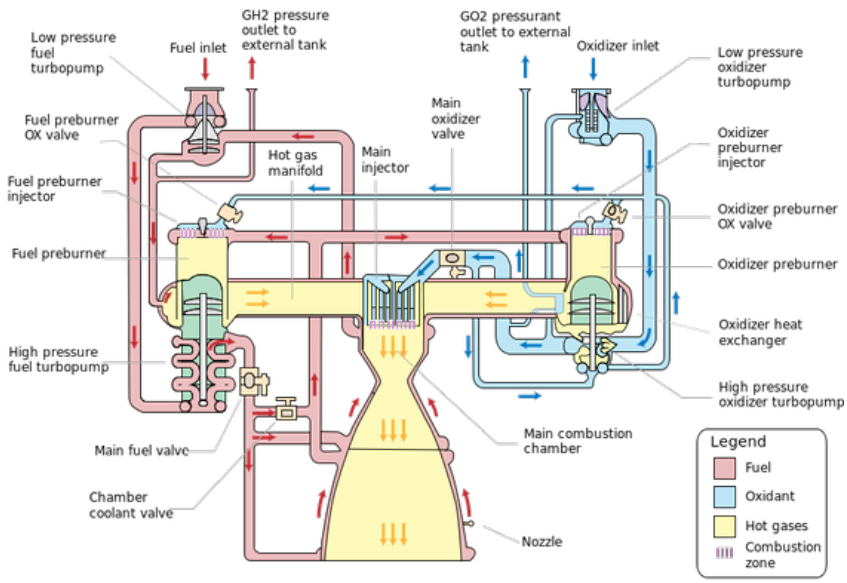

Figure 2.12: Cryogenic engine schematic [23].

Merlin is the engine of Falcon 9's upper stage. It is a recent engine from 2013. It uses liquid oxygen and Kerosene as its propellants [24]. The OF is controlled by the sizing of the piping. It is possible to control this ratio by the flow trimming using a butterfly valve controlled by a servo motor. The engine is cooled by regenerative cooling. Some of the engine's characteristics are in table 2.3.

Table 2.3: Merlin characteristics.

Pressure (bar)	Thrust (kN)	Specific Impulse (Ns/kg)	Burn time (s)	Area ratio	OF
96	716	2766.42	180	16	6.2

Vulcain engine is in the core stage of the european launcher Ariane 5. As table 2.2 shows, its propellants are liquid oxygen and liquid hydrogen. It is, therefore, a cryogenic engine. Its cooling is achieved

by regenerative cooling [25]. Before entering the injetor, the H_2 passes through small tubular channels in the chamber's wall. This wall is made of copper and has a thickness of about 1.5mm. In the injector the propellants are mixed coaxially. The oxygen is injected at the center and the hydrogen at the periphery. The velocity differences between the two propellants create shear forces that produce their atomization. The engine uses turbopumps for both propellants.

Table 2.4: Engine's characteristics.

Pressure (bar)	Thrust (kN)	Specific Impulse (Ns/kg)	Burn time (s)	Area ratio	OF
102	1075	3119.58	605	45	6.2

RD-107 is the engine of the Soyuz launcher. The propellants are liquid oxygen and kerosene. This engine has a gas generator engine cycle in which the turbines work with the steam produced by the catalytic decomposition of H_2O_2 that drives the propellants turbo-pump. As it is possible to see in figure 2.13 it has four combustion chambers but only one turbo-pump. It uses regenerative cooling, as kerosene was used to cool the nozzle before entering the injector. In terms of OF it was introduced an important innovation, allowing it to perform with different ratios.

Table 2.5: RD-107 engine.

Pressure (bar)	Thrust (kN)	Specific Impulse (Ns/kg)	Burn time (s)	Area ratio	OF
58.5	971	2582	150	18.9	Variable

RD-180 is used in the first stage of the american Atlav V [26]. As it is possible to see in figure 2.13 d) it has two chambers. Like Merlin engine, it uses liquid oxygen and kerosene as propellants. It has a staged combustion cycle with a pre-burner, rich in oxygen, and a single turbine. The two-stage fuel pump powers the hydraulic system. It also includes a health monitoring and life prediction system. There was an environmental concern when building this engine, as the start and shutdown of oxidizer eliminate the pollution from unburned kerosene. Other characteristics are presented in table 2.6.

Table 2.6: RD-180 engine.

Pressure (bar)	Thrust (kN)	Specific Impulse (Ns/kg)	Burn time (s)	Area ratio	OF
256.6	4152	3070.53	270	36.4	2.72

RD-253 utilizes dinitrogen tetroxide and unsymmetrical dimethylhydrazine as propellants. It was applied in several launchers from Proton family. It uses a tetroxide with a small quantity of fuel in after-burning through the gas generator. The amount of gas produced passes through the turbine, via the

primary chamber, where it is mixed with fuel. The engine has regenerative cooling, with recirculation of the fuel in the nozzle cooling. The feeding method consists of turbopumps [27]. More characteristics on the engine can be seen in table 2.7.

Table 2.7: RD-253 engine.

Pressure (bar)	Thrust (kN)	Specific Impulse (Ns/kg)	Burn time (s)	Area ratio	OF
152	17635	3099	130	26	2.67

LE-7A is part of the LE-7 family and it was used in the Japanese launcher H-II, in its first stage. The oxidizer is liquid oxygen and the fuel is liquid hydrogen. It has a two stage combustion cycle system. The first engines that were produced had a problem with excessive vibration that led to material fatigue. The feed system uses turbopumps [28]. Table 2.8 shows further information about this engine.

Table 2.8: LE-7 engine.

Pressure (bar)	Thrust (kN)	Specific Impulse (Ns/kg)	Burn time (s)	Area ratio	OF
121	1098	3102	390	51.9	5.9

YF-100 is a Chinese engine is used in the Long March 7 launcher, also known as CZ-7 [29]. It uses liquid oxygen and kerosene. It offers the possibility of throttling achieving 65% of the rated thrust, as can be seen on table 2.9, along with other characteristics. The feeding is done by turbopumps. The oxygen drained from the engine is used to pressurize the oxygen tank, as it passes through a heat exchanger. The control actuators work with pressurized kerosene as hydraulic fluid. The pressurization of the kerosene tank is done using helium. In the preburner, the oxygen is burned with a small amount of kerosene in order to produce enough gas to power the turbine.

Table 2.9: YF-100 engine.

Pressure (bar)	Thrust (kN)	Specific Impulse (Ns/kg)	Burn time (s)	Area ratio	OF
180	1339	3286	155	35	2.7

(a) Merlin engine. [24]

(b) Vulcain engine. [30]

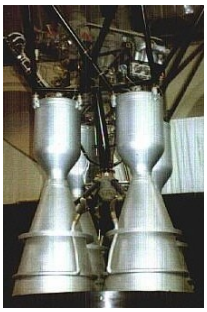

(c) RD-107 engine. [31]

(d) RD-180 engine. [26]

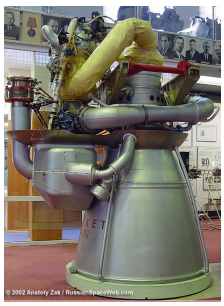

(e) RD-253 engine. [32]

Figure 2.13: Some of the engines described.

Chapter 3

Mathematical Model

3.1 Model

The mathematical model in this project serves to determine if the auto pressurization concept is stable. The objective is to determine the pressure evolution in the tank when the heat transfer is responsible for increasing the remaining fuel's pressure. In order to simplify calculations, the layout considered is layout 6 from section 4.1, which can be seen on figure 3.1.

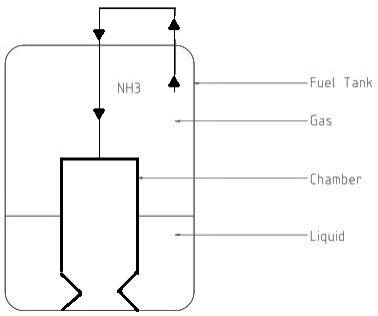

Figure 3.1: Layout number 6 schematic.

The mass in the tank is estimated by a mass balance, in equation 3.6, where $\dot{m}_F$ if the fuel mass flow, m is the fuel mass and $m(0)$ is the initial fuel mass.

$$\frac{\mathrm{d}m}{\mathrm{d}t} = -\dot{m}_F \Rightarrow m = m(0) - \int_0^{\Delta t} \dot{m}_F \mathrm{d}t \tag{3.1}$$

In order to calculate the fuel's mass flow rate - equation 3.2 - it is necessary to know the velocity, which can be calculated with equation 3.3, a version of the Bernoulli equation. Notice that, in this equation, k represents the pressure losses in each pipe section. The term f represents the Darcy friction factor, they can be estimated using available references [33] and [34].

$$\dot{m}_F = \frac{AV}{\nu_g} \tag{3.2}$$

Where A is the area of the piping, V is the velocity and ν_g is the specific volume.

$$P - \Delta h_{loss} = P_0 \Rightarrow \Delta h_{loss} = \frac{V^2}{2\nu_g}\left(\frac{fL}{D} + \Sigma k\right) \Rightarrow V = \sqrt{\frac{2\nu_g\left(P - P_0\right)}{\Sigma k + \frac{fL}{D}}} \tag{3.3}$$

Applying an energy balance in the tank yields equation 3.4, where u and m are defined by equations 3.5 and 3.6, respectively.

$$\dot{Q} = \frac{\mathrm{d}}{\mathrm{d}t}\left(mu\right) + \dot{m}_F h_g \tag{3.4}$$

$$u = u_l + x\left(u_g - u_l\right) \tag{3.5}$$

$$m = \frac{Vol}{V} = \frac{Vol}{\nu_l + x\left(\nu_g - \nu_l\right)} \tag{3.6}$$

where x value is the quality of the mixture. The heat rate is given by:

$$\dot{Q} = AU\Delta T \tag{3.7}$$

A being the area, ΔT the temperature difference and the heat transfer coefficient U definition in given by equation 3.7, as follows:

$$U = \frac{1}{\frac{1}{2\pi r h_i} + \frac{1}{2\pi k} ln\left(\frac{X+L}{r}\right) + \frac{1}{2\pi(X+L)h'_e}} \tag{3.8}$$

where h_i and h'_e are the convection coefficients in the chamber and vaporizer, respectively. The quality x can be estimated by:

$$x(t) = \frac{m_g}{m} = \frac{\int_0^{\Delta t} \dot{Q}/h_{fg} dt}{m(0) - \int_0^{\Delta t} \dot{m}_F \mathrm{d}t} \tag{3.9}$$

To close the problem it is necessary to include an extra equation. Assuming a sonic throat, the mass flow is maximum and equal to:

$$\dot{m}_t = \dot{m}_F + \dot{m}_{ox} = \frac{0.6847 P_0 A^*}{\left(RT_0\right)^{1/2}} \tag{3.10}$$

When applying equation 3.10 it is considered that the throat is sonic. In reference [34] it is possible to find condition 3.13, which ensures supersonic conditions based on the pressure ratio between the chamber and the exit.

$$\frac{P_c}{P_e} > \left(\frac{\gamma_c + 1}{2}\right)^{\frac{\gamma_c}{\gamma_c - 1}} \tag{3.11}$$

This condition is explained by the isentropic relations, which is given by [34]:

$$\frac{P^*}{P_0} = \left(\frac{2}{\gamma + 1}\right)^{\frac{\gamma}{\gamma - 1}} \tag{3.12}$$

In figure 3.2 it is possible to see that a supersonic exhaust requires a sonic throat. In this project it is intended to work with curve H.

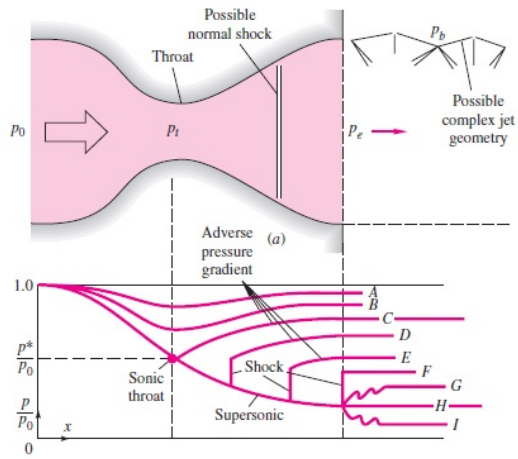

Figure 3.2: Pressure distribution in a convergent-divergent nozzle influenced by back pressures [34].

This requirement leads to:

$$P^* > P_e \Rightarrow \frac{P_0}{P_e} > \frac{P_0}{P^*} \Rightarrow \frac{P_0}{P_e} > \left(\frac{\gamma_c + 1}{2}\right)^{\frac{\gamma_c}{\gamma_c - 1}} \tag{3.13}$$

The exit pressure is 1bar - atmospheric pressure. This means that the exhaust plume will be supersonic for chamber pressures above approximately 2bar.

Method

Given the initial pressure of the tank - set as 20bar - the burning process starts. The flame temperature depends on the oxidizer fuel ratio, (the polynomial that describes the relation is obtained using CEA software). This temperature is crucial to estimate the heat transfer. The heat is absorbed by the fuel in the vaporizer, and its properties will change. Through the energy balance it is possible to determine the new pressure value. This new state, with the updated properties, will result in a different fuel mass flow and, therefore, in a different OF, which will lead to new temperatures in the chamber and therefore, new values of heat rate.

This creates a cycle during the burn, which can be seen of schematic 3.3. The values in blue correspond to the equations that were used.

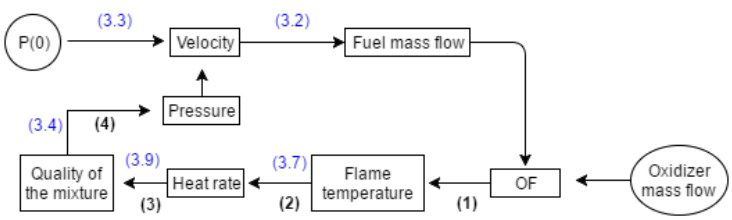

Figure 3.3: Mathematical model flow chart.

The oxidizer mass flow and the initial pressure in the tank are inputs of the model. Step **(1)** includes the polynomial that characterizes the relation between OF and the flame temperature, which can be

seen in figure 1.3. The heat transfer analysis (step **(2)**) depends on equations 3.7 and 3.8. To estimate the quality of the mixture (step **(3)**) with equantion 3.9 the value of the fuel mass (equation 3.6) and the enthalpy of vaporization are required. The enthalpy can be found in the tables from NIST, in appendix B. Finally, step **(4)** includes a solver that determinates the new pressure based on the new properties in the tank.

It is important to refer that this is a simplified mathematical model that does not contemplate some losses during the process. Some of the consulted literature [35], [36] and [37] provide a mathematical model to incorporate this losses by friction and heat transfer. However it was decided to make a simpler model relying on the assumption that the system is isentropic with heat transfer. In fact, the second principle of thermodynamics (equation 3.14), does not discard this possibility for $\mathrm{d}Q < 0$, since $\mathrm{d}\sigma > 0$ [38].

$$\frac{\mathrm{d}Q}{T} + \mathrm{d}\sigma = \mathrm{d}S \tag{3.14}$$

The thermodynamic properties of the saturated fluid were found on NIST [1] and can be consulted in appendix B. The polynomials that correlate pressure with internal energy, enthalpy, etc. were computed from the mentioned saturated property tables, using Matlab.

3.2 Results

In the introduction of this document, in figure 1.3, it is possible to see that there are two regions of operation. One is for low OF values, where the flame temperature changes quickly with the alteration of this ratio, corresponding to the desired operation zone. In the second region, the changes in temperature are more subtle. It is possible to simulate this two cases with the mathematical model.

Figure 3.4 shows the theoretical evolution in the properties for the case of a high OF. In this case it is possible to observe that the slope of the curves change at $t = 17s$. The pressure in the tank decreases, the heat rate and fuel mass flow also decrease.

The model is also capable of estimating the specific impulse and the thrust, using equation 3.15. Where I_{sp} is obtained with CEA software.

$$F = I_{sp}\dot{m} \tag{3.15}$$

However it is possible that these values will differ from the experimental ones, because the specific impulse depends on the burn and expansion efficiencies, and they were computed for the ideal case. Results are presented in figure 3.5.

For a low OF the results are different, as shown on figure 3.6. In this case, the system will slightly increase the fuel mass flow and the tank pressure. As the temperature in the tank increases, the heat rate evolution will decrease. The temperature in the chamber is significantly lower than in the previous case, as it was expected.

[1] National Institute of Standards and Technology

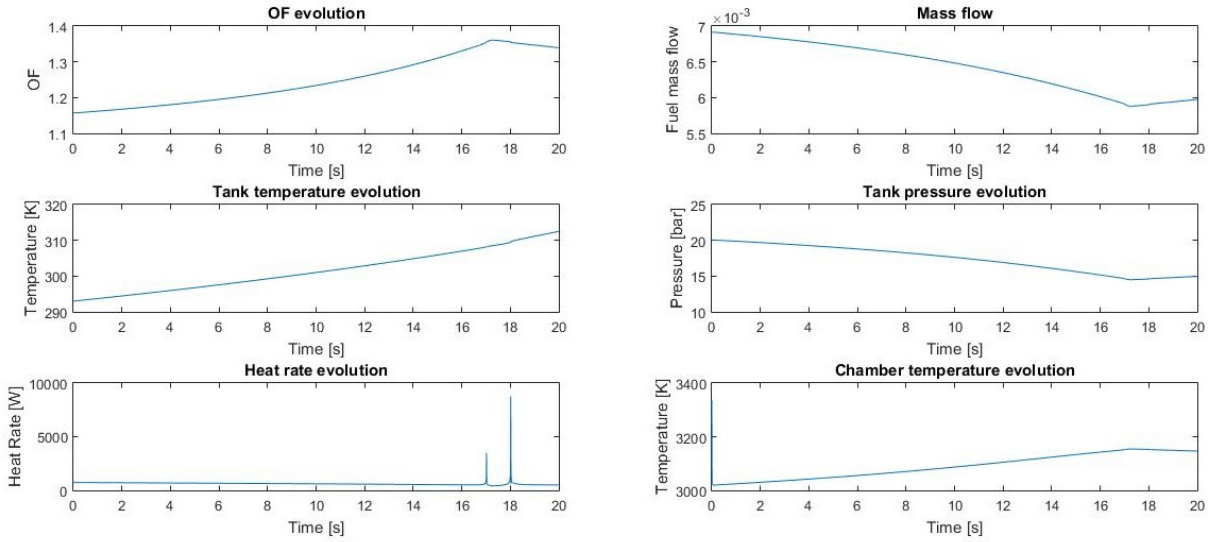

Figure 3.4: Mathematical model results for high OF.

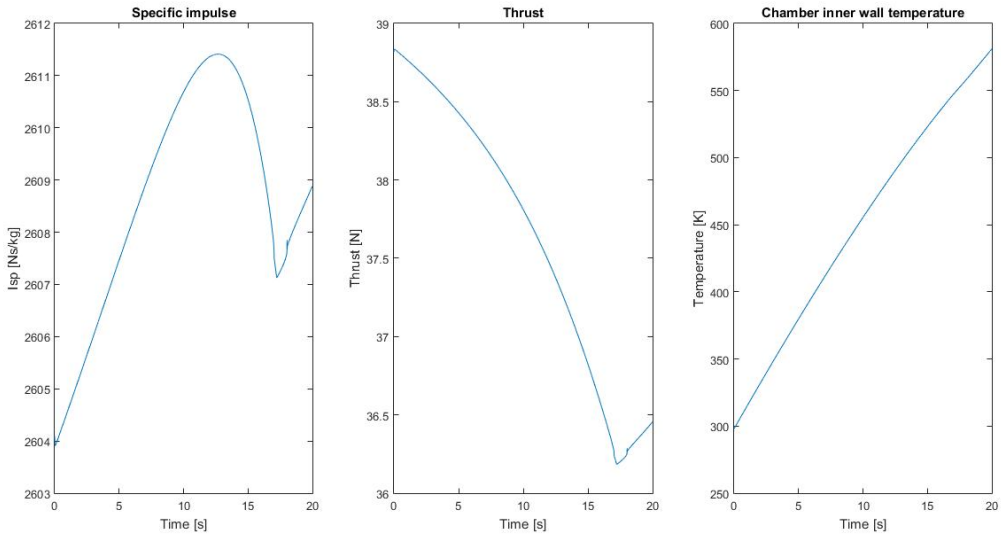

Figure 3.5: Mathematical model results for high OF.

In figure 3.7 it is possible to see that the specific impulse and the thrust for this case is lower.

The results obtained with the mathematical model agree with our expectations. Further in this document these two cases will be compared with experimental results.

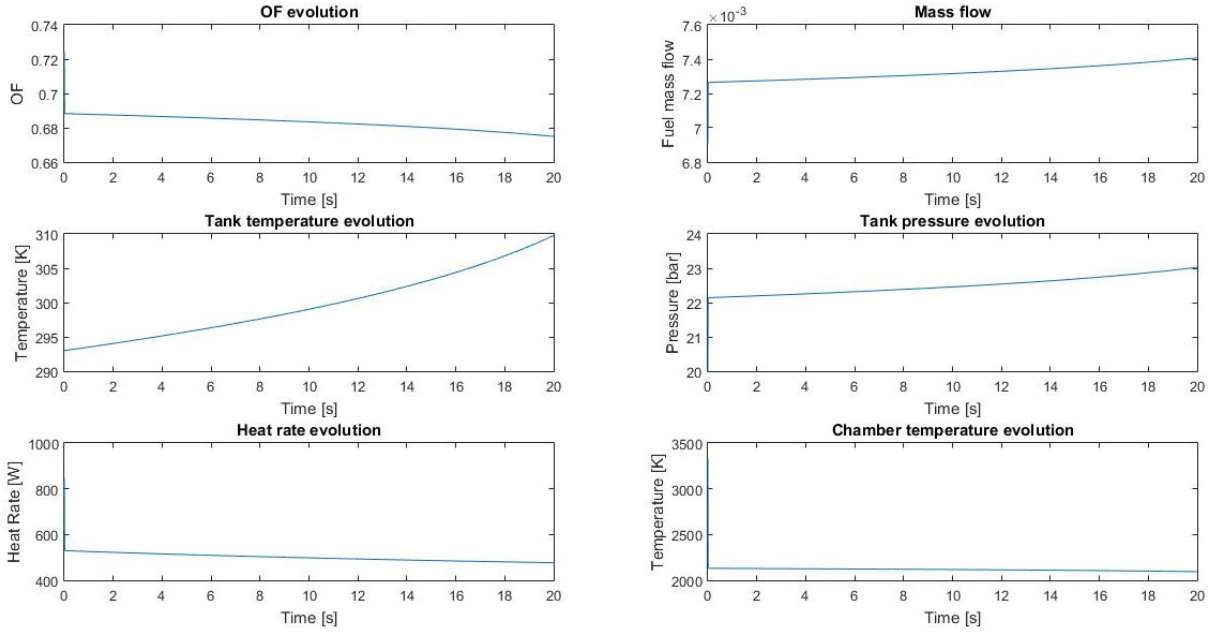

Figure 3.6: Mathematical model results for low OF.

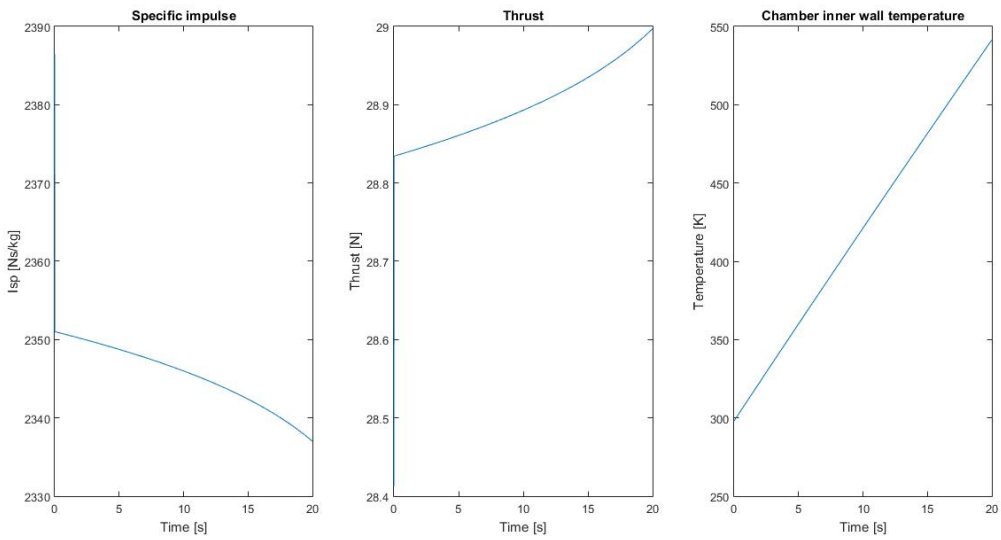

Figure 3.7: Mathematical model results for high OF.

4

Chapter 4

Experimental Work

In this chapter the experimental work developed is presented. In the following sections, the design of the engine, the building process and the final layout are illustrated.

4.1 Layouts Considered

To pass from the design to a system suitable for testing it is necessary to choose a proper layout. In this section the different layouts that were considered are shown and its advantages and disadvantages are analysed.

The first layout, in figure 4.1, includes the pressurization of the fuel tank. This layout was considered when using ethanol. For this layout there is a pressurization line using ammonia. The idea inherent to this system is to have ammonia near the hotter part of the chamber, serving as coolant. When ammonia heats its pressure raises, pushing ethanol to the combustion chamber. This layout has is complex to implement.

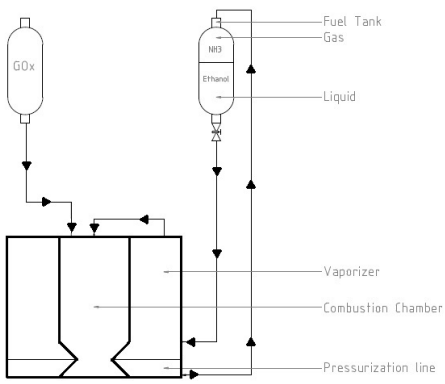

Figure 4.1: Layout number 1 schematic.

The second layout (figure 4.2) has safety problems and should only serve for theoretical studies. Since oxygen is used to pressurize the fuel, in the fuel tank there should be a membrane to prevent

the mixing of the propellants, and consequently, a major fire. In addition, this system does not take advantaged of the heat transfer from the combustion chamber, to pressurize the tank.

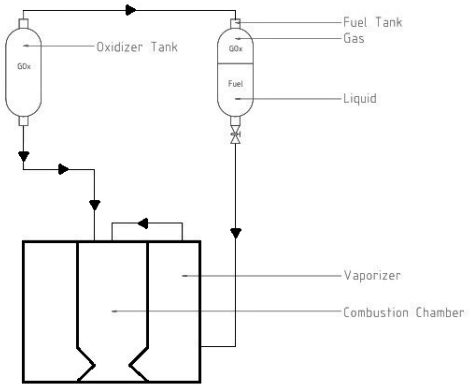

Figure 4.2: Layout number 2 schematic.

In the third layout (figure 4.3), the fuel flows from the tank to the vaporizer and, before entering the combustion chamber, passes inside the tank, exchanging heat and pressurizing it. From all the mentioned layouts, this is the most complex to manufacture. It is a hard task to produce the tank due to the need to incorporate a heat exchanger, which has to be carefully analysed to ensure that the proper amount of heat is exchanged.

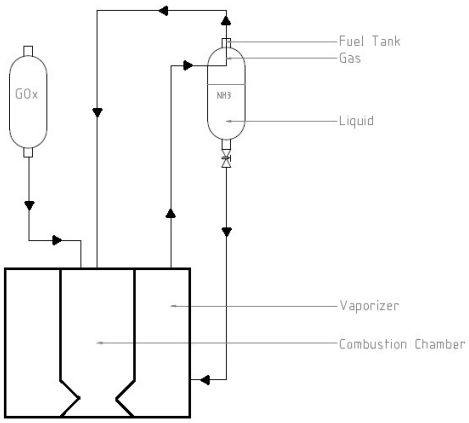

Figure 4.3: Layout number 3 schematic.

On figure 4.4 two layouts are shown. The sixth layout is the most unusual one. In this case, the chamber should be introduced inside the fuel tank. The fuel acts like a coolant and the heat it receives serves to pressurize it. This layout is conceptually simple but the piping implementation is difficult at small scales. In addition, it does not allow flexibility in tests, as it is necessary to place the head of the chamber with the igniter and instrumentation inside the tank. Despite its advantages, it is important to minimize risk so layout 5 was considered instead. It is chosen system , once it provides two possible operation modes: through external pressurization or self pressurization. When connecting the line that enters the upper part of the tank to an high pressure gas line, this gas will be responsible to push the propellant into the combustion chamber. However, the mathematical model used is based on layout 6,

since it is more straightforward.

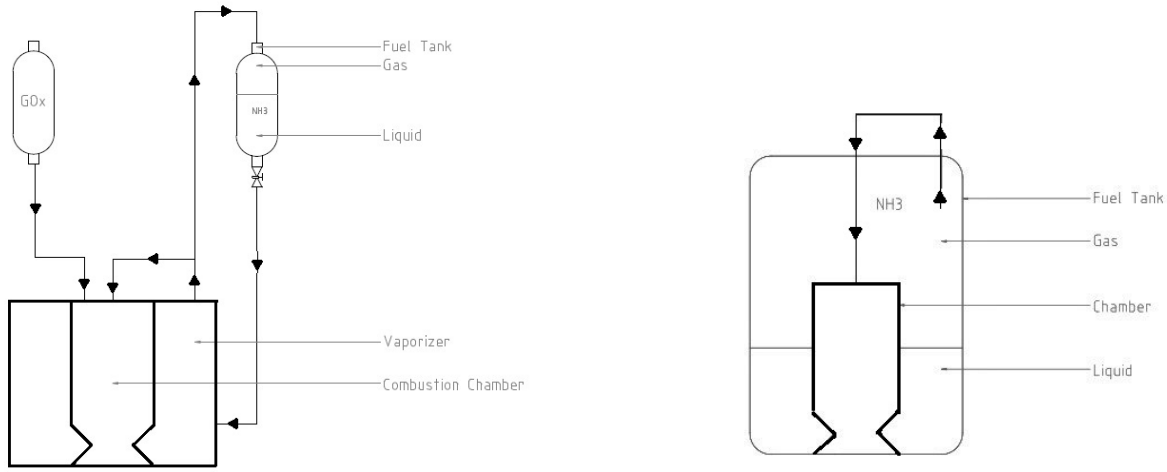

(a) Layout 5

(b) Layout 6

Figure 4.4: Used layouts.

4.2 General Concept

This project consists of the design, building and testing of a small liquid rocket engine. The main objectives of the work were already explained. In this section the system sizing is presented. The departure characteristics were:

Table 4.1: Baseline characteristics.

Pressure	Oxidizer	Fuel	Thrust
15bar	Gaseous Oxygen	To define	25N

To build the small liquid rocket engine, besides the mathematical simulation of the problem, a significant part of the work has to do with sizing. It is an iterative process due to the different options in each step. Nevertheless, as found in literature [3], a sequence of computation was followed: propellant choice, OF calculation, total flow rate computation, nozzle sizing, combustion chamber, chamber wall thickness and cooling. Finally, as part of the problem, the material was chosen and the injectors were designed.

Fuel

The main candidate for the fuel was ethanol. It is cheap, easily available, safe, has reasonable cooling capacity and acceptable performance. However, for the auto-pressurization purpose, ethanol is worse than ammonia or propane. This is because ethanol has a lower vapour pressure at low temperatures. In order to choose a fuel that fulfils the requirements of this project, several parameters were analysed: critical pressure and temperature, enthalpy of vaporization and specific impulse. The values can be

seen in table 4.2. Part of these estimations were done using CEA software and the other information was obtained from NIST.

Table 4.2: Properties of each fuel.

Reactant	Ethanol	Propane	Ammonia
Optimal OF	2	3	1.4
Critical pressure (bar)	63	42.6	112
Critical temperature (K)	514	369	405
Enthalpy of vaporization (@20°C) (kJ/kg)	1030	340	1179
Specific Impulse (N· s/kg)	2462.7	2479.9	2501.6
Chamber temperature (K)	3337.26	3476.2	3109.01
Density (kg/m3)	1.2843	1.1465	1.1141
Area ratio - Ae/At	3.32	3.3	3.21
c^* (m/s)	1709.7	1806.1	1828.5

As it is shown in table 4.2, ethanol and propane have a relatively low critical pressure. In addition, propane has also a low critical temperature. This shows that they are weak candidates for this project, since it desirable to be as far as possible from the critical points, working around standard temperature ($\approx 20°$) with high pressure. Ethanol has another drawback: it has very low pressure in a wide range of temperatures (figure 4.5). This means that the temperature should be higher than the desired to achieve auto-pressurization. Ethanol is not a gas at standard temperature, so its fluid properties are not available in NIST [1] website - where other fluid properties were found (in references [39] and [40] there are polynomials that were used to relate the thermodynamic properties of the saturated fluid with its temperature or pressure). The choice of the propellant was an iterative process and the results are presented in further sections.

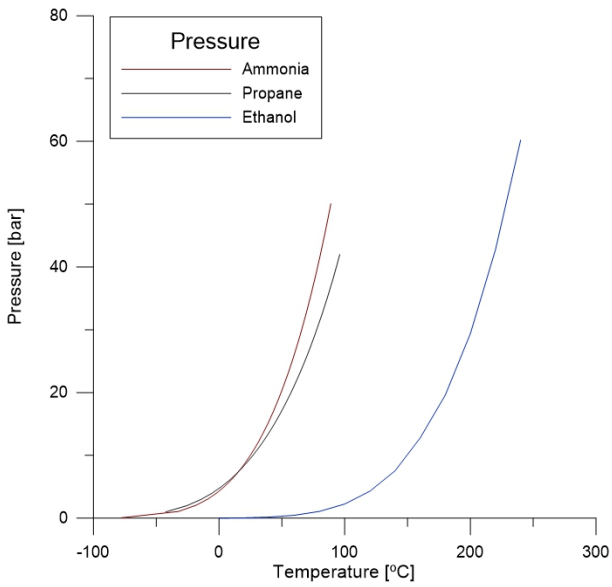

Figure 4.5: Relation pressure-temperature for the considered fuels.

[1] National Institute of Standards and Technology.

Material

Usually, amateur combustion chambers are manufactured from materials with high thermal conductivity, such as copper. This allows high heat rate values, minimizing wall temperatures and the risk of material damage. In the present case copper has some incompatibilities with the considered fuels, because ammonia corrodes copper and copper alloys. Table 4.3 shows the material compatibility with the considered fuels [41] [42].

Table 4.3: Material compatibility.

	Ethanol	Propane	Ammonia
Copper	A	A	D
Aluminium	B	A	A
Stainless Steel (304 and 316)	A	A	A
Nickel Superalloy	A	A	A

Where letters have the following meaning:

- A: Excellent.
- B: Good - Minor effect, slight corrosion or discolouration.
- C: Fair - Moderate effect. It is not recommended for continuous use. Softening, loss of strength, swelling may occur.
- D: Severe effect. It is not recommended for any use.

Accordingly to the previous information, these limitations provide two major candidates: nickel superalloy (also known as Inconel) and stainless steel. Nickel superalloy is expensive and it is difficult to find suppliers, thus it was decided to consider Inconel 625, a more common type of this material. Regarding the stainless steel three types were considered: 316 (1.4401) for its corrosion resistance, 304 (1.4301) because it is cheaper and 2205 (1.4462) for its strength. Mechanical properties are also important: yield strength and melting and service temperatures. It is important to use a material which is capable to stand reasonable pressures under high temperature conditions.

Table 4.4: Material properties.

	Thermal conductivity (W/m° C)	Melting temperature (° C) [43]	Service temperature (° C)	Yield Strength (MPa)
SS 304 [44]	16.2	1400-1450	870	290 annealed
SS 316 [45]	16.2	1375-1400	870	290 (annealed)
SS 2205 [46]	15	1385-1445	300	510 (annealed)
Nickel Superalloy [47]	10	1290-1380	982	872

When comparing the thermal conductivities, they're similar and of the same order of magnitude, therefore they are not an exclusion factor. Despite the mechanical properties of Stainless Steel 2205 the high price doesn't compensate its performance. Furthermore, it has a low service temperature. Nickel super alloy shows the highest yield strength and service temperature, although it is very expensive and difficult to manufacture, which implies in a dramatic increase in costs. Stainless Steel 304 and 316 are good candidates and the choice is purely based on costs: 304 is less expensive to machine and the fabricated components can be delivered faster. Also, a great advantage of stainless steel 316 is the higher corrosion resistance in chlorine-rich and acidic environments, which is irrelevant in our case as the propellants used do not contain chlorine.

Sizing

The sizing process followed was based on what was found in the literature [3]. When the thrust value is fixed - in this case is 25 N - and the specific impulse is estimated with CEA, equation 2.5 gives the total mass flow and, for a given OF, it is easy to estimate the fuel and oxidizer's mass flow.

One of the crucial dimensions is the throat area, given by equation 2.4. This equation gives the maximum throat area to maintain the desired pressure in the chamber. For the different propellants the correspondent diameter is slightly above 3mm, and a value of 3mm was considered.

The equation 2.3 allows the estimation of the exit area, which is about 22.7mm^2. The pressure inside the chamber is relatively small (15bar), which leads to a small difference between the throat and the exit areas when comparing to other engines that operate with much higher chamber pressures. This means that the conic nozzle is a good option, because there is no need for long nozzles or great expansions. Since the performance is not very relevant in this stage of the project, there is no need to implement a more complex contour. Figure 4.6 shows that there are two angles that must be defined to fully calculate the nozzle dimensions - α and β.

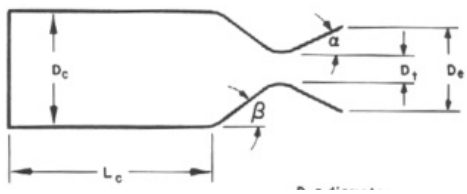

Figure 4.6: Nozzle angles. [3]

According to Krzycki [3], α was chosen as 15° and β as 60° .

For the chamber dimensions the values were already fixed. As it was mentioned before, costs are an important parameter in this project. To minimize the expenses, some of the material from a previous test engine was reused. The chamber's outer diameter was set at 50mm and the complete length is 90mm in order to fit inside an existent component that will serve as the vaporizer. An initial estimation - following literature [3] guidelines - showed that the outer diameter should be approximately 12mm and the length about 70mm. The final design is, then, highly oversized. Although it implies certain losses

and, apparently, a larger area to cool, it also minimizes hazards and has the potential to provide a more efficient mixture. The technical drawing of the chamber can be seen in figure 4.7.

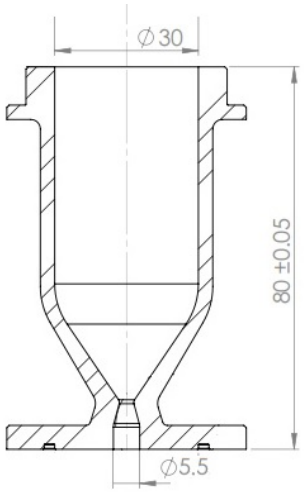

Figure 4.7: Chamber 2D drawing.

In order to finish the chamber sizing, the wall thickness must be calculated. This dimension is directly related to the heat transfer. The wall should be thick enough to withstand the pressures inside the chamber. However, the thickness is inversely proportional to the heat rate, therefore the value should be carefully chosen to avoid compromising the vaporization of the fuel. Increasing the wall thickness increases the thermal inertia of the system. Equation 4.1,gives a first estimation [3].

$$\delta = \frac{P_c D_c}{2F} \tag{4.1}$$

Based on the properties from table 4.4, the minimum thickness values are calculated with equation 4.1, the results are in table 4.5. It is considered that the working stress is the yield strenght dividing by a safety factor.

Table 4.5: Thickness first estimation

Material	Nickel Superalloy	Stainless Steel 304	Stainless Steel 316	Stainless Steel 2205
Thickness (mm)	0.1	0.31	0.31	0.17

These values are very small and do not take into account the high temperature, that compromise the material strength. A safety factor of 4 is introduced to prevent material damage. Further considerations on thickness are explained in the following point.

At last, the jet power of the engine can be calculated with equation 4.2. This value is important to estimate because it gives the order of magnitude of the engine's power.

$$P_{jet} = \frac{1}{2}\dot{m} I_{sp}^2 \tag{4.2}$$

Engine sizing results can be consulted in table 4.8.

Heat transfer and chamber cooling

The heat transfer estimation and simulation was a crucial part of the project because the concept being studied depends on it. It is important to highlight that this was an iterative process with several revisions. There are three major heat transfer processes in regenerative cooling arrangements: convection from the chamber to the inner wall, conduction through the wall and convection to the cooling fluid. Radiation is, usually, neglected in this case. Figure 4.8 shows a typical temperature profile.

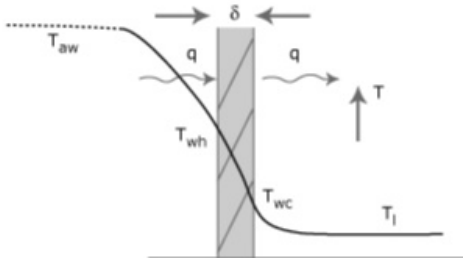

Figure 4.8: Heat transfer profile.

The throat area is the critical region of the engine due to its high heat flux. In this case, the convergent and divergent part are also small in size, which means that they are an important region to cool.

The general equation for the heat rate by convection is given by

$$\dot{Q} = h_g(T_{aw} - T_{wh})A \tag{4.3}$$

Where the h_g is the convection coefficient, T_{aw} is equivalent to T_c, the temperature of the chamber, T_{wh} is the temperature at the inner wall and A is the area. The general equation heat rate by conduction is

$$\dot{Q} = \kappa A \frac{T_{wh} - T_{wc}}{\delta} \tag{4.4}$$

Where κ is the thermal conductivity of the material and δ is the wall thickness. To facilitate the calculation of the heat transfer the chamber was divided into three main regions, as figure 4.9 illustrates: combustion chamber - 1, convergent section - 2, and divergent section - 3.

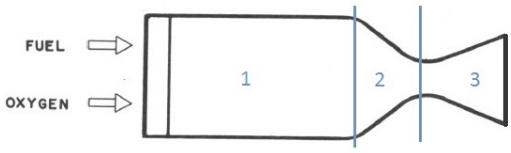

Figure 4.9: Chamber division for the heat transfer study.

An important point in the cooling process is the coolant's ability to absorb the heat from the chamber. It depends on its heat of vaporization, specific heat and mass flow rate. For the desirable vaporizing rate

it is possible to estimate the rate of heat absorption. These estimations indicate whether the considered fuels have the capacity to absorb a reasonable amount of heat. For the three fuels considered, and the desired mass flow rate, the heat transfer were estimated and can be seen in table 4.6.

Table 4.6: Fuel's cooling capacities.

	Ammonia	Ethanol	Propane
$\dot{Q}$ (W)	5485.98	3444.28	1490.92

Convection at exhaust side Regarding the convection in the chamber, the coefficient was computed using the simplified Bartz Equation from reference [48]

$$h_g = \frac{0.026}{D_t^{0.2}} \left(\frac{P_c}{c^*}\right)^{0.8} \left(\frac{D_t}{D}\right)^{1.8} c_p \mu_e^{0.2} \left(\frac{T_c}{< T >}\right)^{0.8-0.2w} \tag{4.5}$$

where the coefficient w is approximately 0.6, $< T >$ is the average between wall and throat temperature, D is the diameter of the considered area, D_t is the throat diameter, c_p is the specific heat, μ is the viscosity of the mixture and P_c is the pressure in the chamber. As equation 4.5 shows, h_g depends on the local diameter. In order to estimate a more accurate value of this coefficient it is calculated for each considered section. To conclude this process it is necessary to know the inner wall temperature and the combustion temperature. As the latter is obtained with the CEA software, the adopted strategy was to define the former temperature as the service temperature of the material and see if the coolant has the capability of absorbing the required amount of energy.

Conduction in the wall Assuming steady-state, the heat rates from different transfer processes are similar in each section, as equation 4.6 translates.

$$\dot{Q}_{conv.gas} = \dot{Q}_{cond.wall} = \dot{Q}_{conv.coolant} \tag{4.6}$$

The heat rate for the conduction in the chamber wall is estimated by equations 4.7, provided by reference [49].

$$\dot{Q} = 2\pi\kappa\Delta T \int \frac{1}{\ln\left(\frac{r_{ext}(X)}{r_{int}(X)}\right)} dX \tag{4.7}$$

where r_{ext} and r_{int} are the functions of the external and internal radii, respectively. In the case of the cylinder, these radii are constant. In the case of the conical nozzles, the radii are linear functions easily defined by two known radii values. Therefore, we have:

$$r_{ext_1}(X) = -1.259X + 0.0189 \tag{4.8}$$

$$r_{ext_2}(X) = 8.0357X - 0.01205 \tag{4.9}$$

$$r_{int}(X) = r_{ext}(X) + \delta(X) \tag{4.10}$$

From equation 4.6, the heat rate on the wall is known. The term $\delta(X)$ is constant for the divergent part and linear for the convergent one. For the equations that define the radii, the position X depends on the referential used, which is aligned with the center of the chamber cylinder and the origin is placed at the beginning at each section (figure 4.10).

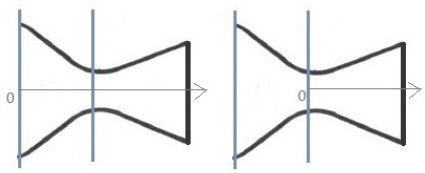

Figure 4.10: Referencial for each section.

Convection at vaporizer The combustion chamber will be assembled inside an already manufactured part 4.11, which will perform as a vaporizer, where it is intended that the fuel boils. This must be analysed in detail due to the different regimes of boiling.

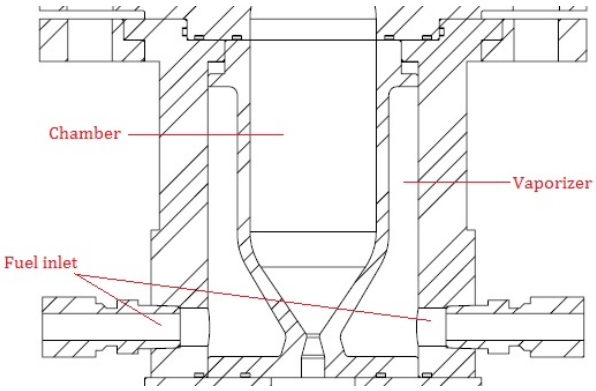

Figure 4.11: 2D with chamber inside the vaporizer.

As it was mentioned before, usually, in regenerative cooling, the cooling flow is calculated to ensure that the liquid does not pass to the gaseous state. Boiling can easily enter the regime of film boiling, which dramatically decreases heat transfer. However, since gaseous injection is intended, in this case the evaporation of the fuel is an objective. Figure 4.12, from reference [49], shows a typical boiling curve for water. Water is not the coolant used, but the curve is similar for other fluids, as well.

Operation is desired in the nucleate boiling regime. This regime is stable and provides reasonably high heat flux values. When the coolant's temperature increases and diverges from its saturation temperature, it slightly enters the film boiling, passing through a transition boiling regime, where bubble formation is rapid enough to form a vapour film. This is an unstable regime, which oscillates between nucleate and film boiling. The film boiling region occurs after the Leidenfrost point [50], where heat flux is minimum - point D. Therefore in our study it is important to calculate maximum and minimum heat fluxes

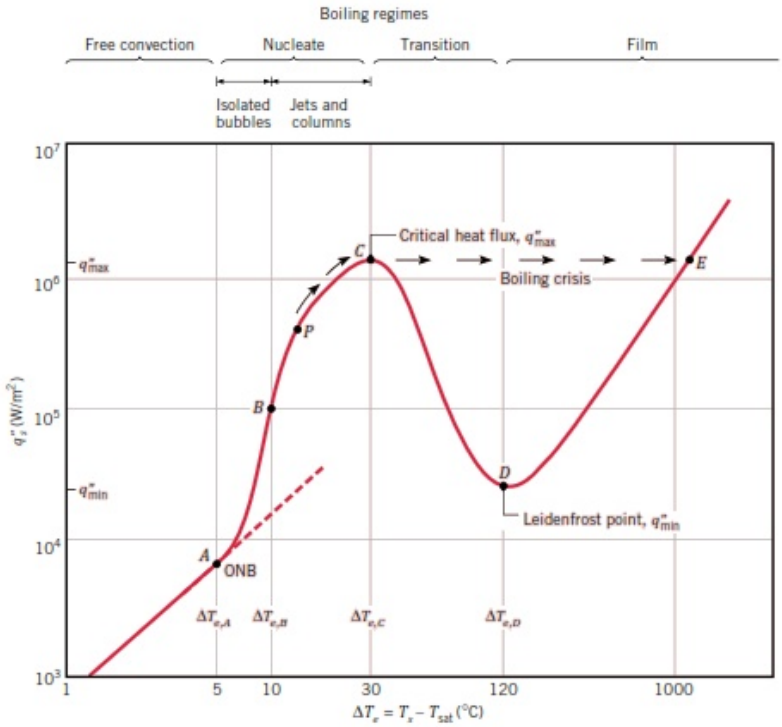

Figure 4.12: Typical boiling curve for water at 1atm. [49]

for the given fuels; estimate the Leidenfrost temperature; predict the heat flux with evaporation; ensure that the working region is in nucleate boiling. For nucleate boiling, the following equation describes the heat flux

$$q'' = \mu_l h_{fg} \rho_g \left(\frac{g\left(\rho_l - \rho_g\right)}{\sigma} \right)^{\frac{1}{2}} \left(\frac{c_{p_l} \Delta T_e}{C_{sf} h_{fg} Pr^n} \right)^3 \tag{4.11}$$

It is called the Rohsenow equation. In this equation there are two parameters that should be determined experimentally: C_sf and n. The assumed values for this two parameters were defined as 0.013 and 1.7, respectively, due to the similarities of molecular polarity [49] between ammonia and water molecules. Rohsenow equation allows the calculation of the heat flux during nucleate boiling. For this regime, the maximum heat flux is given by equation 4.12.

$$q''_{max} = 0.131 h_{fg} \rho_g \left(\frac{\sigma g\left(\rho_l - \rho_g\right)}{\rho_g} \right)^{\frac{1}{4}} \tag{4.12}$$

The value 0.131 is defined as a constant used for cylinders [49]. Once this point is achieved, and if the temperature continues to increase, the heat flux decays consistently, entering the transition regime, until it reaches is minimum, estimated by equation 4.13.

$$q''_{min} = 0.09 h_{fg} \rho_g \left(\frac{\sigma g\left(\rho_l - \rho_g\right)}{\left(\rho_g + \rho_g\right)^2} \right)^{\frac{1}{4}} \tag{4.13}$$

Where 0.09 was determined experimentally [49].

When entering the film boiling regime the behaviour of the fluid changes. This regime occurs when

the temperature difference - surface and liquid - exceeds the Leindenfrost point, which is given by equation 4.14, found in reference [50].

$$T_{LDF} = T_l + \frac{0.844T_{cri}\left(1 - exp\left(-0.016\left[\frac{\left(\frac{\rho_s}{M_s}\right)^{1.330}}{\sigma_l}\right]^{0.5}\right)\right) - T_l}{exp\left(3.066 \times 10^6\beta\right) erfc\left(1758\sqrt{\beta}\right)} \tag{4.14}$$

where β [50] is

$$\beta = \frac{1}{\kappa_s \rho_s c_{p_s}} \tag{4.15}$$

As expected, the Leidenfrost point depends not only on the fluid properties but also on the surface properties. The heat flux equation [49] for this type of boiling is more complicated to calculate than for nucleate boiling. It is important to introduce the Nusselt number - Nu, which is the ratio between the heat that is transferred by convection and by conduction. It relates with convection coefficient through equation 4.16 [51].

$$Nu = \frac{h_c L}{\kappa} \tag{4.16}$$

Literature shows that there is an analogy between film boiling and laminar film condensation, so their equations are similar [49]. For vertical surfaces the prediction through this equality isn't the most adequate, although it was decided to use it due to the lack of consistent information for this case, because satisfactory predictions were obtained [49]. In this case, the average Nusselt number - $\overline{Nu}$ - is used

$$\overline{Nu} = \frac{\overline{h}_{conv} D}{\kappa_g} = 0.62\left[\frac{g\left(\rho_l - \rho_g\right) h'_{fg} D^3}{V_g \kappa_g \left(T_s - T_{sat}\right)}\right]^{\frac{1}{4}} \tag{4.17}$$

where h $'_{fg}$ is given by

$$h'_{fg} = h_{fg} + 0.80 c_{p,g}\left(T_s - T_{sat}\right) \tag{4.18}$$

When the temperature is above 300° C, radiation starts to play an important role. This happens because the radiation across the vapour film increases up to a point where it should not be neglected. Radiation will also lead to the increase of the film thickness. The total coefficient is given by 4.19 if the coefficient from radiation is less than the coefficient from convection.

$$\overline{h}^{4/3} = \overline{h}_{conv} + \frac{3}{4}\overline{h}_{rad} \tag{4.19}$$

Where

$$\overline{h}_{rad} = \frac{\varepsilon \sigma_{Boltz}\left(T_s^4 - T_{sat}^4\right)}{T_s - T_{sat}} \tag{4.20}$$

Most of the surface parameters needed to estimate the Leidenrost point - density, surface tension and molecular weight - were found on SolidWorks material database.

Simulations and Results From the equations above heat transfer was calculated and its results are shown in table 4.7.

Table 4.7: Results of analytical thermal analysis.

			Ammonia	Ethanol	Propane
		$\dot{Q}$ (W)	5484.98	3444.28	1490.92
		T_1 (K)		1143	
Convection	1	T_0 (K)	3109.01	3337.26	3476.2
		h_g	401.58	557.221	576.79
		$\dot{Q}$ (kW)	4.72	6.55	6.78
	2	T_0 (K)	2952.28	3196.43	3324.07
		h_g (W/(m^2 · K))	1169.3	1622.5	1679.48
		$\dot{Q}$ (kW)	2217.19	3076.51	3184.58
	3	T_0 (K)	2369.86	2717.23	2808.24
		h_g (W/(m^2 · K))	8389.83	11641.49	12050.41
		$\dot{Q}$ (kW)	2166.87	3006.69	3112.303
		$\dot{Q}_{convection}$=$\dot{Q}_{conduction}$			
Conduction	1	T_2 (K)	723	666	659
	2/3	T_2 (K)	500	333	326
Convection		q"$_{max}$ (MW/m^2)	2.353	0.995	0.077
		T_{LDF} (K)	331.2	453.9	315.8
		q" (MW/m^2)	21200	0.276	961

Table 4.7 shows that ammonia has greater cooling capability when compared to the other fuels, as it is possible to see by its value of $\dot{Q}$. Also, it is less probable that it enters in the film boiling region, because the value on q''_{max} is higher than for the other two fuels. The Leidenfrost is not expected to be achieved during the test with either one of the considered fuels. The values presented are the worst case scenario, as it was a conservative approach. It is expected that the heat transfer values and correspondent temperature remain below these.

To conclude a FEM thermal analysis was performed using the CAD software SolidWorks. Several simulations were done in order to understand the transient conditions of the system and its behaviour when exposed to the different heat flux coefficients. The inner temperature was defined accordingly to those obtained in CEA and three convection coefficients were added in section 1, 2 and 3, defined in figure 4.9. In the wall, the conduction depends on the material. For the outer wall different coefficients were used:

- h_g for nucleate boiling for three different temperatures (beginning and middle)
- h_g correspondent to maximum heat flux
- h_g correspondent to minimum heat flux

Although the coefficient was not calculated in previous steps, through equation 4.21 it can be estimated. Simulations were also important to fixate the wall thickness. Section 1 has a constant thickness of 3mm. For the convergent part the thickness is variable. As the diameters are small, it was decided to have a thicker wall in the throat, so that the extra material ensures mechanical resistance and protection against throat abrasion. The thickness varies linearly from 3mm to 5mm in throat, and remains 5mm in the divergent part.

$$q'' = h_g \Delta T \Leftrightarrow h_g = \frac{q''}{\Delta T} \tag{4.21}$$

In figure 4.13 there are two images with results from the thermal simulations with the maximum and minimum heat flux. It is possible to see that in both simulations, as it was expected, the critical area is the throat. In both cases the wall temperature passes the material melting point and for the maximum heat transfer coefficient, the maximum temperature is 1972K. Although it is a high value, it corresponds to the adiabatic flame temperature, which means that the real value will be significantly lower, and so will be the wall temperature. The rest of the chamber is exposed to reasonable temperatures. In the simulation represented in figure 4.13 b, using the minimum heat transfer coefficient - in the film boiling region - the simulation shows that the temperature reached does not allow adequate cooling. The throat wall temperature is higher than 2500K and the chamber's wall is around 1400K. This proves that film boiling should be avoided so that the engine can perform for the stipulated time without material damage.

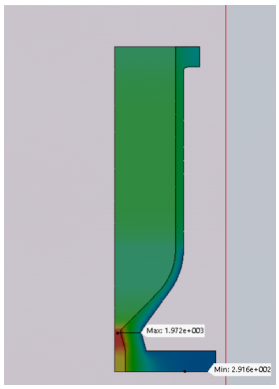

(a) Simulation with maximum heat transfer.

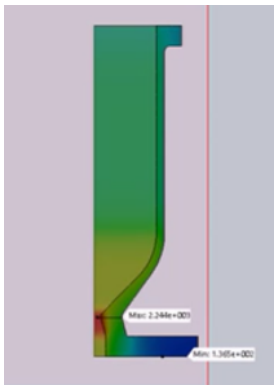

(b) Simulation with minimum heat transfer.

Figure 4.13: Thermal simulation.

The simulations indicate that the system takes approximately 10 seconds to achieve equilibrium. This is important to fix the test time. It was set to 20 seconds.

Igniter

One of the desired features of the design was a reusable ignition to avoid reinstalling a new component or consumable after each test. Although it was considered to make an igniter, the idea of using a standard plug was appealing. It is an inexpensive component and easy to adapt to fit in the test stand. Both spark and glow plugs were considered. A spark plug has the timing problem, which may cause a

hard start if there is a reasonable amount of mixture when the spark is created or, on the contrary, the spark may occur when there isn't enough propellant to burn. Additionally, a spark plug requires a high voltage source, which makes the glow plug a safer solution. Therefore, it was concluded that the glow plug is a plausible option for the system. There are two types of glow plugs: metal and ceramic. The ceramic plugs withstand higher temperatures, however they are more expensive. The chosen glow plug can be seen in figure 4.14.

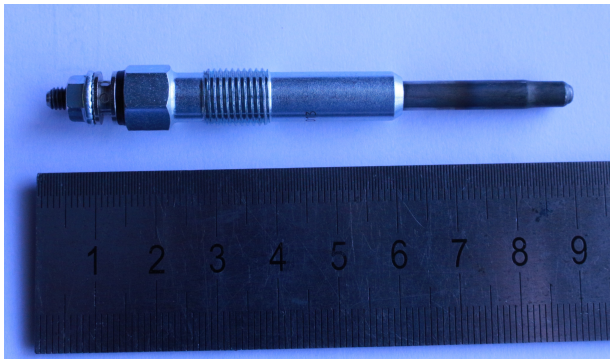

Figure 4.14: Glow plug used.

This glow plug is suitable to include in the designed head of injection using a standard bored compression fitting (figure 5.3).

Injector

Flame instabilities have been the cause of multiple accidents with rocket engines, as for example the failure of F-1 and Titan-II engines [52]. Also, they can cause performance degradation as the exhaust plume will be unsteady. To stabilize the flame it is necessary to create a recirculation bubble. This can be achieved by using a bluff body or having a swirl flow. It was decided that two types of injectors would be manufactured: a simpler one, similar to the one reviewed in chapter 2.2, and one with a swirl. The idea of having two injectors is to see if there are measurable differences between them. As the reactants are injected in gaseous phase, and there is little information available for this kind of injection in these engines, it is important to test different approaches. The simplest injector is based on a pintle injector, presented in the state of art, section 2.2. The same injector is used for fuel - the inner tube - and oxidizer - the outer tube. The holes from where the fuel flows are radial, which creates a similar effect to the bluff body. The oxygen flows through the outer tube, which is close to the inner tube. In order to be able to manufacture it in Omnidea's instalations, it was decided that the holes should be as simple as possible. The initial idea was to drill the injection holes with a 30° angle, providing a tangent velocity to the flow. This idea was abandoned during the manufacture process. Therefore, the injector has four equally spaced holes without inclination.

The swirl injector creates a flow with a tangent velocity. High swirl flows are also able to produce a recirculation bubble when the swirl number - S - is higher than 0.6. The swirl number is a ratio between axial and radial velocity. When it is fixed, it is possible to estimate the blade inclination through equation

4.22 [53].

$$S = \vartheta \frac{r}{2B} \left(1 - \left(\frac{r_h}{r}\right)^2\right) \tag{4.22}$$

Where

$$\vartheta = \frac{\omega_1}{\nu_1} \tag{4.23}$$

When the radii difference isn't significant, as in this case, the swirl equation can be replaced for 4.24.

$$S = \frac{2}{3} \tan \phi \tag{4.24}$$

To have a swirl number higher than 0.6 it is necessary that ϕ is higher than 42° . It is set as 60° .

When designing injectors it is important to compute the diameter of holes for the desired pressure drop. In this case the design was made so that the chamber operates at 15bar and the upstream pressure is kept at 20bar. Using the flow equation 2.7, in chapter 2 for subsonic flow it is possible to predict the desired values for the diameters. In the mentioned equation, P_c is the chamber pressure and P is the tank pressure.

Fixing C_d as unity, for the fuel the minimum value for the hole diameter is approximately 0.5mm. For the oxygen the area that should be taken into consideration is the lateral area from the truncated cone, given by equation 4.25. For this case the minimum distance between the outer wall and injector is 1mm. These values are crucial to determine the hole's diameter and the tube length.

$$A = \pi \left(R + r\right) s \tag{4.25}$$

Both the simple and swirl injectors can be seen in figure 4.15.

(a) Simple injector. The picture shows 8 holes, but only 4 were properly drilled.

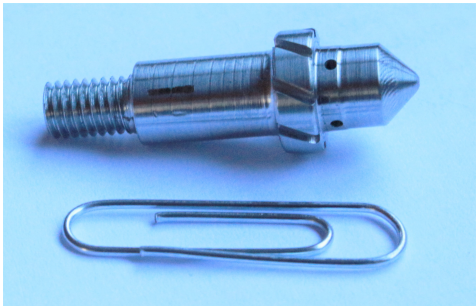

(b) Swirl injector.

Figure 4.15: Injectors used during the test campaign.

Injector tips are exposed to very high temperatures. The initial ideia, in order to avoid material decomposition, was to use nickel superalloy. As it was mentioned before, nickel super alloy is expensive and difficult to work. Therefore it was decided to produce it at Omnidea. A simple injector was made from stainless steel to test the material resistance. Figure 4.16 shows the injector after two burn tests. Although there are some darker deposits, there is no evidence of material decomposition or abrasion.

Figure 4.16: Injector after two burn tests.

When assembling the injector without swirl it was detected that it was slightly bent. This causes an asymmetric flame and can originate material damage. The swirl injector was design differently in order to mitigate this issue.

Conclusions: Final design

The final characteristics of the engine can be found in table 4.8.

Table 4.8: Engine and propellant properties.

	Item	Unit	Value
ENGINE	OF		1.4
	Total mass flow	kg/s	0,00999
	I_{sp}	m/s	2501,6
	Power	kW	31.3
	Chamber diameter	mm	30
	Throat diameter	mm	3
	Area ratio		3.2
	Chamber pressure	bar	15
	Chamber material		Stainless Steel 304
	Burn time	s	
OXIDIZER	Oxygen		
	Pressure	bar	40
	Temperature	K	293
FUEL	Ammonia		20
	Pressure	bar	40
	Temperature	K	∼300

The final design of the engine can be seen in the figure 4.17, that shows a cross section of the engine assembly. As it was already pointed out, reusing parts of a previous experiment was paramount, in order to reduce costs and schedule delays. In figure 4.17 all the already existent parts are marked.

The injection head's design was designed at Omnidea, and its review was part of the work developed in this master thesis. This particular part was designed to include the injection parts, the ignition and the instrumentation needed in the chamber - thermocouple and pressure port. Figure 4.18 shows the design of the injection head in detail.

In the center there is the injection hole, and the four wholes in the periphery will accommodate instrumentation and the igniter. Photos of the manufactured part can be seen on the subsection 5.1.

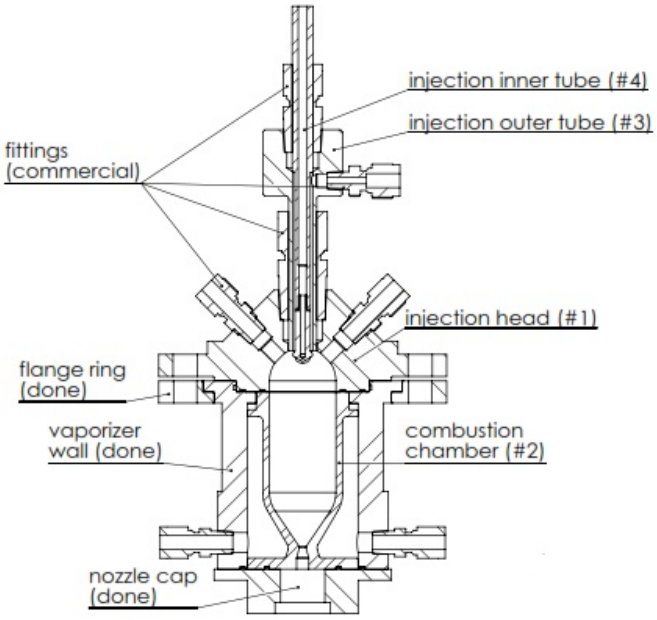

Figure 4.17: 2D engine assembly.

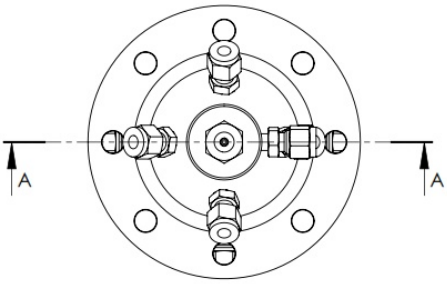

(a) Top view.

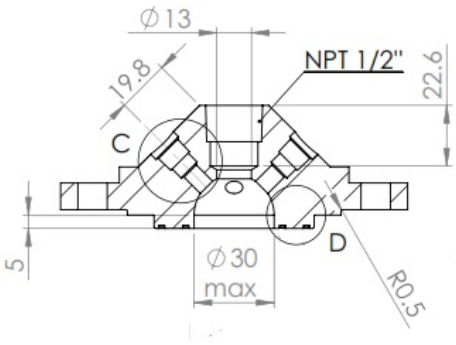

(b) A-A cut view.

Figure 4.18: Injection head 2D.

Chapter 5

Tests

The information regarding the tests is explained in this chapter.

5.1 Test Stand

Although the design of the test stand was not included in this work, part of its construction, choice of instrumentation and supervision were actually done during this master thesis. The stand in use can be seen in figure 5.1.

Figure 5.1: Test stand assembly in the test facilities.

The layout in test, as it was mentioned before, is layout number 5 from figure 4.4. The final schematic accordingly to the layout configuration is in figure 5.2, in the next page.

The dotted line represents the self-pressurization line. In the schematic it is possible to see the location of the valves, filter and instrumentation.

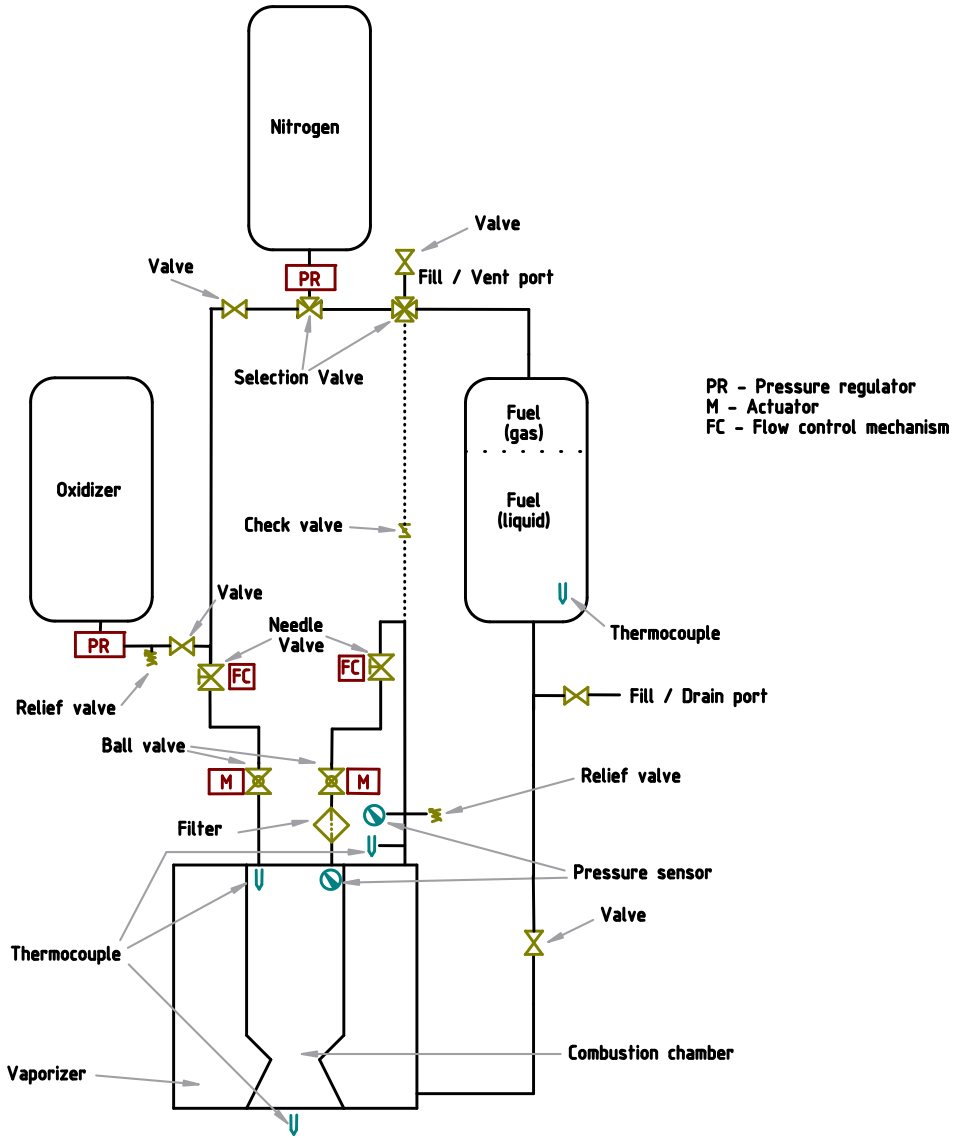

Figure 5.2: Schematic of the test stand.

Material

The materials in the test stand have to withstand the test campaign, which means that their durability and resistance is important. For the piping it was used a stainless steel tube of 1/4" diameter, with the thinnest wall available. The internal diameter is about 4mm.

The vaporizer and the nozzle cap (figure 4.17) are also made of stainless steel. The flange ring is made of carbon steel.

Instrumentation

The main parameters were measured: pressure, temperature and thrust. Those were the most important parameters that must be monitored during tests, to check if the engine is operating according to expectations. Therefore, four thermocouples were installed in the chamber, vaporizer line, fuel tank and at the exhaust plume. Two pressure sensors measure the pressure in the vaporizer line and in the chamber. The instrumentation of the chamber is installed in the injection head and can be seen on figure 5.3. A load cell measures the thrust. This load cell is installed under the test stand and has a correction factor due to its position. It withstands the stand's weight and the thrust value must be multiplied by 0.85. This correction has to do with the cell's position in the test stand, which can be seen in figure 5.4.

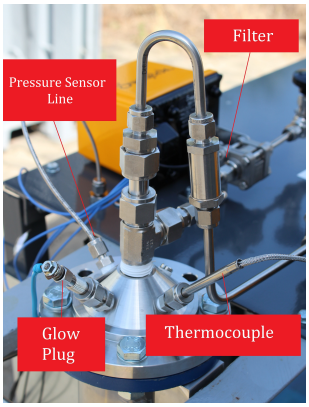

Figure 5.3: Injection head with chamber's instrumentation.

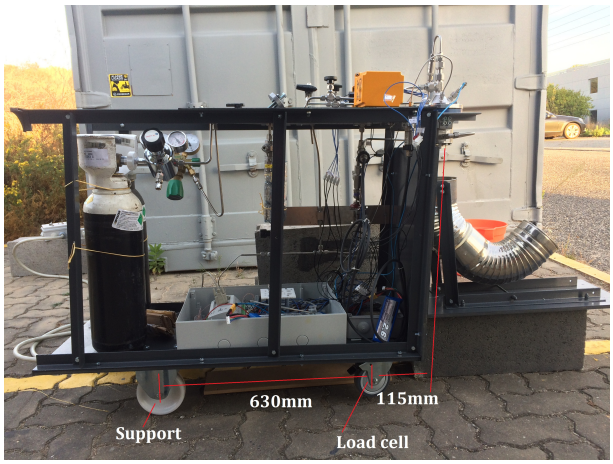

Figure 5.4: Position of the load cell.

These sensors are linked to a data logger, which is able to record signals coming from 8 different channels and has a maximum recording capacity of 1000 samples per second. For the test campaign, samples were record every 20ms. It has a HMI [1] that allows the remote monitorization of the parameters during the test.

Finally, two video cameras were installed.

[1] Human-to-machine interface

The instrumentation used and its specifications can be seen below in table 5.1.

Table 5.1: Instrumentation specifications.

Instrument	Brand	Model	Range	Error
Pressure sensor	Swagelok	PTI-S-AG400-12AQ	0 - 100 bar	$<$0.5% LPC
Thermocouple K	Omega	TC-K-NPT-U-72	TO 650 ^{o}C	0.75%
Thermocouple K	F Louro	-	-	-
Load Cell	Burster	8532	0 - 500 N	$<$1%

To evaluate of the vaporizer, the instrumentation was placed at its exit. This means that there should not be a significant difference in pressure, which probably does not happen with the temperature. This should be taken into account when analysing the results.

Flow Control

To provide the proper OF in the chamber two flow control needle valves were installed in both the oxygen and the fuel lines. As flow meters were not available, this is an economic approach that has some limitations, but is adequate for the research carried out. Also, it allows to set the desired drop of pressure. The needle valves in use are from Swagelok [54]. This type of valves allow throttling in order to have the desired mass flow rate. They have a linear relation between the flow coefficient C_v and the number of turns of the stem. This correlation is different for liquid and gases and, for the latter case, for high and low pressure drops - subsonic or sonic throat.

The valve were installed upstream of the combustion chamber, therefore the reactants pass through them in the gaseous state. The flow rate was mainly controlled by the needle valves. Experience shows that with bottles regulated to 25bar it is possible to achieve 15 bar in the chamber. Therefore, for low pressure drop the mass flow is given by equation 5.1, setting the constant N_2 as 6950 [54].

$$\dot{m} = N_2 C_v P_1 \left(1 - \frac{2\Delta P}{3P_1}\right) \sqrt{\frac{\Delta P}{\rho_1 G_g T_1}} \tag{5.1}$$

The equation above can be manipulated to obtain the value of the coefficient - C_v. Figure 5.5 shows the relation between this coefficient and the number of turns, so one can estimate the number of turns to achieve a certain flow coefficient.

To facilitate the set up of the needle valves the number of turns was converted to the height of the valve. Table 5.2 shows the needle valve adjustment requirements for each combination.

To make it possible to operate the system from a safely, downstream of the needle valves there are two ball valves controlled by an actuator. Figure 5.6 shows the valves and the actuators on the test stand.

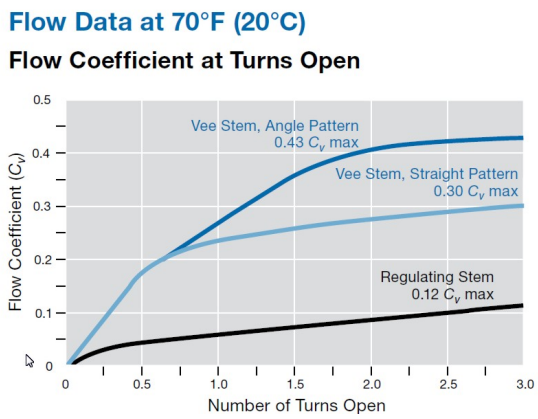

Figure 5.5: Flow coefficient as function of the number of turns.

Table 5.2: Flow control valve settings.

		Simple Injector (*Oxygen injector area is 0.788mm²*)		Swirl Injector (*Oxygen injector area is 9.67mm²*)	
		Ethanol	Ammonia	Ethanol	Ammonia
Mass flow [kg/s]	Fuel	0.003	0.0042	0.003	0.0042
	Oxidizer	0.007	0.0058	0.007	0.0058
Fuel's injector area [mm²]		1		3.14	
Flow coefficient	Fuel	0.013	0.003	0.011	0.0025
	Oxidizer	0.02	0.017	0.017	0.014
Number of turns	Fuel	0.26	0.06	0.22	0.05
	Oxidizer	0.4	0.34	0.34	0.28
Heigh [mm]	Fuel	2.7	2.6	2.68	2.54
	Oxidizer	2.8	2.8	2.77	2.72

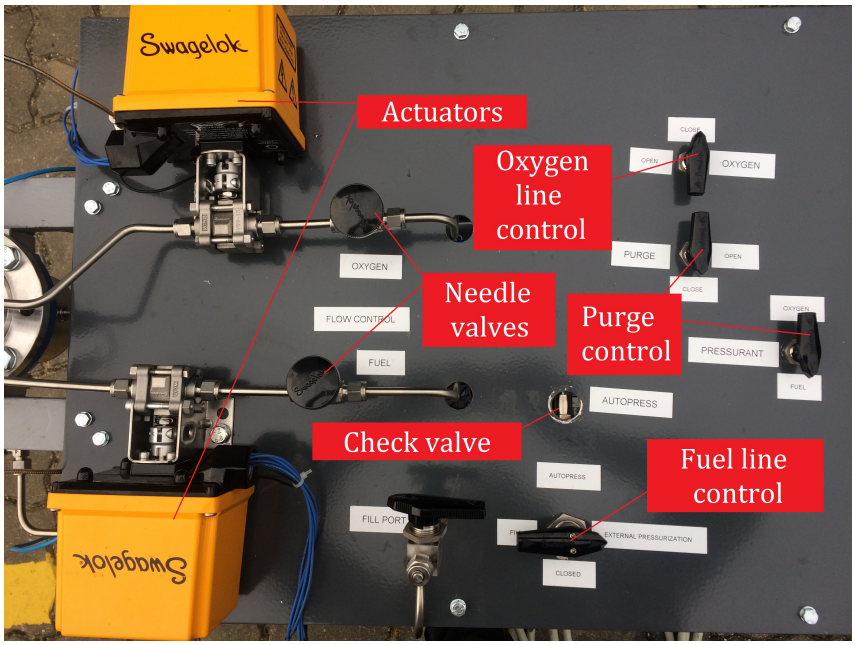

Figure 5.6: Valves and actuators on the test stand.

These valves allow changing the test's operation mode. The pressurized nitrogen can flow through the oxygen or fuel lines. In the first case, it acts as a purge to clean the line. In the second case, it can

also be used to pressurize the fuel. In the fuel line, the selector valve must be changed accordingly to the desired action: fill the tank, close the line, set the test for autopressurization or external pressurization. In the fuel line there by a check valve, that was relevant for the self-pressurized operation.

Safety Procedures

Besides the safety concerns that are exposed in section 5.2, the test stand integrates two relief valves that will open in case the pressure exceeds 60bar.

To allow the operators to keep a safe distance from the test stand, it is operated remotely using the control in figure 5.7. The cable is 5 meters long, which allows the operators to be in a safe place, protected by a wall.

Figure 5.7: Control box.

The control box allows to open and choose the main valves of the stand and to turn on the ignition. Timings and sequences are explained in the following section.

Reactants

As shown in figure 5.8, the reactant's bottles are permanently stored in the back of the test stand. The oxygen bottle contains about 1kg of oxygen gas.

(a) Nitrogen bottle - left. Oxygen bottle - right.

(b) Fuel bottle.

Figure 5.8: Bottles from the reactants.

To fill the fuel tank there are two possible lines - figure 5.9. In the case of ethanol, it is relatively easy to fill the tank. The port used to fill the tank is the drain/fill port. It is necessary to vent the fuel's line, which is achieved with the fill/vent port. For the tests where ammonia is used as fuel, it is necessary to be aware of the safety concerns regarding ammonia handling. It is also desirable to cool down ammonia's tank to ease the process. The ports to fill the fuel's tank are the inverse of the ones used for ethanol.

(a) Fill/vent port to fuel tank.

(b) Drain/fill port to fuel tank.

Figure 5.9: Fill ports in the test stand.

If there is remaining fuel in the tank it can be drained through the fill/drain port.

5.2 Test Plan

Objectives

This small liquid engine was built in order to prove the concept of self-pressurization. On this test sequence the ultimate goal is to assess the concept's feasibility. To achieve that it is necessary to ensure first the engine's required performance. Some intermediate goals are also defined:

- Successful, and stable burn;
- Repeatable, reliable and prompt ignition.

Test strategy

Assumptions

- The system is similar to the theoretical one - chapter 3 - when operating under self pressurization;
- Only valid tests are considered;
- Environment disturbances in the variables are not significant - for example, propellant's temperature fluctuation.

Principles

- Tests focus mainly on the evolution of the parameters during the burn;
- Test cycles begin after cold/static tests are performed;
- Validation criteria is similar in each cycle.

Cold/Static tests There are several tests that must be conducted before the burn tests.

- Glow plug timing, temperature and input requirements – it is important to know the time required for the glow plug to reach a desirable temperature and the type of energy source available;
- Pressure drop through the system to be included in the mathematical model;
- Leak testing – search for leaks;
- Injection test - injection flow test;
- Cold test - operation test without ignition.

Execution Strategy

To facilitate the data treatment, each test type has a specific code and is enumerated accordingly to its chronological order.

Test	Glow plug timer	Pressure drop	Leak testing	Injection testing	Cold testing	Burn
Code	GP	PD	L	I	C	B

Test order Since ethanol is easier and safer to handle, and despite what was concluded in the theoretical approach, the first tests were done with it. This allowed us to familiarize with the test procedures and became aware of stability problems. Before conducting the study of autopressurization it is important to perform some experiments in order to obtain data about engine's response.

In table 5.3 the reader can see the planned combinations. It is important to highlight that, in the last row, the autopressurization with ethanol is dependable on the data obtained in previous tests, due to the poor pressurization capability of ethanol - explained in section 4.2.

Table 5.3: Reactants combinations to test.

Order	Pressurization	Fuel	Oxydizer	Repetitions
1	Nitrogen	Ethanol	Gaseous oxygen	3
2	Nitrogen	Ammonia	Gaseous oxygen	3
3	Auto	Ammonia	Gaseous oxygen	3
4	Auto	Ethanol	Gaseous oxygen	3

Further information regarding the tests (safety concerns, risks, etc.) can be consulted in appendix C.

5.3 Results

5.3.1 Ethanol - External Pressurization

Ethanol was used in the first tests in order to understand the engine's behaviour, its stability and validate test stand operations with a fuel easier to handle. The test with external pressurization corresponds to the case where the nitrogen is responsible to pressurize the fuel tank, which means that the fuel line represented by the dotted line in figure 5.2 is not used.

Three different tests are presented below:

- Test 1 - The combustion chamber used in this test is an old chamber from a previous test stand. The injector is the simple one, inspired by the pintle.
- Test 2 - In this test the combustion chamber used was the designed for this project and the injector is the swirl injector. The fuel flow control valve was adjusted for gas flow.
- Test 3 - The difference between this test and the previous one is the fuel flow control valve. In this case it was adjusted for liquid flow.

Test 1 Due to delays in the chamber manufacturing the first test was conducted with a chamber from previous hybrid rocket prototype. This chamber was not designed to allow good heat transfer. It was oversized due to safety concerns. The throat was located close to the fluid outlet, thus not taking advantage of the cooling effect from the fuel flow.

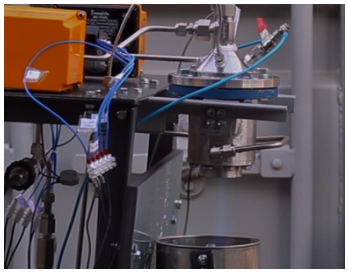

(a) Plume during test.

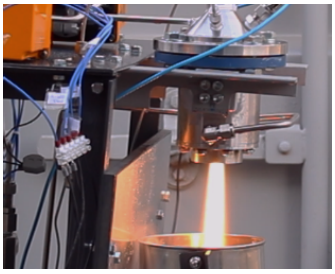

(b) Chamber burned out.

Figure 5.10: Image record of the first burn test.

This initial experiment confirmed the importance of efficient heat transfer in rocket engines. The chamber used had the throat close to the injection head, and the coolant fluid reaches this region at high temperature. This fact caused the throat's burning (figure 5.11). After this test it was decided to limit the operation time when using ethanol.

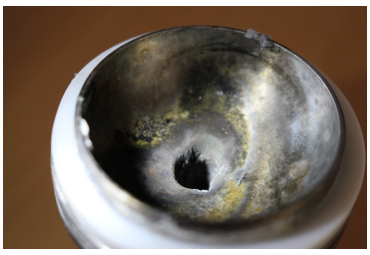

Figure 5.11: Chamber damage.

The data collected during the test is shown in figure 5.12.

In figure 5.12b it is possible to see that the pressure is stable through most of the burn. There are very small oscillations in the

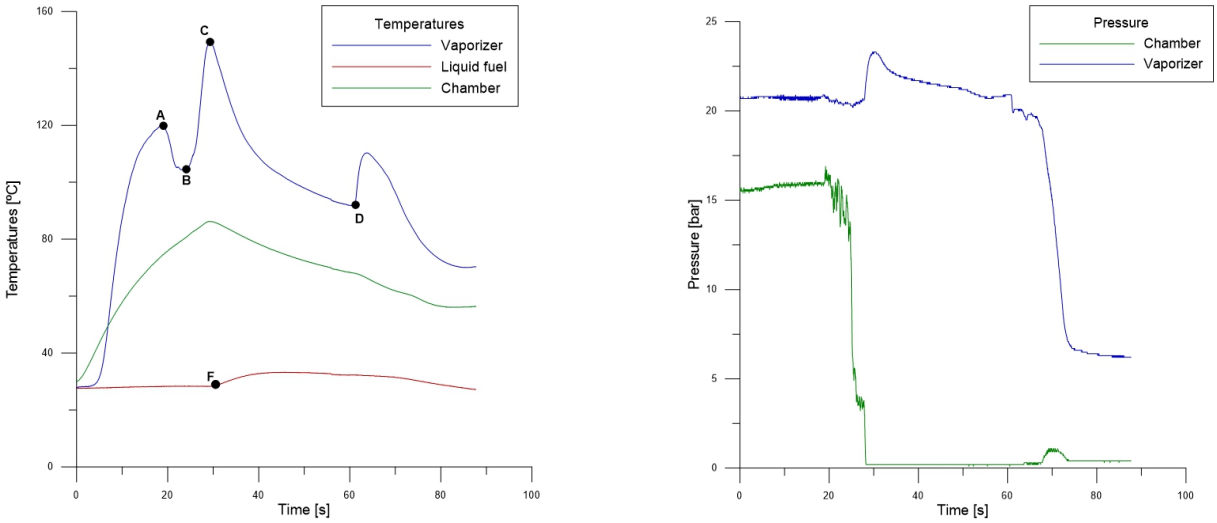

(a) Temperature evolution during the test.

(b) Pressure evolution during the test.

Figure 5.12: Properties evolution during test.

chamber's pressure except in the end of the hot fire, due to the burning. In figure 5.12a several important points are marked. The first thing to notice is that the temperature obtained at the exit of the vaporizer is higher than in the chamber. This is due to the location of the thermocouple inside the chamber. Probably, due to its positioning in the injection head, it does not read accurately the temperature inside the chamber. From the liquid fuel temperature it is possible to see that there is one single change, which corresponds to point F, when ethanol ended and nitrogen - the pressurization gas - started to enter the fuel's tank. Nitrogen's temperature is above ethanol's, which explains the increase of temperature. When analysing the vaporizer temperature there are three peaks in the curve, similar to what happens in figure 4.12. The first peak, in point A, is explained by the transition in the boiling regime. Ethanol's phase diagram shows that, when pressurized, ethanol needs a significant temperature to boil. At point A, the heat flux is probably maximum, and there is the transition to film boiling, causing the suddenly decrease of temperature until point B. During film boiling, the wall overheats significantly, causing the fuel to heat up again until point C, which happens slightly after point F when the engine ran out of fuel and the temperature in the vaporizer starts to decrease. In point D there is another temperature increase. It happened during the purge of the lines and is explained due to the position of the vaporizer's thermocouple. In fact, it is placed at the exit of the vaporizer, which means that when the purge takes place, the hot ethanol inside the vaporizer passes through the thermocouple causing this peak.

Test 2 The second test already included the chamber designed for this project and the swirl injector. During the test, the exhaust plume was unstable. Figure 5.13 shows that this irregularity is not observed in the chamber's pressure, which was almost constant during the burn. However, when analysing the temperature's chart, it is notorious that the temperature of the vaporizer was not high enough to boil the ethanol. At the registered pressure, ethanol's temperature should be above 100° in order to boil, which did not happen. When analysing the pressure plot one can see that the difference between the pressures in the chamber and in the vaporizer is constant during the burn, which means that there was

no change in ethanol's state.

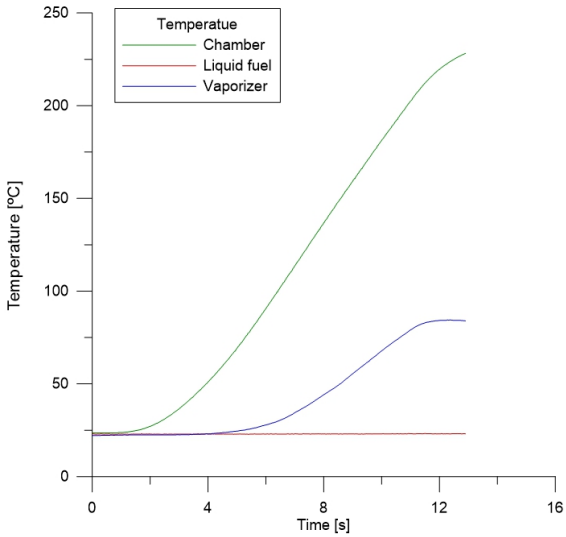

(a) Temperature evolution during the test.

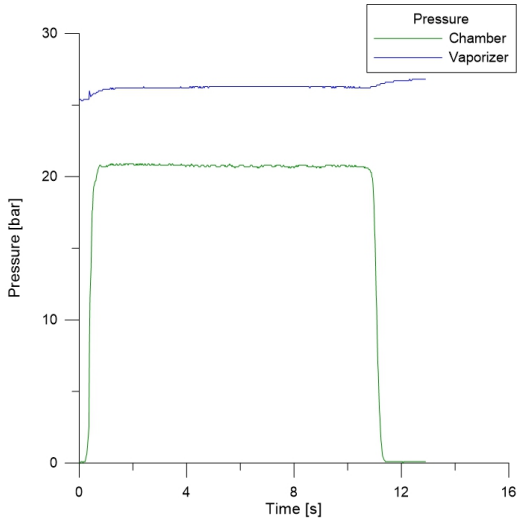

(b) Pressure evolution during the test.

Figure 5.13: Properties evolution during test.

With ethanol entering the chamber in the liquid phase, the flow control valve was not properly set for this eventuality, and there was an excess of fuel inside the chamber causing the aforementioned instability. In addition, the swirl injector has a larger injection area for both propellants, which means that the flow rate must be corrected in the flow control valves, which are the main responsible for the pressure drop. This was corrected before the third test therefore, the values shown at table 5.2 were changed accordingly to the equation for the pressure drop when liquid is passing by the needle valves [54].

Test 3 As mentioned before, the flow control valve was properly set to the case where liquid is passing through the valve. The plume - which can be observed in figure 5.14 - was clear and bright, and the burning was stable.

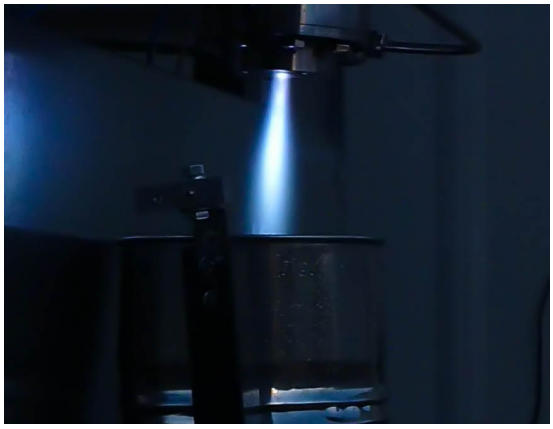

Figure 5.14: Plume from test 3.

Figure 5.15 shows the data collected during the test. The temperature in the vaporizer exceeds the

chamber temperature beyond a certain point. As it was mentioned before, this does not mean that the chamber's temperature was effectively lower, since the chamber's thermocouple is placed in a region where the recorded data depends on the flame position. In this case the flame was distant from the injector and, therefore, from the thermocouple.

In FEM simulations, the temperature suffered a significant increase at about 10 seconds from the beginning of the burn, after which it begins to stabilize. This can also be observed in figure 5.15.

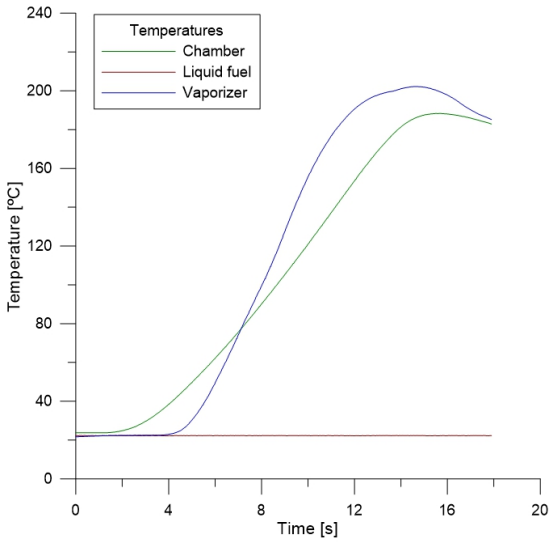

(a) Temperature evolution during the test.

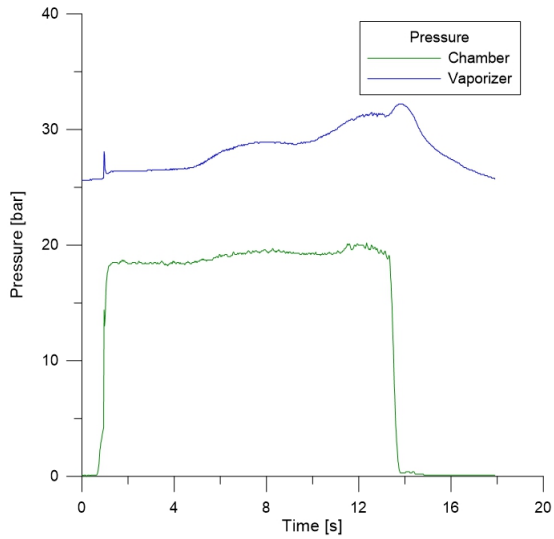

(b) Pressure evolution during the test.

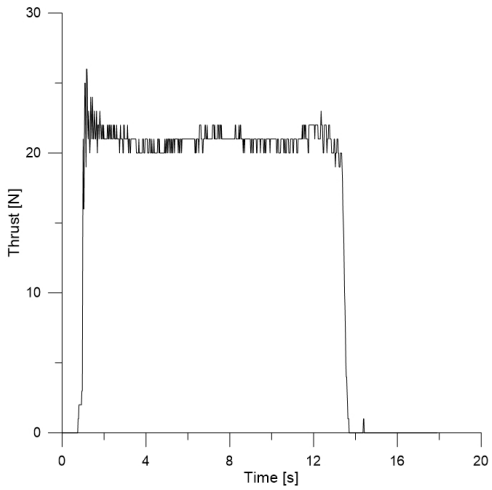

(c) Thrust evolution during the test.

Figure 5.15: Properties evolution during test.

The temperature reached in the vaporizer was enough for the vaporization of ethanol to occur, which is confirmed by the pressure graphic. The difference between the pressure in the chamber and the vaporizer increases, confirming boiling.

As for the thrust, its value is around the predicted - 25N. The oscillations in the sensor reading can be explain by the vibrations in the structure.

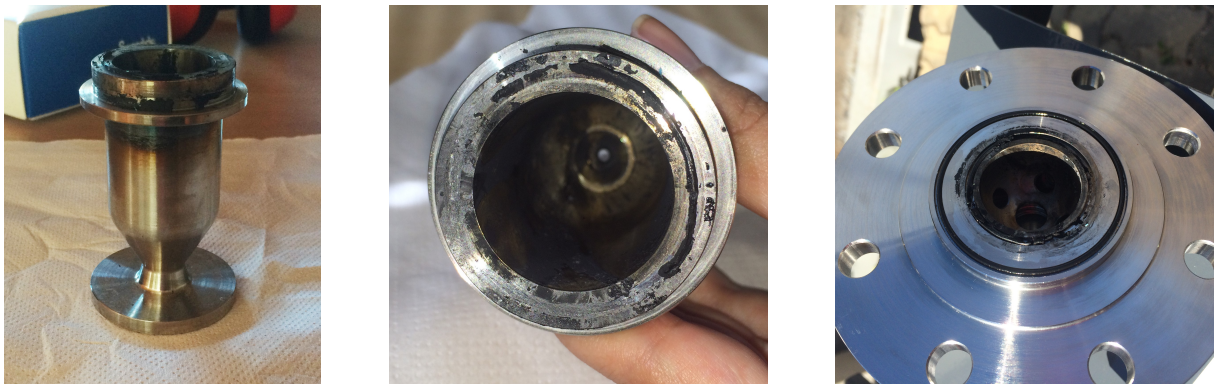

Figure 5.16: Chamber and injection head after test.

Figure 5.16 shows the combustion chamber after the third test. There was no major damage, although the o-rings used to seal the engine melted and had to be replaced. The ethanol enters the vaporizer atthe level of the throat. This assures that this area is properly cooled. The hot fluid exits at a higher level, forcing the fluid circulation in that direction. In the figure above it is possible to see that the chamber has a small damage at the outer wall, where the stainless steel shows different colors. This is caused by wall overheating. The region where the damage was spotted is in the opposite side of the hot fluid exit, meaning that this particular area was not properly cooled. Inside the chamber there are flame curved traces, related to the swirl direction but there was no significant damage and the throat was intact. The injection head shows that the flame was significantly close.

The phase diagram of ethanol and the its boiling are analysed in the section 6.

5.3.2 Ammonia - External Pressurization

Similar to the previous set of tests, the nitrogen is used to pressurize the fuel tank. All the tests with ammonia used the combustion chamber designed for this project and the swirl injector.

Two tests are presented in this subsection:

- Test 1 - The flow control valves are set as indicated in table 5.2.
- Test 2 - The difference between test 1 and 2 is that the second one occurred when the chamber's temperature was higher than the room temperature, because another fire test had taken place few minutes before it.

Test 1 With ammonia as fuel it is more difficult to have a successful ignition. In the first test with ammonia there were two failed attempts to start the engine due to lack of ignition.

To have a successful burn it is necessary to keep the glow plug powered for a longer time - about 6 seconds - than in the case with ethanol. The results of this test can be seen in the figure 5.17. The burn was shorter to avoid running out of fuel, which can cause material damage.

Ammonia is in liquid state, under a pressure between 8 and 12 bar, which means that when it enters the vaporizer it starts to expand, and its temperature will decrease. Contrary to what happened

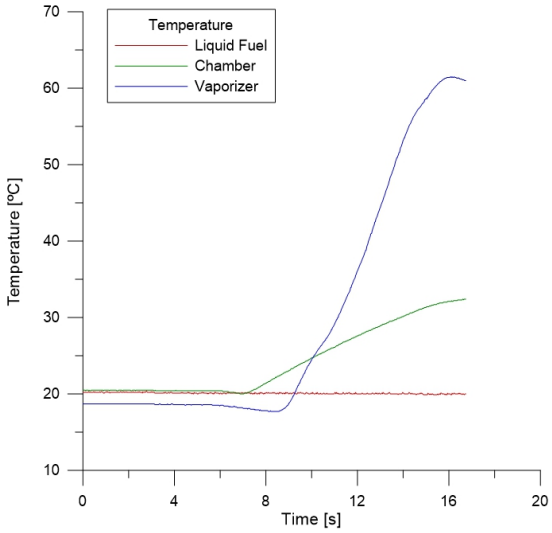

(a) Temperature evolution during the test.

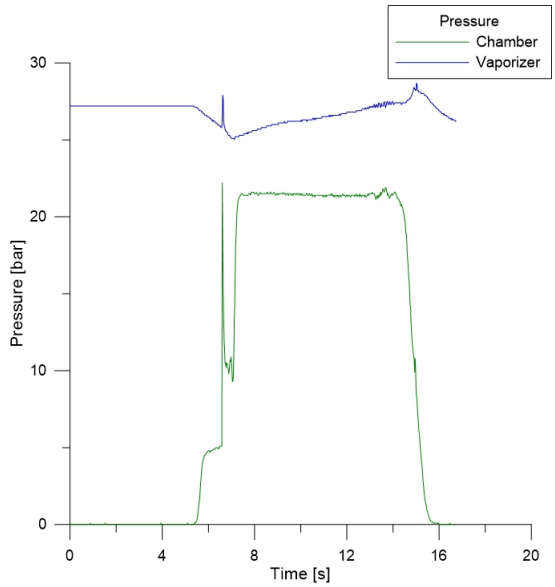

(b) Pressure evolution during the test.

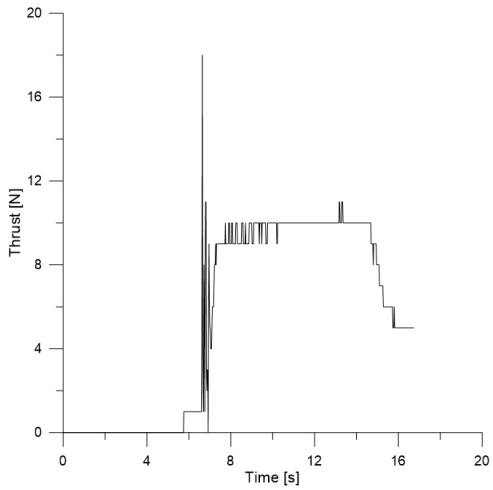

(c) Thrust evolution during the test.

Figure 5.17: Properties evolution during test.

with ethanol, ammonia's liquid temperature has some fluctuations, small enough to be neglected. The temperature chart shows that the temperature increases quickly, although it reaches temperatures lower than the ones achieved with ethanol. Nevertheless, the burning time was roughly half the one obtained with ethanol. It was predicted with CEA that the flame temperature would be lower with ammonia, then with ethanol. This means that is less likely to have damage in the combustion chamber, once using ammonia implies lower temperatures and better cooling.

In the pressure chart, the line correspondent to the chamber pressure has a sharp fall in the beginning of burning, after the valves are open. This irregularity represents a small hard start. It means that when the mixture was lit there was already a significant amount of mixed reactants in the chamber. While the chamber's pressure is stable, the vaporizer pressure increases, which implies an increase of pressure loss between the vaporizer and the chamber, possibly related to the vaporization of ammonia.

The value of the thrust is below the expected. It is possible that the OF is not defined properly and

there is an excess of oxygen entering the chamber, which will affect thrust.

The engine's behaviour is promising regarding autopressurization, because the temperatures are kept under 100° showing a satisfactory cooling, boiling and pressurization.

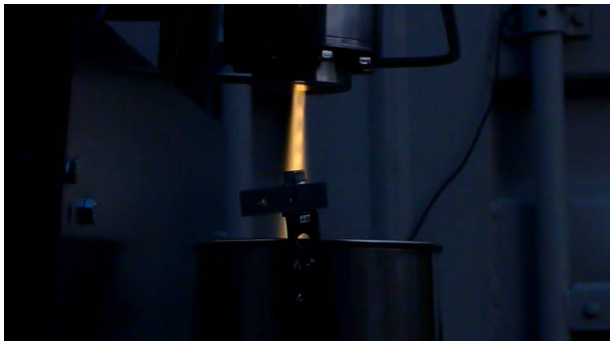

Figure 5.18: Plume during test.

Figure 5.18 shows the plume with a diamond pattern, which indicates that the exit is supersonic and the hypothesis of a sonic throat is sustained. The flame was almost constant, assuring the stability of the engine.

Test 2 The second test with external pressurization was made shortly after a previous test, which means that the combustion chamber was already at high temperature.

In figure 5.19, from the temperature plot it is possible to conclude that the flame was closer to the thermocouple than in previous tests. The chamber's temperature reached almost 400 ° C. The temperature in the vaporizer, even in this test, did not reach the high temperatures that were observed in the ethanol case. This allows longer operating times than with ethanol.

In the pressure chart, the two lines behave quite differently from the previous test. There is a hard start at the beginning of the burn. The chamber pressure shows a sharp decay around 7 seconds after the beginning, because the ammonia ran out. As it was mentioned before, this test was performed after an autopressurized test, which means that part of the ammonia was already spent. Regarding the vaporizer's pressure, represented by the blue line, it shows three different stages.

The thrust achieved during the test was satisfactory, around 23N, for a projected value of 25N. It starts to drop when the fuel tank runs out of ammonia. It is possible that the OF value was not suitable, especially when ammonia starts to evaporate. However, with the lack of instrumentation to actively control the fuel mass flow rate, the results are satisfactory.

After the test the chamber was open. The detection of a leak in the vaporizer indicated that the o-rings integrity was compromised during the test. The photos of the several parts can be seen in figure 5.20.

The glow plug shows a great amount of dark deposits, as well as a blue one, although in less quantity. The injection head is darker than in previous tests and also shows deposits. The injector shows that the flame was closer to it, which explains the burned appearance and confirms the readings of the thermocouple. In the chamber it is possible to see that there was no major damage, and the

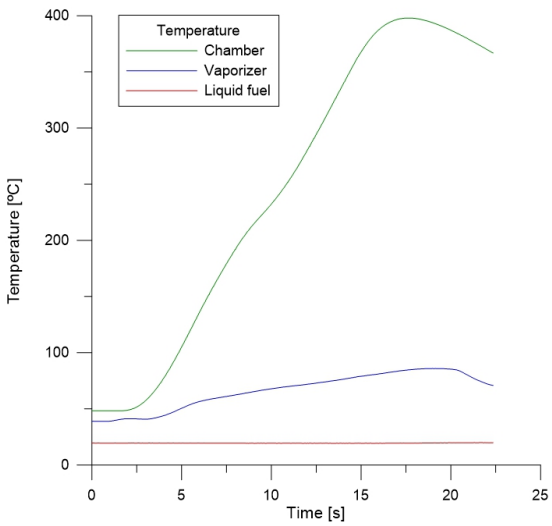

(a) Temperature evolution during the test.

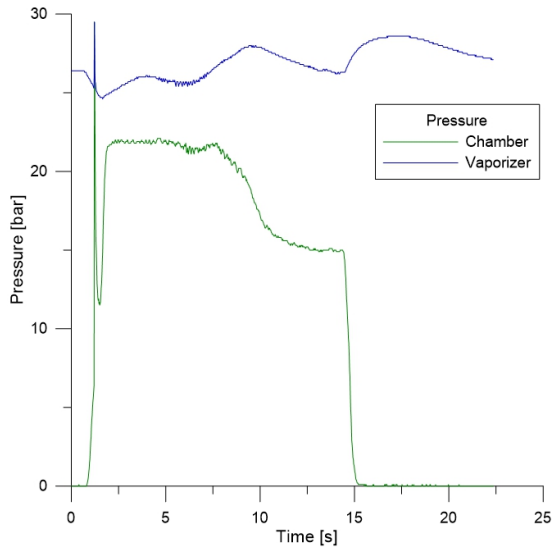

(b) Pressure evolution during the test.

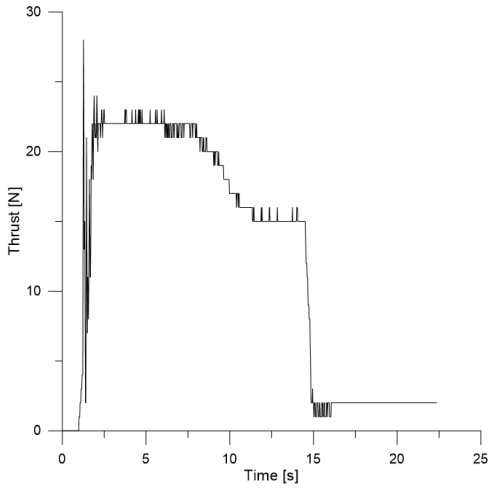

(c) Thrust evolution during the test.

Figure 5.19: Properties evolution during test.

(a) Glow plug.

(b) Injection head.

(c) Injector.

(d) Chamber outside.

(e) Chamber inside.

(f) O-rings.

Figure 5.20: Engine parts after test.

throat remained intact. However, the o-ring melted, which means that there were higher temperatures than expected.

5.3.3 Ammonia - Autopressurization

For the two self-pressurized tests the four position selection valve of the test stand is positioned to connect the autopressurization line (dotted line in the figure 5.2).

- Test 1 - Test with high OF.
- Test 2 - Test with low OF.

Test 1 To begin the autopressurized test it is necessary to fill the piping with pressurized gas. The nitrogen bottle must remain closed during the test and the four way valve must be switched to autopressurization.

The results of the test can be seen in figure 5.21.

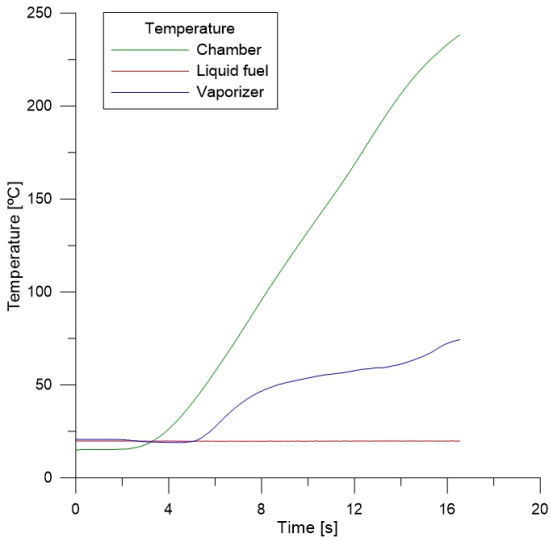

(a) Temperature evolution during the test.

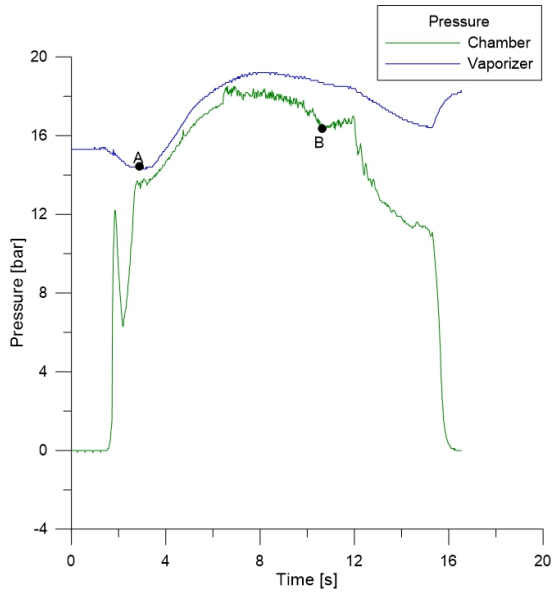

(b) Pressure evolution during the test.

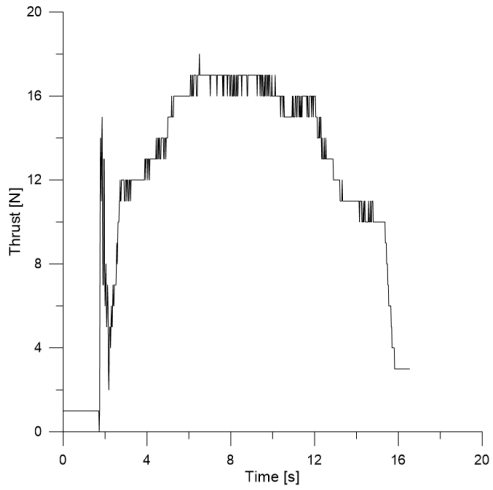

(c) Thrust evolution during the test.

Figure 5.21: Properties evolution during test.

From the pressure plot it is possible to see that the vaporizer line has the same tendency predicted

by the mathematical model (figure 3.4). The depression marked by point A is the point where nitrogen in the fuel's line stops being responsible for the pressurization. Thereafter there is a pressure increase due to regenerative cooling, as it was predicted. However, in the case of the chamber pressure, the pressure starts to increase, as expected, and then it decays till point B. There is a small increase afterwords, followed by a decay, until the valves are closed around 14 seconds after the beginning. During the test the sound emitted suggested an unstable operation, which is visible from the constant fluctuations of the chamber's pressure.

Test 2 Due to the results of the previous test it was decided to change the pressure in the bottles in order to work with a lower OF. Therefore the oxygen bottle was regulated to 20bar and the fuel's line was initially pressurized to 18bar. The flow control valves were also adjusted with the same height - about 3mm.

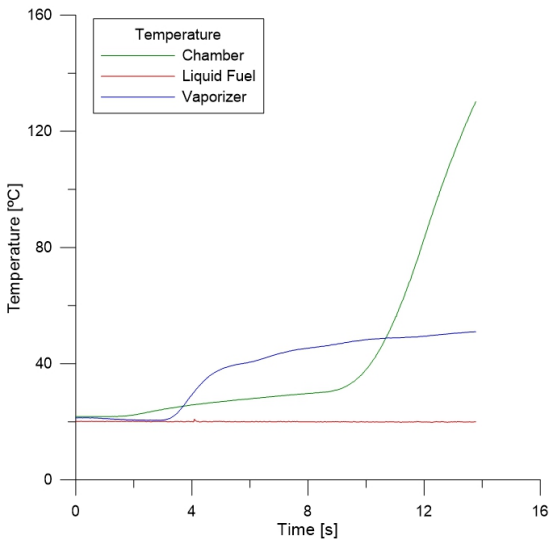

(a) Temperature evolution during the test.

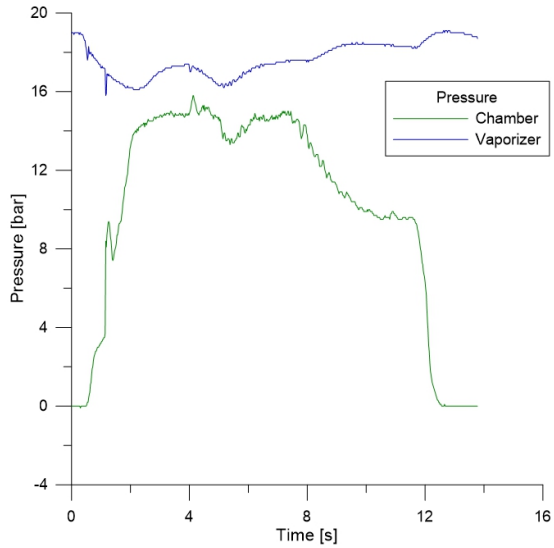

(b) Pressure evolution during the test.

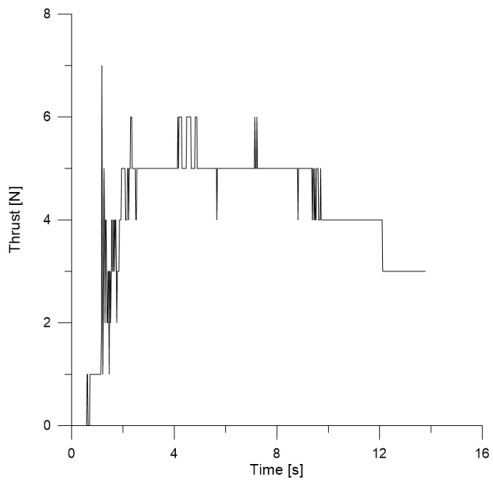

(c) Thrust evolution during the test.

Figure 5.22: Properties evolution during test.

Figure 5.22 shows that the pressure in the chamber is more stable than in the previous case and the

pressure in the vaporizer shows a growth trend.

Figure 5.23 shows the plume obtained. Although in the photo it appears to be bright, during the test there was a clear oscillation between a bright and a dim plume.

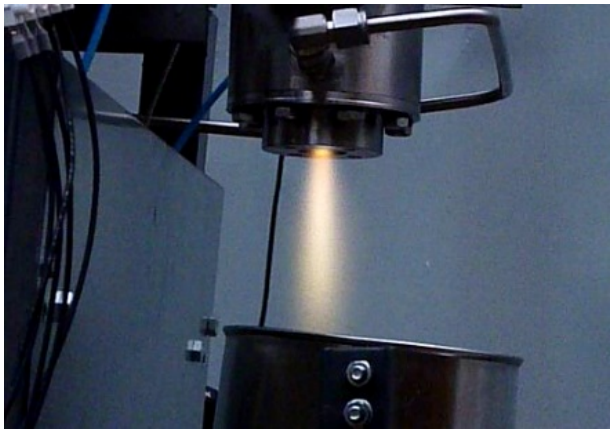

Figure 5.23: Plume during test.

Further comments on the test results can be seen in chapter 6, where there is an extensive analysis of the obtained results.

Chapter 6

Discussion

The work developed in this master thesis aimed to design, build and test a small liquid rocket engine. The main goal of this project was to study the feasibility of having a self-pressurized engine, avoiding external pressurization with inert gases or turbo pumps. The system had to be as simple as possible - including the injection and the ignition.

When choosing the layout, it was decided to build a system where it would be possible to perform a phased test campaign, starting by the external pressurization, looking at the stability and efficiency of the heat transfer by regenerative cooling - crucial to the self-pressurization process. In addition, knowing the behaviour of the externally pressurized system, it is easier to address self-pressurization and compare the differences.

During the preliminary design several choices were made, which included the fuel, material and sizing. From the three fuel candidates, ammonia was chosen for its cooling characteristics and adequate critical temperature and pressure. Experiments showed that it was a good choice, despite its ignition problems, which often caused a hard start. In the first tests, where the engine was working with ethanol, the temperature rose above the expected and to avoid material damage it was necessary to limit the time of operation. In addition, even with high temperatures, it was difficult to boil ethanol, due to the high pressure in the vaporizer.

The ethanol phase diagram, in figure 6.1a, shows that for the working pressure of the vaporizer the temperature should be above 100° C in order to boil. Furthermore, in tests where this temperature was achieved in the vaporizer, there was material damaged. The phase diagram of ammonia, figure 6.1b, shows that for a pressure around 20bar ammonia boils at about 50° C, which is a great advantage compared to ethanol.

Figure 6.2 shows the evolution of the enthalpy of vaporization and specific heat with temperature, for both fluids.

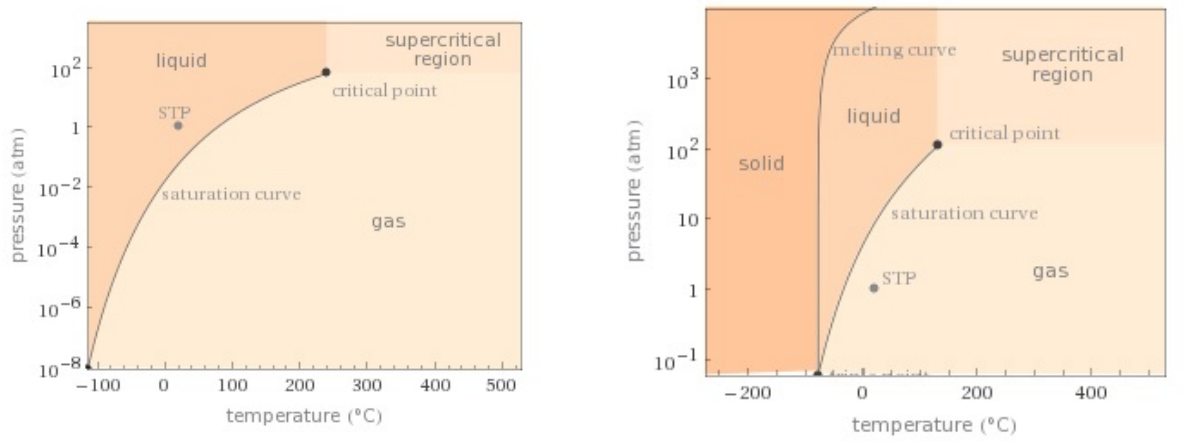

(a) Ethanol

(b) Ammonia

Figure 6.1: Phase diagrams [55].

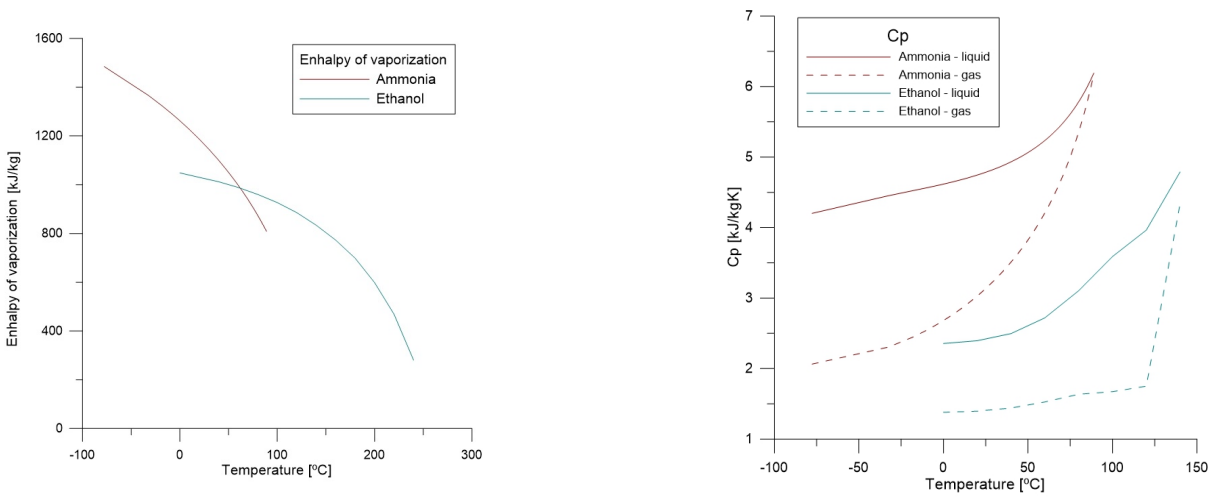

(a) Enthalpy of vaporization.

(b) Specific heat.

Figure 6.2: Phase diagrams.

For low temperatures (below 50° C), the enthalpy of vaporization is higher for ammonia and when there is no boiling, the specific heat is also higher for ammonia. This proves the advantage of using ammonia for the cooling of the combustion chamber, especially when there is no evidence of boiling. Figure 6.2 b) shows that in order to change the fuel's temperature one Kelvin, ammonia requires a greater amount of energy than ethanol. Therefore, in case of regenerative cooling with ethanol higher temperatures are achieved.

Another problem arises when boiling is not achieved. The flow control valves are adjusted for a gas flow. Therefore, whenever there is a liquid, which density is higher, the OF changes completely. This was the main cause of failure of the second ethanol test.

The absence of major material damage in the chamber proves the success of the system dimensioning. This shows that there was no need of building the chamber with a more expensive material, as the chosen stainless steel was able to handle chamber's pressure and temperature. It was a conservative

approach, as the system was oversized, but it allowed the safeguard of the system's integrity.

The use of a simple injector was another objective of this work. Between an injector with or without swirl, the swirler injector was preferable, as it minimizes the asymmetry of the flame. When the simple injector was used, after the chamber was opened, the asymmetry of the flame became obvious, because one of the injector sides had more deposits than the other. The damage in the first chamber was also asymmetrical.

The re-startable ignition was also successful through the use of a glow plug, which was able to withstand all the tests made.

When the system worked with external pressurization, results were close predictions.

For the two fuels used, the chamber's pressure evolution was stable with no major oscillations during the burn, as it is possible to see in figure 6.3. The values of this pressure were around 20bar, which is higher than the predicted. The pressure in the chamber depends on the regulated pressure of the propellant bottles. The pressure drop between the bottle and the chamber is due to the flow control valves and the injector. As the swirler injector has a large area, it results in a small drop of pressure, which means that the drop will be mainly assured by the flow control valve.

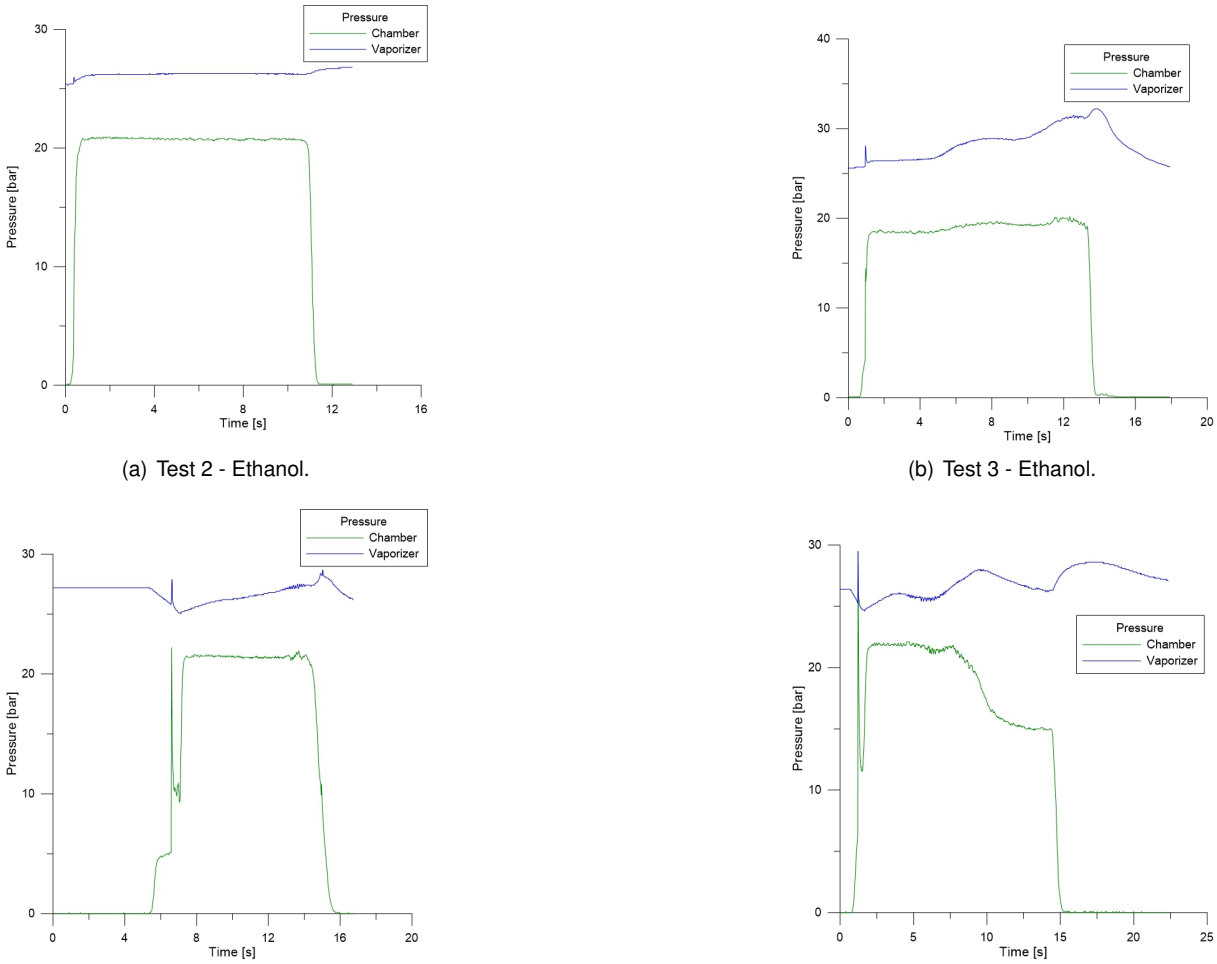

(a) Test 2 - Ethanol.

(b) Test 3 - Ethanol.

(c) Test 1 - Ammonia.

(d) Test 2 - Ammonia.

Figure 6.3: Pressure evolution during tests.

In the ammonia tests it is possible to identify the occurrence of a hard start. The difficulty to ignite

ammonia was confirmed and caused these hard starts. Experience showed that the glow plug should be powered for about 5 seconds before opening the valves and the ignition should start about 1 second after the valves were open.

It was observed that in several tests there was an increase of the vaporizer pressure. This can be explained by fuel boiling, which explains the pressure steps visible in the results. When looking to the temperature evolution in figure 6.4, and recalling the phase diagrams in figure 6.1, whenever there is an increase of vaporizer temperature this fact confirms a change of phase from liquid to gas.

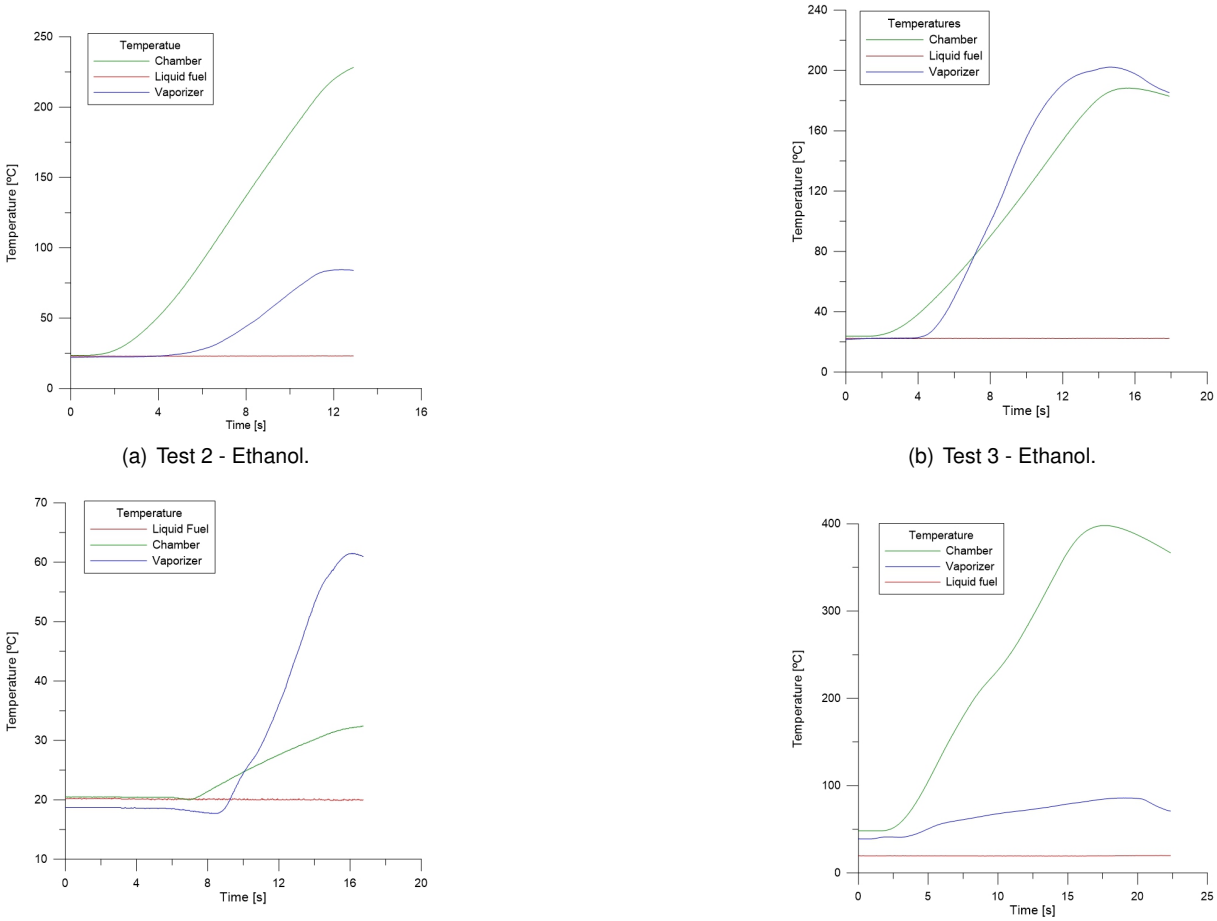

(a) Test 2 - Ethanol.

(b) Test 3 - Ethanol.

(c) Test 1 - Ammonia.

(d) Test 2 - Ammonia.

Figure 6.4: Temperature evolution during tests.

The place where thermocouples were installed greatly influences readings. Chamber's temperature were much lower than the expected. Theoretical considerations show that the difference between the flame temperature of ethanol and ammonia is not very significant, which means that the major discrepancies during the tests can be explained by the flame position. We can conclude that the flame was closer to the injector in test 2 with ammonia. In the vaporizer ethanol's temperature were much higher, as it was expected.

In terms of temperature stabilization, FEM simulations predicted pointed that the system would reach the steady state regime 10s after the ignition. Observations did not confirm this result.

The engine was designed for a thrust of about 25N and the values obtained experimentally were close, except for the first test with ammonia, which produced about 10N of thrust. It is important to

refer the incapacity of controlling the mass flow accurately in this test stand because the needle valves used are not fit for such small values. In addition, heating changes the liquid density, which will cause a change in the fuel mass flow.

The final objective of this project was to study the feasibility of having a self-pressurized system. Using the heat from the combustion chamber to pressurize the fuel tank. The system must be self-regulated relying on the flame temperature adjustment for different OF values.

The first test using self-pressurization was set with a high OF. The flow control valves were settle for an initial fuel pressure of about 15bar and an oxidizer pressure of 25bar.

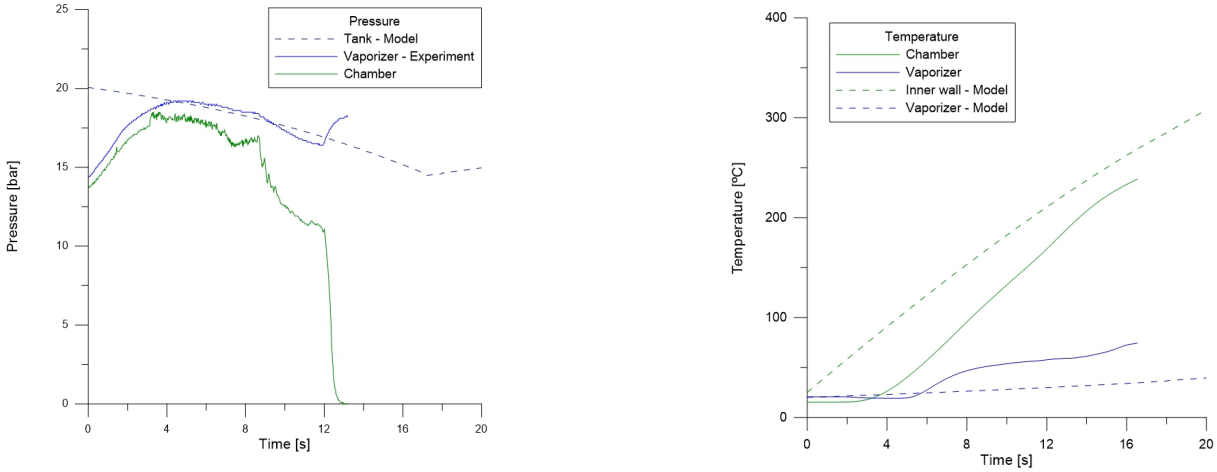

(a) Pressure (b) Temperature

Figure 6.5: Comparison between experimental and analytical results for higher OF.

In figure 6.5 the results from the mathematical model and those obtained experimentally are compared. The vaporizer pressure follows the same trend of the predicted pressure in the tank. However, since the burn was not able to withstand an operation time of 20 seconds, the pressure in the chamber began to drop sharply and the valves were closed. Fluctuations on the chamber's pressure can be correlated to flame instabilities.

Regarding the temperatures, results shows that the chamber temperature is closer to the inner wall temperature than to the flame temperature. As the thermocouple is far from the flame, the reading in the thermocouple actually results from the heat transfer from convection. The temperature observed in the vaporizer is higher than the model prediction. This can be explained by the model assumptions, in the code in order to minimize the computation time. To estimate the temperature of the fluid inside the vaporizer, the model uses the heat rate and the vaporizer's fluid specific heat, which means that the convection coefficient is not included directly in this estimate.

Figure 6.6 shows that according to predicitons, the pressure in the tank will exceed the value of the pressure in the vaporizer at some point. When this occurs, the check valve closes and the pressure tank drops, as well as the pressure in the vaporizer. This implies that the fuel mass flow entering the chamber decreases and the plume fades away, as observed during the test.

The thrust obtained in this test was about 16N, which is lower than expected. It is normal that some inefficiencies occur, and the mass flow can also be lower than the design values.

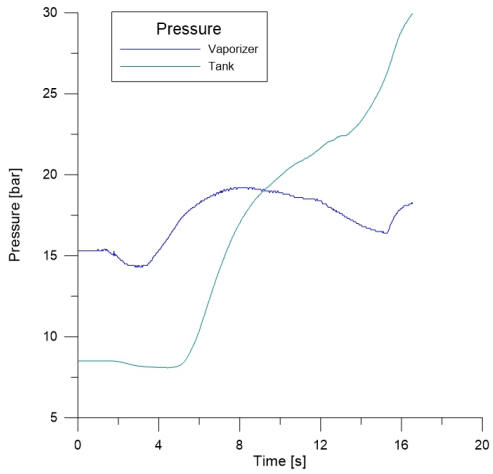

Figure 6.6: Estimation of tank pressure evolution.

When the system works with higher values of OF it is expected that the corrections are less significant.

In the second self-pressurized test the flow control valves are adjusted to obtain a lower OF.

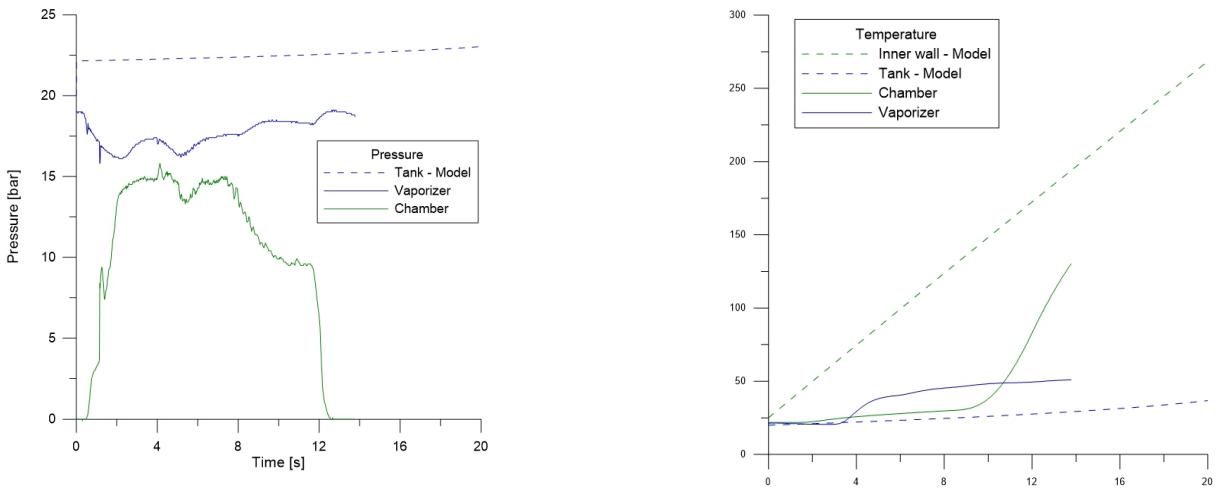

(a) Pressure

(b) Temperature

Figure 6.7: Comparison between experimental and analytical results for lower OF.

In figure 6.7a, the chamber pressure shows a sharp drop near second 6, but the avarage value is around 14bar, close to the design value of 15bar. Regarding temperature, near second 6 there is a small increase in growth rate, which increases. This reinforces the idea of a self-adjustment of the system. At about 8 seconds there is a drop of chamber pressure, until the valves are closed. At the beginning of the burn there is still a small hard start.

The vaporizer pressure plot show that the predicted trend is obtained experimentally. Comparing the model to the test results it is possible to see that there is a similar increase in both cases. Although, in the experimental case the pressure is lower, this has to do with the regulated pressure in the propellants bottles, which was lower than the original prediction. Despite the similar trend, in the experimental data there is an oscillation that was not expected. As it is possible to see in figure 5.2, there is a check valve

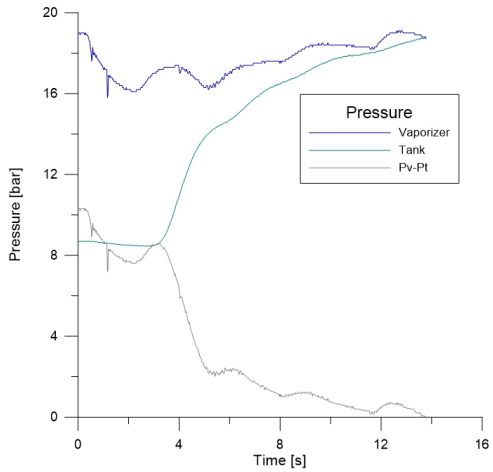

Figure 6.8: Estimation of tank pressure evolution.

in the line that connects the vaporizer to the tank, in order to prevent the fluid from going in the opposite direction, whenever the tank pressure is above the vaporizer's. This check valve opens when condition 6.1 is verified.

$$P_v > P_T + (0.49\text{to}1.1)bar \tag{6.1}$$

and closes when condition 6.2 is applied.

$$P_T < P_v + 0.21bar \tag{6.2}$$

The tank does not have a pressure sensor. Although, the thermocouple of the vaporizer is placed at its exit, it can be assumed that there is no significant change in temperature, and it is possible to calculate the pressure, because the fluid is saturated. This will predict when the pressure in the tank is above the vaporizer pressure and, therefore, when the valve should be closed.

Figure 6.8 shows the prediction of the tank pressure. In the plot it was added the line correspondent to the difference between the two pressures was added, in order to understand when the valve is closed. From second 8, the pressure difference decreases until it is virtually zero. This corresponds to a visible oscillation in the vaporizer pressure.

Figure 6.7b compares the experimental temperatures with those estimated by the model. In this case it is reasonable to assume that the the flame was far from the chamber's thermocouple, as the pressure that was recorded is significantly lower than the one predicted. It is important to refer that the vaporizer pressure starts to increase drastically when the pressure in the chamber decays, making the flame move to a higher point of the chamber. In the case of the vaporizer temperature the experimental value is higher than the predicted, similarly to the previous case.

Neither one of the self-pressurized tests was able to withstand for 20 seconds. Pressure graphics show that, contrary to what was expected, the pressure in the chamber starts to decay after about 8 seconds of the burn start. This was one of the unexpected results. When observing figure 5.2, in the

biforcation of the vaporizer's line, there are two different lines of piping. One of them leads to the tank and the other goes to the chamber. In the chamber line there are three components where pressure losses may occur: injector, filter and flow control valve. In the case of the tank line there is only the check valve. The pressure loss between the vaporizer and the chamber will be higher, which means that there is a greater amount of flow in the tank direction. This will lead to a decrease of fuel mass in the chamber and the burn would start to expire. This might explain the low thrust that was obtained during the test - around 5N.

With condition 3.13 it is possible to conclude that the plumes observed in the tests were supersonic.

After the exposed facts and assumptions, the self-pressurizing concept is considered feasible. However, it is crucial to collect more data from the tests.

The predictions that were made using the mathematical model are considered a fair approach to the experimental results. The discrepancies are explained by the implementations and limitations of the model.

Both the model and the tests confirm that the ideal operating region is for low OF values.

Chapter 7

Conclusions

This master thesis marks the beginning of a company's project to build a successful engine. It was a work based on research and development that, as it was expected, had successful and unsuccessful outcomes.

7.1 Achievements

In this project it was possible to accomplish the initial objectives. To sum up, the project was divided in two main parts: external pressurization and self-pressurization operating modes.

The external pressurized system was stable and behaved as expected. It was possible to build a simple and low cost engine, properly sized and in which the heat transfer was well estimated. The heat transfer analysis was an important issue, which prevented damages and, therefore, the success of the test campaign. The data collected leads to the conclusion that, with ammonia, the objective of having gaseous injection was achieved.

The second part of the work, confirmed that the self-pressurized system is a feasible concept. However, results obtained were far from predictions, which means that both mathematical model and the implemented layout need further improvements. The fact that the system was able to sustain an effective burn during a brief time was already a success.

In the beginning of this document there is an explanation about how the system can be self-stable through the change of the flame temperature with the OF. Experience and the model showed that there are actually differences when operating with low and high OF.

7.2 Future Work

For the next demonstrations of the engine the pressure drop in the line between the vaporizer and the tank must be increased to avoid the decrease in the fuel's mass flow to the chamber.

The company intends to increase the engine's capacity. Therefore, the chamber was resized in order to achieve a thrust of 300N, changing as little as possible the methodology adopted so far.

To increase thrust is necessary to increase pressure, in order to achieve reasonable dimensions and a sonic throat. The relief valves installed can go up to 70bar, so the chamber's pressure is fixed at 50bar. The results of the resizing can be seen in table 7.1.

Table 7.1: Engine properties.

	Item	Unit	Value
ENGINE	OF		1.4
	Total mass flow	kg/s	0,1030
	I_{sp}	m/s	2912.3
	Power	kW	458
	Chamber diameter	mm	30
	Throat diameter	mm	6
	Area ratio		7.66
	Chamber pressure	bar	50
	Material		Inconel
	Burn time	s	
OXIDIZER	Oxygen		
	Pressure	bar	60
	Temperature	K	293
FUEL	Ammonia		
	Pressure	bar	60
	Temperature	K	∼320

For these new characteristics a new fuel tank should be installed with a capacity of 2L.

In future work the concern with the oversizing can be rethought as the safety will be continuously proven. For instance, the wall thickness can be decreased, as the present thickness induces too much thermal inertia in the system. In further considerations the material of the o-rings should be changed to a more resistant to temperature. The temperature achieved in the o-ring area is higher than what was expected, causing the degradation of the o-rings, which compromised the system integrity.

In order to allow a deeper study of the engine, several instruments should be added to the test stand. In the future there should be a flow meter, which would help understanding the mass flow evolution. When the mass flow is known it is easier to understand the irregularities detected in experimental data. Also, including a pressure sensor in the tank would help understanding the evolution of the tank's pressure. Other configurations of the system can also be tested - for example, building the chamber inside the tank. The plume's temperature is also unknown, acquiring a new thermocouple should also be considered.

The study of the flame and its stability is important in further work, as it is a major source of rocket instabilities.

The unexpected problems that occured during the experiment - as the short burn period - should be corrected in the future work.

Bibliography

[1] G. Sutton and O. Biblarz. *Rocket Propulsion Elements*. Bsp Books Pvt. Ltd., 2001. ISBN 0471326429. doi: 10.1017/CBO9781107415324.004.

[2] W. Arbit, H.; Bissell, W.R.; Cardenas, M.P.; Cross, E.H.; Gaspar, K.C.; Iii, E.D.J.; Perry, J.G.; Stanley. *Modern Engineering for Design of Liquid-Propellant Rocket Engines*. AIAA, 1962. ISBN 1600864007.

[3] L. J. Krzycki. How to Design, Build and Test Small Liquid-Fuel Rocket Engines. pages 1–71, 1967.

[4] T. S. T. Hiraiwa and T. Tomita. Research Works of Ethanol Propulsion Sytem For The Future Rocket-Plane Experimental Vehicle. *47th AIAA/ASME/SAE/ASEE Joint Propulsion Conference*, (6114):1–9, 2011.

[5] Pressure-fed cycle diagram. `https://en.wikipedia.org/wiki/Pressure-fed_engine`. Visited: 2016-10.

[6] Gas Generator Diagram. `https://en.wikipedia.org/wiki/Gas-generator_cycle`. Visited: 2016-10.

[7] Expander Diagram. `https://en.wikipedia.org/wiki/Expander_cycle`. Visited: 2016-10.

[8] Staged Combustion Diagram. `https://en.wikipedia.org/wiki/Staged_combustion_cycle`. Visited: 2016-10.

[9] B. J. McBride and S. Gordon. Computer Program for Calculation of Complex Chemical Equilibrium Compositions and Applications: II-User Manual and Program Description, 1996.

[10] S. Gordon and B. J. McBride. CEA Analysis, 1994. URL `http://www.grc.nasa.gov/WWW/CEAWeb/RP-1311.pdf`.

[11] F. Ma, J.-Y. Choi, and V. Yang. Thrust Chamber Dynamics and Propulsive Performance of Single-Tube Pulse Detonation Engines. *Journal of Propulsion and Power*, 21(3):512–526, 2005. doi: 10.2514/1.8182.

[12] Space Exploration. `http://claudelafleur.qc.ca/Spacecrafts-index.html#Launchvehicle`, . Visited: 2016-10.

[13] Space Launch Report. http://www.spacelaunchreport.com/library.html#lvdata, . Visited: 2016-10.

[14] NASA. http://blogs.nasa.gov/spacestation/wp-content/uploads/sites/240/2015/09/Soyuz_TMA-18M_liftoff11.jpg. Visited: 2016-09.

[15] Liquid Rocket Propellants. https://en.wikipedia.org/wiki/Liquid_rocket_propellant. Visited: 2016-07.

[16] L. Schoenman. LOX/Propane and LOX/Ethanol Combustion Chamber Heat Transfer. *J. Propulsion*, 7(4):538–548.

[17] W. E. Welsh and A. B. Witte. A Comparison of Analytical and Experimental Local Heat Fluxes in Liquid-Propellant Rocket Thrust Chambers. *Journal of Heat Transfer*, 84(1), 1961.

[18] Copenhagen Suborbitals. https://copenhagensuborbitals.com/roadmap/bpm2-engine/. Visited: 2016-06.

[19] M. Meyer, D. Linne, and D. Rousar. Forced convection boiling and critical heat flux of ethanol in electrically heated tube tests. *36th AIAA Aerospace Sciences Meeting and Exhibit*, (1055), 1998. doi: 10.2514/6.1998-1055. URL http://arc.aiaa.org/doi/10.2514/6.1998-1055.

[20] T. H. S. T. T. S. M. Takegoshi, R. Suzuki and F. Ono. Effect of Triangular Fins on Critical Heat Flux of Ethanol. *47th AIAA/ASME/SAE/ASEE Joint Propulsion Conference*, (5624):1–8, 2011.

[21] G. A. Dressler and J. M. Bauer. TRW Pintle Engine Heritage and Performance Characteristics. *AIAA*, pages 2000–3871, 2000.

[22] R.-H. Chen, J. F. Driscoll, J. Kelly, M. Namazian, and R. W. Schefer. A Comparison of Bluff-Body and Swirl-Stabilized Flames. *Combustion Science and Technology*, 71:197–217, 1990. doi: 10.1080/00102209008951632.

[23] Engine schematic. https://www.quora.com/How-does-cryogenic-engine-work. Visited: 2016-09.

[24] Merlin. https://en.wikipedia.org/wiki/Merlin_(rocket_engine_family). Visited: 2016-09.

[25] Vulcain - Astronautix. http://www.astronautix.com/v/vulcain.html, . Visited: 2016-09.

[26] RD-180. http://www.astronautix.com/r/rd-180.html, . Visited: 2016-09.

[27] RD-253 - Astronautix . http://www.astronautix.com/r/rd-253-11d48.html, . Visited: 2016-09.

[28] LE-7 - Astronautix . http://www.astronautix.com/l/le-7.html. Visited: 2016-09.

[29] YF-100 - Astronautix . http://www.astronautix.com/y/yf-100.html. Visited: 2016-09.

[30] Vulcain. https://en.wikipedia.org/wiki/Vulcain, . Visited: 2016-09.

[31] RD-107 - Astronautix . http://www.astronautix.com/r/rd-107.html, . Visited: 2016-09.

[32] RD-253. http://www.russianspaceweb.com/rd253.html, . Visited: 2016-09.

[33] Pressure Loss. http://www.katmarsoftware.com/articles/pipe-fitting-pressure-drop.htm. Visited: 2016-07.

[34] F. White. Fluid Mechanics. *McGraw-Hill,New York*, page 862, 2010. ISSN 1364-0321. doi: 10.1111/j.1549-8719.2009.00016.x.Mechanobiology. URL http://www.amazon.com/Mechanics-Student-McGraw-Hill-Mechanical-Engineering/dp/0077422414.

[35] J. N. Beri. Flow through nozzles - frictional and heat transfer effects, 1960.

[36] W. G. Watson. Nozzle Flow with Heat Transfer and Friction. *Aircraft Engineering and Aerospace Technology, Vol. 27*, pages 339–345, 1955.

[37] A. Bandyopadhyay. Modeling of Compressible Flow with Friction and Heat Transfer using the Generalized Fluid System Simulation Program (GFSSP). *Thermal Fluid Analyst Workshop*, 2007.

[38] M. J. Moran and H. N. Shapiro. *Fundamentals of Engineering Thermodynamics*. John Wiley & Sons, Inc., West Sussex, fifth edition, 2006.

[39] T. F. Sun, C. a. Ten Seldam, P. J. Kortbeek, N. J. Trappeniers, and S. N. Biswas. Acoustic and Thermodynamic Properties of Ethanol from 273.15 to 333.15K and up to 280MPa. *Physics and Chemistry of Liquids*, 18(2):107–116, 1988.

[40] H. S. P. Dilan. A Fundamental Equation For The Calculation Of The Thermodynamic Properties Of Ethanol. *International Journal of Thermophysics*, 25:1–17, 2003.

[41] BAL SEAL Engineering. Chemical Compatibility Chart Metallic Materials Used in Bal Seal Products. *Techincal Report TR-60C*, pages 1–28, 1999.

[42] Material Compability. http://www.coleparmer.com/Chemical-Resistance. Visited: 2016-06.

[43] Stainless Steel Melting Point. http://www.bssa.org.uk/topics.php?article=103. Visited: 2016-06.

[44] A. S. Corporation. Product Data Sheet: Stainless Steel 304 304L. *AK Steel*, pages 7–8, 2014. URL http://www.aksteel.com/pdf/markets{_}products/stainless/austenitic/304{_}304l{_}data{_}sheet.pdf.

[45] AK Steel Corporation. Product Data Sheet: Stainless Steel 316/316L. *AK Steel*, page 2, 2007. ISSN 15420086. doi: 10.1016/B978-0-444-89875-3.50030-2.

[46] A. S. Corporation. Product Data Sheet: Stainless Steel 2205 Duplex. pages 6–7.

[47] Inconel Alloy 625. *www.Specialmetals.com*, 625(2):1–28, 2013. doi: SMC-066.

[48] MIT. Rocket Propulsion Classes - Lecture 7. (3):1–16. URL https://ocw.mit.edu/courses/aeronautics-and-astronautics/16-512-rocket-propulsion-fall-2005/lecture-notes/.

[49] F. P. Incropera, D. P. DeWitt, T. L. Bergman, and A. S. Lavine. *Fundamentals of Heat and Mass Transfer*. 2007. ISBN 9780471457282. doi: 10.1073/pnas.0703993104.

[50] J. D. Bernardin and I. Mudawar. The Leidenfrost Point: Experimental Study and Assessment of Existing Models. *Journal of Heat Transfer*, 121(4):894, 1999. doi: 10.1115/1.2826080.

[51] D. Roncati. Iterative calculation of the heat transfer coefficient. *Progettazione Ottica Roncati*, (2).

[52] R. H. Freeman. Understanding Space Launch Vehicle Complexity: A Case Study in Combustion Instabilities. *Procedia Computer Science*, 61:307–312, 2015. doi: 10.1016/j.procs.2015.09.142. URL http://dx.doi.org/10.1016/j.procs.2015.09.142.

[53] A. K. Gupta, D. G. Lilley, and N. Syred. *Swirl Flows*. Abacus Press, 1984. ISBN 0-85626-175-0.

[54] Swagelok. Valve Sizing - Technical Bulletin . pages 277–318, 2004. URL http://www.swagelok.com/downloads/webcatalogs/EN/MS-06-84.PDF.

[55] Phase Diagrams - Wolfram Alpha. https://www.wolframalpha.com/. Visited: 2016-10.

[56] Praxair. Ammonia , anhydrous Ammonia , anhydrous Safety Data Sheet P-4562. pages 1–9, 2015.

Appendix A

Mathematical model code

```
%---------------MODELO MATEMÁTICO----------------%
%------------------MAIN FUNCTION------------------%
%---Master Thesis - Small liquid rocket engine----%
%------Prove of concept - Auto pressurization-----%
%-----------Mariana P. Pascoa M. Marques----------%
close all
clear all
clc

%VARIABLES
k=15;   %thermal capacity of stainless steel

%Temperatures
t0c = zeros(1,2000); %stagnation temperature at chamber
t0conv = zeros(1,2000); %stagnation temperature at convergent part
t0div = zeros(1,2000); %stagnation temperature at divergent part

t1c = zeros(1,2000); %temperature at chamber inner wall
t1conv = zeros(1,2000); %temperature at convergent inner wall
t1div = zeros(1,2000); %temperature at divergent inner wall

t2c = zeros(1,2000); %temperature at chamber outter wall
t2conv = zeros(1,2000); %temperature at convergent outter wall
t2div = zeros(1,2000); %temperature at divergent outter wall

t3 = zeros(1,2000); %tank temperature

Isp = zeros(1,2000); %Isp vector
thrust = zeros(1,2000);  %thrust


%Pressure
p_chamber = zeros(1,2000); %chamber pressure
    p_chamber(1)=13; %[bar]
p = zeros(1,2000);  %tank pressure
    p(1)=15; %[bar]
p_drop_inj = 5;


%Heat flux
hfluxc = zeros(1,2000); %heat flux coefficient in the chamber
hflux_conv = zeros(1,2000);
hflux_div = zeros(1,2000);
heat_rate = zeros(1,2000); %heat rate coefficient in the chamber

%initial temperatures
    %chamber
t0c(1) = 3337.26;
t0conv(1) = 3196.43;
t0div(1) = 2717.23;

    %wall temperatures start at ambient
t1c(1) = 25 + 273;
t1conv(1) = 25 + 273;
t1div(1) = 25 + 273;
```

```
t2c(1) = 25 + 273;
t2conv(1) = 25 + 273;
t2div(1) = 25 + 273;
t3(1) = 20 + 273;

%Mass, title
mf = zeros(1,2000); %fuel mass
    mf(1) = 0.2; %initial mass [KG]
mfg = zeros(1,2000); %fuel gasous mass
    mfg(1) = 0; %initial mass [KG]
mfl = zeros(1,2000); %fuel liquid mass
    mfl(1) = mf(1); %initial mass [KG]
x = zeros(1,2000); %steam quality
    x(1)=0;  %initial steam quality
mf_dot = zeros(1,2000); %fuel mass flow
mox_dot = 0.005;  %oxygen mass flow 0.0058

%burn time
t_burn = 20; %[s]

%Piping area
A = pi*.003^2;

%Constant
cstar = 1828.5;

i=1;
time = zeros(1,2000);
time(1)=0;
    %time
        for j= 1:1:1999
         time(i+1)= time(i)+ 0.01;
         i=i+1;
        end

for i = 1:1:2000

    %velocity
        v = sqrt((2*abs(p(i) - p_chamber(i))*10^5)/(250*compute_rhog(p(i))));
    %mass
        mf_dot(i)= A*v*compute_rhog(p(i));

             mf(i+1)= mf(i)-mf_dot(i)*0.01;

    %heat
        hfluxc(i) = (0.026/0.003^0.2)*((p_chamber(i)*10^5)/cstar)^0.8 * (0.003/0.03)^1.8 * ...
            compute_cpl(p(i)) * (1.01e-4)^0.2 * (2*t0c(i)/(t0c(i)+t1c(i)))^(0.8-0.2*0.6);
        hflux_conv(i) = (0.026/0.003^0.2)*((p_chamber(i)*10^5)/cstar)^0.8 * (2*0.003/(0.03+0.003))^1.8 *...
            compute_cpl(p(i)) * (1.01e-4)^0.2 * (2*t0conv(i)/(t0conv(i)+t1conv(i)))^(0.8-0.2*0.6);
        hflux_div(i) = (0.026/0.003^0.2)*((p_chamber(i)*10^5)/cstar)^0.8 * (2*0.003/(0.0055+0.003))^1.8 * ...
            compute_cpl(p(i)) * (1.01e-4)^0.2 * (2*t0div(i)/(t0div(i)+t1div(i)))^(0.8-0.2*0.6);

        h3 = compute_miu(p(i)) * ((9.81*(compute_rhol(p(i))-compute_rhog(p(i))))/compute_sigma(p(i)))^0.5 * ...
            (compute_cpl(p(i))/(0.013*compute_pr(p(i))^1.7))^3*((t2c(i)-t3(i))/(10^3*compute_hfg(p(i))))^2;

        uc = 1/((1/(pi*0.03*hfluxc(i)))+((1/(2*pi*k))*log((0.015+0.003)/0.015))+(1/(pi*(0.03+0.003)*h3)));
        uconv = 1/((1/(pi*0.03*hflux_conv(i)))+((1/(2*pi*k))*log((0.00825+0.004)/0.015))+(1/(pi*(0.00825+0.005)*h3)));
        udiv = 1/((1/(pi*0.03*hflux_div(i)))+((1/(2*pi*k))*log((0.00425+0.004)/0.015))+(1/(pi*(0.00425+0.005)*h3)));

        Q_dotc(i) = ((t0c(i)-t3(i))*pi*0.03*0.0538*uc);
        Q_dotconv(i) = (uconv*(t0conv(i)-t3(i))*pi*(0.015+0.0015)*0.017);
        Q_dotdiv(i) = (udiv*(t0div(i)-t3(i))*pi*(0.0015+0.00275)*0.009);

        Q_dot(i) = Q_dotc(i) + Q_dotconv(i) + Q_dotdiv(i);

    %titulo

       if i==1
           x(i+1) = (Q_dot(i)*0.01)/(10^3*compute_hfg((p(1)+p(i))/2)*mf(i+1));
         else
          x(i+1) = x(i) + (Q_dot(i)*0.01)/(10^3*compute_hfg((p(1)+p(i))/2)*(mf(i+1)));
       end

          mfg(i+1) = x(i+1) * mf(i+1);
          mfl(i+1) = mf(i+1) - mfg(i+1);

    %new wall temperature
```

```
    if i<2000

        t1c(i+1) = t1c(i) + (Q_dotc(i)*0.01*.003)/(pi*0.03*0.0538*k);
        t1conv(i+1) = t1conv(i) + (Q_dotconv(i)*0.01*.003)/(pi*(0.015+0.0015)*0.017*k);
        t1div(i+1) = t1div(i) + (Q_dotdiv(i)*0.01*.003)/(pi*(0.0015+0.00275)*0.009*k);

        t2c(i+1) = t2c(i) + (Q_dotc(i)*0.01)/(15*pi*0.03*0.0538)*0.003;
        t2conv(i+1) = t2conv(i) + (Q_dotconv(i)*0.01)/(15*pi*(0.015+0.0015)*0.017)*0.003;
        t2div(i+1) = t2div(i) + (Q_dotdiv(i)*0.01)/(15*pi*(0.0015+0.00275)*0.0098)*0.003;

        t3(i+1) = t3(i) + (Q_dot(i)*0.01)/(mf(i+1)*compute_cpl(p(i)));

    end
    %OF
        OF(i) = mox_dot/mf_dot(i);

    %new chamber temperature
     if i<2000
        t0c(i+1) = -246.38*OF(i)^5 + 2001.6*OF(i)^4 - 5538.6*OF(i)^3 + 5126.6*OF(i)^2 + 1199.8*OF(i) + 271.01;
        t0conv(i+1) = t0c(i+1) - 300;
        t0div(i+1) = t0c(i+1) - 500;
     end

    %new pressure on the tank
    hg = 10^3*compute_hg((p(i)+p(1))/2);

    syms y

    eqn = mf(i+1) * ( 66.6*y^3 - 2835*y^2 + 58168.1*y + 108902.3 + x(i+1)*(-66.6*y^3+2035*y^2- ...
        44068.1*y + 1315797.7)) == 0.01*(mf_dot(i)*hg-Q_dot(i))+ mf(i)*(compute_uf((p(i)+p(1))/2)+x(i)*...
        (compute_ug((p(i)+p(1))/2)- compute_uf((p(i)+p(1))/2)));

    solx = solve(eqn,y)

    pressure = double(solx)

    if i<2000
    if (pressure(1))>0 && (pressure(2))>0 && abs(p(i) - (pressure(1))) > abs(p(i) - (pressure(2)))
        p(i+1) = (pressure(2));
    elseif (pressure(1))>0 && (pressure(2))>0 && abs(p(i) - (pressure(1))) < abs(p(i) - (pressure(2)))
        p(i+1) = (pressure(1));
    elseif (pressure(3))>0 && p(i+1)==0
        p(i+1) = (pressure(3));
    elseif (pressure(3))>0 && abs(p(i)-p(i+1))> abs(p(i)-(pressure(3)))
        p(i+1) = (pressure(3));
    end
    end

%    deltap(i) = ((Q_dot(i)-mf_dot(i)*hg)/(mf(i+1)*(10^3*compute_uf((p(1)+p(i))/2)+...
%        x(i+1)*(10^3*compute_ug((p(1)+p(i))/2))-10^3*compute_uf((p(1)+p(i))/2))))*0.01;
%
%     if i<2000
%     p(i+1) = p(i)+deltap(i);
%     end

    %new pressure on the chamber
    if i<2000
    p_chamber(i+1) = p(i+1) - p_drop_inj;
    end

    Isp(i) = -61.568*OF(i).^4 + 655.52*OF(i).^3 - 2451.1*OF(i).^2 + 3558.3*OF(i) + 863.16;

    thrust(i) = Isp(i)*(mox_dot + mf_dot(i));
end

%PLOTS
hold on

figure
subplot(3,2,1)
plot(time,OF)
xlabel('Time [s]')
ylabel('OF')
title('OF evolution')

subplot(3,2,2)
```

```
plot(time,mf_dot)
xlabel('Time [s]')
ylabel('Fuel mass flow')
title('Mass flow')

subplot(3,2,3)
plot( time, t3)
xlabel('Time [s]')
ylabel('Temperature [K]')
title('Tank temperature evolution')

subplot(3,2,4)
plot(time,p)
xlabel('Time [s]')
ylabel('Pressure [bar]')
title('Tank pressure evolution')

subplot(3,2,5)
plot(time,Q_dot)
xlabel('Time [s]')
ylabel('Heat Rate [W]')
title('Heat rate evolution')

subplot(3,2,6)
plot( time, t0c)
xlabel('Time [s]')
ylabel('Temperature [K]')
title('Chamber temperature evolution')

figure
subplot(1,3,1)
plot (time, Isp)
xlabel('Time [s]')
ylabel('Isp [Ns/kg]')
title('Specific impulse')

subplot(1,3,2)
plot(time, thrust)
xlabel('Time [s]')
ylabel('Thrust [N]')
title ('Thrust')

subplot(1,3,3)
plot( time, t1c)
xlabel('Time [s]')
ylabel('Temperature [K]')
title ('Chamber inner wall temperature')
```

Appendix B

Saturated Fuel Properties

B.1 Ammonia

LIQUID PHASE

T (ºC)	P (bar)	Rho (kg/m^3)	V (m^3/kg)	Int Energy	Enthalpy	Entropy	Cv	Cp	SoundSp	J-Thomson	Viscosity	Thrm Cond	Sigma	Hfg
-77.658	0.0609	732.91	0.0013644	-0.010561	-0.0022515	-5.40E-05	2.9343	4.2022	2124.3	-0.023362	undefined	undefined	undefined	1484.4023
-32.407	1.0609	680.83	0.0014688	195.86	196.01	0.9003	2.8533	4.4525	1761.6	-0.018473	0.00025224	0.66262	0.044411	1366.79
-18.163	2.0609	662.76	0.0015088	259.71	260.02	1.158	2.8295	4.5228	1660.2	-0.016666	0.0002096	0.61605	0.039221	1323.28
-8.7258	3.0609	650.36	0.0015376	302.52	302.99	1.3229	2.8141	4.5701	1593	-0.015305	0.00018745	0.58615	0.035899	1292.41
-1.4822	4.0609	640.6	0.001561	335.67	336.3	1.4466	2.8026	4.6084	1541.2	-0.014133	0.00017286	0.56373	0.033414	1267.5
4.4748	5.0609	632.4	0.0015813	363.12	363.92	1.5465	2.7934	4.6421	1498.2	-0.013067	0.00016213	0.54564	0.031411	1246.08
9.5758	6.0609	625.24	0.0015994	386.76	387.73	1.631	2.7858	4.673	1461.2	-0.012066	0.0001537	0.53038	0.029728	1227.17
14.062	7.0609	618.84	0.0016159	407.67	408.81	1.7044	2.7793	4.7024	1428.4	-0.011107	0.00014681	0.51714	0.02827	1209.99
18.082	8.0609	613.01	0.0016313	426.51	427.82	1.7696	2.7737	4.7306	1398.7	-0.010178	0.00014099	0.50541	0.026984	1194.08
21.735	9.0609	607.64	0.0016457	443.71	445.2	1.8283	2.7688	4.7581	1371.6	-0.0092683	0.00013597	0.49486	0.02583	1179.3
25.092	10.061	602.63	0.0016594	459.59	461.26	1.8819	2.7645	4.7852	1346.4	-0.0083728	0.00013157	0.48525	0.024783	1165.34
28.203	11.061	597.92	0.0016725	474.38	476.23	1.9313	2.7608	4.8119	1322.9	-0.0074864	0.00012765	0.47642	0.023824	1152.17
31.107	12.061	593.46	0.001685	488.24	490.27	1.9771	2.7574	4.8386	1300.8	-0.0066055	0.00012412	0.46824	0.02294	1139.63
33.833	13.061	589.23	0.0016971	501.31	503.53	2.0199	2.7544	4.8652	1280	-0.0057272	0.00012092	0.46062	0.022118	1127.47
36.405	14.061	585.18	0.0017089	513.7	516.1	2.0602	2.7518	4.8918	1260.1	-0.0048493	0.00011799	0.45346	0.021351	1115.9
38.842	15.061	581.3	0.0017203	525.49	528.08	2.0981	2.7495	4.9186	1241.2	-0.0039697	0.00011529	0.44673	0.020631	1104.72
41.16	16.061	577.56	0.0017314	536.75	539.53	2.1342	2.7474	4.9455	1223	-0.003087	0.00011279	0.44035	0.019953	1093.77
43.372	17.061	573.95	0.0017423	547.54	550.51	2.1684	2.7456	4.9726	1205.6	-0.0021997	0.00011046	0.4343	0.019312	1083.29
45.488	18.061	570.46	0.001753	557.9	561.07	2.2011	2.744	5	1188.8	-0.0013065	0.00010828	0.42853	0.018705	1072.93
47.517	19.061	567.07	0.0017635	567.89	571.25	2.2324	2.7426	5.0276	1172.6	-0.00040647	0.00010624	0.42303	0.018127	1062.95
49.468	20.061	563.77	0.0017738	577.52	581.08	2.2624	2.7414	5.0556	1156.9	0.00050149	0.00010431	0.41775	0.017577	1053.12
51.347	21.061	560.56	0.0017839	586.85	590.6	2.2913	2.7404	5.084	1141.6	0.0014183	0.00010249	0.41269	0.017051	1043.6
53.16	22.061	557.42	0.001794	595.88	599.84	2.3191	2.7396	5.1127	1126.8	0.0023447	0.00010076	0.40782	0.016548	1034.16
54.913	23.061	554.35	0.0018039	604.65	608.81	2.346	2.739	5.1419	1112.5	0.0032816	9.91E-05	0.40313	0.016066	1024.89
56.61	24.061	551.35	0.0018137	613.18	617.54	2.372	2.7385	5.1715	1098.4	0.0042297	9.75E-05	0.3986	0.015603	1015.86
58.254	25.061	548.41	0.0018235	621.48	626.05	2.3972	2.7381	5.2016	1084.8	0.0051897	9.60E-05	0.39423	0.015157	1006.95
59.851	26.061	545.52	0.0018331	629.57	634.34	2.4216	2.7379	5.2321	1071.4	0.0061624	9.46E-05	0.38999	0.014729	998.16
61.402	27.061	542.68	0.0018427	637.46	642.45	2.4453	2.7378	5.2632	1058.3	0.0071483	9.32E-05	0.38588	0.014315	989.45
62.91	28.061	539.88	0.0018523	645.17	650.37	2.4684	2.7379	5.2949	1045.6	0.0081482	9.19E-05	0.38189	0.013916	980.93
64.379	29.061	537.13	0.0018617	652.72	658.13	2.4909	2.7381	5.3271	1033	0.0091628	9.07E-05	0.37801	0.01353	972.47
65.811	30.061	534.42	0.0018712	660.1	665.73	2.5128	2.7384	5.3599	1020.8	0.010193	8.94E-05	0.37424	0.013157	964.07
67.208	31.061	531.75	0.0018806	667.34	673.18	2.5342	2.7389	5.3933	1008.7	0.011238	8.83E-05	0.37057	0.012796	955.82
68.571	32.061	529.11	0.00189	674.43	680.49	2.5551	2.7395	5.4274	996.86	0.012301	8.71E-05	0.36698	0.012446	947.61
69.903	33.061	526.5	0.0018993	681.39	687.67	2.5755	2.7402	5.4622	985.23	0.01338	8.60E-05	0.36349	0.012106	939.53
71.205	34.061	523.92	0.0019087	688.23	694.73	2.5955	2.741	5.4977	973.79	0.014478	8.49E-05	0.36008	0.011776	931.47
72.479	35.061	521.37	0.001918	694.95	701.67	2.6151	2.7419	5.5339	962.53	0.015594	8.39E-05	0.35674	0.011456	923.43
73.726	36.061	518.84	0.0019274	701.56	708.51	2.6342	2.7429	5.5709	951.44	0.016729	8.29E-05	0.35348	0.011145	915.59
74.947	37.061	516.34	0.0019367	708.06	715.24	2.6531	2.7441	5.6087	940.52	0.017884	8.19E-05	0.35029	0.010843	907.66
76.144	38.061	513.86	0.0019461	714.46	721.87	2.6715	2.7453	5.6473	929.76	0.019059	8.10E-05	0.34716	0.010548	899.93
77.318	39.061	511.4	0.0019554	720.77	728.41	2.6897	2.7467	5.6868	919.15	0.020256	8.01E-05	0.3441	0.010262	892.09
78.469	40.061	508.96	0.0019648	726.99	734.86	2.7075	2.7482	5.7272	908.67	0.021476	7.92E-05	0.3411	0.0099823	884.44
79.6	41.061	506.54	0.0019742	733.13	741.23	2.725	2.7497	5.7686	898.34	0.022717	7.83E-05	0.33815	0.0097102	876.67
80.709	42.061	504.13	0.0019836	739.18	747.52	2.7422	2.7514	5.811	888.14	0.023983	7.74E-05	0.33526	0.0094449	869.08
81.799	43.061	501.74	0.0019931	745.15	753.74	2.7592	2.7532	5.8543	878.06	0.025273	7.66E-05	0.33241	0.009186	861.46
82.871	44.061	499.36	0.0020026	751.05	759.88	2.7759	2.7552	5.8988	868.1	0.026588	7.58E-05	0.32962	0.0089335	853.92
83.924	45.061	496.99	0.0020121	756.89	765.95	2.7924	2.7572	5.9444	858.25	0.027929	7.50E-05	0.32688	0.0086869	846.35
84.96	46.061	494.64	0.0020217	762.65	771.96	2.8087	2.7593	5.9911	848.52	0.029297	7.42E-05	0.32418	0.0084461	838.74
85.979	47.061	492.29	0.0020313	768.35	777.91	2.8247	2.7615	6.0391	838.89	0.030693	7.34E-05	0.32152	0.0082109	831.29
86.982	48.061	489.96	0.002041	773.99	783.8	2.8405	2.7639	6.0883	829.37	0.032118	7.27E-05	0.3189	0.007981	823.8
87.969	49.061	487.63	0.0020507	779.58	789.64	2.8561	2.7663	6.1389	819.94	0.033573	7.20E-05	0.31633	0.0077563	816.26
88.941	50.061	485.31	0.0020605	785.11	795.42	2.8715	2.7689	6.1909	810.6	0.035059	7.12E-05	0.31379	0.0075366	808.88

VAPOR PHASE

T (ºC)	P (bar)	Rho (kg/m^3)	V (m^3/kg)	Int Energy	Enthalpy	Entropy	Cv	Cp	SoundSp	J-Thomson	Viscosity	Thrm Cond	Phase
-77.658	0.0609	0.064081	15.605	1389.3	1484.4	7.593	1.5566	2.0628	354.12	17.114	undefined	undefined	vapor
-32.407	1.0609	0.92861	1.0769	1448.6	1562.8	6.5778	1.7092	2.3047	386.73	6.3975	8.08E-06	0.021017	vapor
-18.163	2.0609	1.7297	0.57814	1464.2	1583.3	6.3477	1.7907	2.4446	394.03	4.9868	8.50E-06	0.021894	vapor
-8.7258	3.0609	2.5097	0.39846	1473.5	1595.4	6.2106	1.8535	2.5583	397.93	4.2751	8.79E-06	0.022606	vapor
-1.4822	4.0609	3.2786	0.30501	1479.9	1603.8	6.1121	1.9064	2.6581	400.38	3.8183	9.01E-06	0.023229	vapor
4.4748	5.0609	4.0411	0.24746	1484.8	1610	6.035	1.9527	2.7491	402.03	3.4903	9.19E-06	0.023795	vapor
9.5758	6.0609	4.8001	0.20833	1488.6	1614.9	5.9714	1.9943	2.8339	403.16	3.2389	9.35E-06	0.02432	vapor
14.062	7.0609	5.5572	0.17995	1491.7	1618.8	5.9172	2.0324	2.9143	403.93	3.0375	9.49E-06	0.024814	vapor
18.082	8.0609	6.3137	0.15839	1494.2	1621.9	5.8697	2.0677	2.9911	404.44	2.8711	9.62E-06	0.025285	vapor
21.735	9.0609	7.0705	0.14143	1496.4	1624.5	5.8275	2.1006	3.0653	404.76	2.7304	9.73E-06	0.025736	vapor
25.092	10.061	7.8285	0.12774	1498.1	1626.6	5.7894	2.1317	3.1374	404.92	2.6094	9.84E-06	0.026171	vapor
28.203	11.061	8.5881	0.11644	1499.6	1628.4	5.7546	2.161	3.2077	404.95	2.5037	9.94E-06	0.026594	vapor
31.107	12.061	9.3499	0.10695	1500.9	1629.9	5.7226	2.1889	3.2766	404.88	2.4102	1.00E-05	0.027005	vapor
33.833	13.061	10.114	0.09887	1501.9	1631	5.6928	2.2156	3.3445	404.72	2.3268	1.01E-05	0.027408	vapor
36.405	14.061	10.882	0.091899	1502.8	1632	5.665	2.2412	3.4115	404.49	2.2518	1.02E-05	0.027802	vapor
38.842	15.061	11.652	0.085821	1503.5	1632.8	5.6389	2.2658	3.4779	404.2	2.1837	1.03E-05	0.02819	vapor
41.16	16.061	12.426	0.080475	1504.1	1633.3	5.6142	2.2895	3.5437	403.85	2.1216	1.04E-05	0.028571	vapor
43.372	17.061	13.204	0.075733	1504.6	1633.8	5.5908	2.3124	3.6093	403.45	2.0647	1.04E-05	0.028949	vapor
45.488	18.061	13.986	0.071499	1504.9	1634	5.5685	2.3346	3.6746	403.02	2.0122	1.05E-05	0.029322	vapor
47.517	19.061	14.773	0.067693	1505.2	1634.2	5.5472	2.3561	3.7398	402.54	1.9636	1.06E-05	0.029691	vapor
49.468	20.061	15.563	0.064253	1505.3	1634.2	5.5268	2.3771	3.805	402.03	1.9184	1.07E-05	0.030058	vapor
51.347	21.061	16.359	0.061128	1505.4	1634.2	5.5073	2.3974	3.8704	401.49	1.8762	1.07E-05	0.030422	vapor
53.16	22.061	17.159	0.058277	1505.4	1634	5.4884	2.4173	3.9359	400.92	1.8367	1.08E-05	0.030785	vapor
54.913	23.061	17.965	0.055663	1505.4	1633.7	5.4702	2.4367	4.0018	400.32	1.7996	1.09E-05	0.031147	vapor
56.61	24.061	18.776	0.053259	1505.3	1633.4	5.4526	2.4557	4.068	399.7	1.7647	1.09E-05	0.031507	vapor
58.254	25.061	19.592	0.05104	1505.1	1633	5.4355	2.4743	4.1347	399.06	1.7318	1.10E-05	0.031867	vapor
59.851	26.061	20.414	0.048985	1504.8	1632.5	5.419	2.4925	4.2019	398.4	1.7007	1.10E-05	0.032227	vapor
61.402	27.061	21.242	0.047076	1504.5	1631.9	5.4029	2.5104	4.2698	397.73	1.6711	1.11E-05	0.032588	vapor
62.91	28.061	22.076	0.045297	1504.2	1631.3	5.3872	2.5279	4.3383	397.03	1.6431	1.12E-05	0.032949	vapor
64.379	29.061	22.917	0.043637	1503.7	1630.6	5.3719	2.5451	4.4076	396.32	1.6164	1.12E-05	0.033311	vapor
65.811	30.061	23.763	0.042082	1503.3	1629.8	5.357	2.5621	4.4776	395.6	1.5909	1.13E-05	0.033674	vapor
67.208	31.061	24.616	0.040623	1502.8	1629	5.3424	2.5788	4.5486	394.86	1.5666	1.13E-05	0.034039	vapor

68.571	32.061	25.476	0.039252	1502.3	1628.1	5.3281	2.5952	4.6206	394.11	1.5433	1.14E-05	0.034406	vapor
69.903	33.061	26.343	0.037961	1501.7	1627.2	5.3141	2.6114	4.6936	393.34	1.521	1.15E-05	0.034775	vapor
71.205	34.061	27.217	0.036742	1501	1626.2	5.3004	2.6274	4.7677	392.57	1.4996	1.15E-05	0.035147	vapor
72.479	35.061	28.099	0.035589	1500.4	1625.1	5.2869	2.6431	4.843	391.78	1.4791	1.16E-05	0.035522	vapor
73.726	36.061	28.987	0.034498	1499.7	1624.1	5.2737	2.6587	4.9195	390.98	1.4593	1.16E-05	0.0359	vapor
74.947	37.061	29.884	0.033463	1498.9	1622.9	5.2606	2.6741	4.9974	390.17	1.4402	1.17E-05	0.036282	vapor
76.144	38.061	30.789	0.03248	1498.1	1621.8	5.2478	2.6893	5.0768	389.35	1.4219	1.18E-05	0.036667	vapor
77.318	39.061	31.701	0.031544	1497.3	1620.5	5.2352	2.7044	5.1576	388.53	1.4041	1.18E-05	0.037057	vapor
78.469	40.061	32.622	0.030654	1496.5	1619.3	5.2227	2.7193	5.24	387.69	1.387	1.19E-05	0.037452	vapor
79.6	41.061	33.552	0.029804	1495.6	1617.9	5.2104	2.734	5.324	386.85	1.3704	1.19E-05	0.037851	vapor
80.709	42.061	34.49	0.028993	1494.6	1616.6	5.1982	2.7487	5.4099	385.99	1.3543	1.20E-05	0.038255	vapor
81.799	43.061	35.438	0.028218	1493.7	1615.2	5.1862	2.7632	5.4976	385.13	1.3387	1.21E-05	0.038665	vapor
82.871	44.061	36.395	0.027476	1492.7	1613.8	5.1743	2.7776	5.5873	384.26	1.3236	1.21E-05	0.039081	vapor
83.924	45.061	37.361	0.026766	1491.7	1612.3	5.1625	2.7918	5.679	383.39	1.3089	1.22E-05	0.039503	vapor
84.96	46.061	38.337	0.026084	1490.6	1610.7	5.1509	2.806	5.7729	382.5	1.2946	1.22E-05	0.039932	vapor
85.979	47.061	39.323	0.02543	1489.5	1609.2	5.1394	2.8201	5.8691	381.61	1.2807	1.23E-05	0.040368	vapor
86.982	48.061	40.32	0.024802	1488.4	1607.6	5.1279	2.8341	5.9677	380.71	1.2672	1.24E-05	0.040811	vapor
87.969	49.061	41.327	0.024197	1487.2	1605.9	5.1166	2.8479	6.0688	379.81	1.254	1.24E-05	0.041262	vapor
88.941	50.061	42.345	0.023616	1486	1604.3	5.1053	2.8618	6.1726	378.9	1.2411	1.25E-05	0.041722	vapor

B.2 Ethanol

THERMAL-FLUIDS CENTRAL
connecting the global thermal fluids community

Search Thermal-Fluids Central
Entire Website Search

Home Encyclopedia Journals eBooks eResources Jobs Events News Who's Who Links

Home » Encyclopedia » Index » Thermophysical_Properties:_Ethanol

Thermophysical Properties: Ethanol

From Thermal-FluidsPedia

Ethanol, C2H5OH, Molecular Mass: 46.0, (T_{sat} = 78.3 °C; T_m = -114.5 °C)

T Temp. °C	p_v saturation pressure (10^5 Pa)	latent heat (kJ/kg)	ρ_ℓ liquid density (10^3 kg/m³)	ρ_v vapor density (kg/m³)	μ_ℓ liquid viscosity (10^{-3} N-s/m²)	μ_v vapor viscosity (10^{-5} N-s/m²)	k_ℓ liquid thermal conductivity (W/m-K)	k_v vapor thermal conductivity a (W/m-K)	σ liquid surface tension (10^{-3}N/m)	$c_{p,\ell}$ liquid specific heat b (kJ/kg-K)	$c_{p,v}$ vapor specific heat c (kJ/kg-K)
0	0.012	1048.4	0.901	0.036	1.7990	0.774	0.183	0.0117	24.4	2.27	1.34
20	0.058	1030.0	0.800	0.085	1.1980	0.835	0.179	0.0139	22.8	2.40	1.40
40	0.180	1011.9	0.789	0.316	0.8190	0.900	0.175	0.0160	21.0	2.57	1.48
60	0.472	988.9	0.770	0.748	0.5880	0.959	0.171	0.0179	19.2	2.78	1.54
80	1.086	960.0	0.757	1.430	0.4320	1.030	0.169	0.0199	17.3	3.03	1.61
100	2.260	927.0	0.730	3.410	0.3180	1.092	0.167	0.0219	15.5	3.30	1.68
120	4.290	885.5	0.710	6.010	0.2430	1.157	0.165	0.0238	13.4	3.61	1.75
140	7.530	834.0	0.680	10.670	0.1900	1.219	0.163	0.0256	11.2	3.96	
160	12.756	772.9	0.650	17.450	0.1500	1.293	0.161	0.0272	9.0		
180	19.600	698.8	0.610	27.650	0.1200	1.369	0.159	0.0288	6.7		
200	29.400	598.3	0.564	44.480	0.0950	1.464	0.157	0.0395	4.3		
220	42.800	468.5	0.510	74.350	0.0725	1.618	0.155	0.0321	2.2		
240	60.200	280.5	0.415	135.500	0.0488	1.948	0.153		0.1		

Property$_a$	Temp.	a_0	a_1	a_2	a_3	a_4	a_5	Error(%)
p_v (10^5Pa)	0 – 240 °C	-4.4114	8.7650-2b	-6.3182-4	3.9958-6	-1.4340-8	2.0359-11	1.24
$h_{\ell v}$ c (kJ/kg)	0 – 240 °C	1048.6	-1.0921	1.0651-2	-2.0693-4	1.1231-6	-2.4928-9	0.12
ρ_ℓ (10^3kg/m³)	0 – 240 °C	-1.0791-1	-7.7201-3	1.5906-4	-1.6139-6	7.1873-9	-1.2075-11	0.50
ρ_v (kg/m³)	0 – 240 °C	-3.3681	5.2492-2	5.1630-5	-1.9542-6	8.6893-9	-1.1451-11	4.95
μ_ℓ (10^{-3}Ns/m²)	0 – 240 °C	5.8942-1	-2.2540-2	1.0283-4	-8.8574-7	4.7884-9	-9.7493-12	0.39
μ_v (10^{-6} Ns/m²)	0 – 240 °C	-2.5759-1	4.5249-3	-3.1212-5	3.9144-7	-2.3733-9	5.1450-12	0.29
k_ℓ (W/m-K)	0 – 240 °C	-1.6976	-1.2505-3	7.5291-7	5.2361-8	-3.4986-10	6.4599-13	0.10
k_v (W/m-K)	0 – 220 °C	-4.4346	3.3797-3	2.1001-4	-3.4778-6	2.0462-8	-4.0325-11	3.75
σ^c (10^{-3} N/m)	0 – 240 °C	24.419	-8.1477-2	-1.1450-4	8.6540-7	-7.6432-9	1.9148-11	2.15
$c_{p,\ell}$ (kJ/kg-K)	0 – 140 °C	0.81763	2.6793-3	1.3888-5	-4.3856-11	-4.4424-10	1.5104-12	0.01
$c_{p,v}$ (kJ/kg-K)	0 – 120 °C	2.9255-1	1.2271-3	8.0938-5	-1.8513-6	1.6850-8	-5.3880-11	0.11

Figure B.1: Ethanol table.

Appendix C

Safety Concerns

Safety Concerns During the project some choices were influenced by the safety concerns inherent to the reactants in use. The following list mentions some of this concerns.

Ethanol
It is highly flammable. It can be irritating to the skin and in case of contact with eyes, they must be washed immediately. It must be stored in a ventilated place, and the container should be tightly closed. It may form an explosive mixture with air, but it is chemical stable under normal conditions. The products of the combustion are carbon monoxide and carbon dioxide. It may attack some plastics, rubber and coatings.
Ammonia
From the reactants in use, ammonia is the only one that represents a potential concern for the environment as it is very toxic to aquatic life. Ammonia is flammable, may explode if heated, is toxic when inhaled, causes skin burns and is corrosive, especially to copper alloys. The container should be kept in a cool place. The handling must be made carefully, avoiding drag, roll, slide or drop and requiring the use of adequate chemical protect gloves, safety glasses and protective shoes.
Oxygen
Gaseous oxygen is highly flammable and can easily explode. Its handling requires that every component is free of oils or grease. Oxygen also reacts violently with asphalt, kerosene, cloth, paint, tar and dirt. When in contact with eyes or skin no effects are expectable however, above a certain concentration ($\sim 75\%$), the can cause nausea, vertigo and convulsions. When handling oxygen, some practices must be adopted: the components that will be in contact with oxygen must be clean and the valves must be opened slowly.
Nitrogen
It is a pressurized gas, which risks an explosion when heated. It should be stored in an aired place. The container must be inspected regularly to ensure that there are no leaks. Safety glasses, shoes and gloves should be used when handling it. Nitrogen is asphyxiating when inhaled in high concentrations. It is an inert gas, so it neither reacts nor ignites.

Test management

The test management includes all the planning and logistics associated with each test. The test campaign is divided into two main parts: experiments with ethanol and with ammonia. The material involved and the requirements to perform the tests are presented bellow.

Material Besides the test stand, some other material is needed. This includes the following list.

- Gloves and safety glasses, when handling ammonia.
- Water for the deflector.
- Ear protection during the tests.
- Large syringe to fill the fuel's tank with ethanol.
- Beaker to measure the ethanol.
- Cameras to record videos.
- Cold sleeve to cool ammonia's tank, assuring that it is filled with liquid ammonia.
- Fire extinguisher.

Environment The tests were performed in an open space. The choice of this environment has to do with reactants safety requirements. The test stand is portable and will be installed before every set of tests. Operators must stay in a location without line of sight.

Procedures Regarding the objectives of each test, the following procedures were defined.

1. Ignition
   The glow plug has an input voltage of 11V, although the maximum current is not specified. To ensure that the power source is adequate, and that the ignition through a glow plug is feasible, preliminary tests were performed. The description is presented in table C.1 and the glowing plug can be seen in figure C.1.

Table C.1: Test procedures for the igniter.

Code	Objective	Designation
I1	Record the temperature of the plug.	The plug is connected to a generator that provides 11V and 5A. A thermocouple is attached to the glowing part. The data logger records the temperature variation.
I2	Record the temperature of the plug.	Similar to I1. Plug is conected to a car battery.
I3	Check if the plug temperature is enough to ignite ethanol.	Similar conditions to I2. The plug is put in contact with ethanol.
I4	Assure that the power source on the test stand is enough to make the plug glow.	Similar to I2, but the power source is a 20V battery.

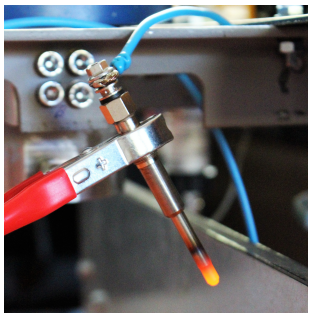

Figure C.1: Glow plug being tested with the test stand's ignition system.

2. Pressure drop

   The pressure drop value can be estimated through a hot fire test. Fixing the pressure from the reactants on their bottles, it is possible to obtain the pressure decay in the system, measuring the chamber pressure.

3. Leaks

   Leak testing is a crucial part of test procedures. Due to the several valves it is possible to isolate parts of the piping, and test for leaks separately. Several leak tests were conducted in every assembled part. When leakage was detected, the piping was sprayed with a mixture of water and soap. A bubble formation indicates the location of a leak, as shown in figure C.2.

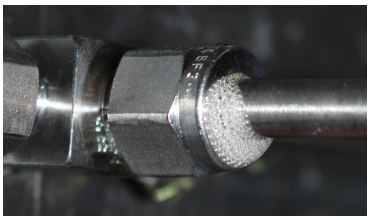

Figure C.2: Illustration of a leak detection.

4. Injection

   During the assembly, the first injector was tested in order to see if there were any leaks and to confirm that the geometry of the flow was as intended.

5. Cold flow test

   Before each burn test with a new propellant combination, a cold flow test was planned. This test is important to determine if there is ignition without using the glow plug. Also, it is a dynamic test that allows the inspectation of all systems apart from the igniter. During the cold flow test it is possible to verify pressures, flows and the overall function of the test stand.

6. Hot fire test

   The hot fire tests are the most important of the project. Their description and objectives can be seen in table C.2.

Table C.2: Burn tests description and objectives.

Code	Objective	Description
B1.1	Test system feasibility with ethanol and external pressurization.	Burn test using ethanol as fuel. Due to delays in the manufacturing of the combustion chamber, in the first test a chamber from a previous motor prototype was used.
B1.2 B1.3	Test system feasibility with ethanol and external pressurization.	Burn test using ethanol as fuel. The combustion chamber designed for this project is used.
B2.1 B2.2 B2.3	Test system feasibility with ammonia and external pressurization.	Test conditions are similar to B1.3, but the fuel used was ammonia.
B3.1 B3.2 B3.3	Test autopressurization with ammonia.	Test conditions are similar to B2.3 but autopressurization is used instead of external pressurization. Ammonia's vapour pressure at ambient temperature is enough to drive it from the tank to the combustion chamber.

For every test there is a check list - table C.3 - to ensure that there are no forgotten steps and all safety precautions are followed.

Table C.3: Test check list.

Order	Description
1	Guarantee that the main valves are closed.
2	Fill the fuel tank.
3	Pressurize oxygen line with nitrogen.
4	Configure test stand.
5	Turn on cameras and data logger.
6	Begin test.
7	Close valves.
8	Check the stand integrity.
9	Turn off cameras and data logger.
10	Purge system.

At last, for these tests, and to minimize errors in operations, table C.4 shows the position of the valves for each pressurization case and the timing for the control interface. Notice that the operator should begin by turning on the glow plug, which takes approximately one second to become incandescent. Reactants must enter the chamber at different times, to avoid a hard start, the fuel being the first. The glow plug should be kept lit until ignition occurs.

Table C.4: Test set up combination and control sequence and timing.

Valve	Position
Oxygen	Open
Fuel	External Pressurization
Purge	*Indifferent*
Pressurant	Fuel
Oxygen	Open
Fuel	Autopressurization
Purge	*Indifferent*
Pressurant	Fuel

Time (s)	1	2	3	4	5	6	7	8	9	10	11	12	13	14	15	16	17	18	19	20
Ignition																				
Oxygen																				
Fuel																				

Risks The following table summarize the risks. The impact column refers to the impact on the test campaign and not on the individual test.

Hazards Similar to the previous topic, the following table shows the hazards associated with the tests.

Table C.5: Risks associated with the test campaign.

Risk	Likelihood	Impact	Damage Control Procedures
Failed Ignition	Low for ethanol. Medium for ammonia.	Low	Restart test.
Hard Start	Low	Medium	Check for compromising hardware failures. Continue test and guarantee that the valve opening follows the check list.
Valve Open Failure	Low	Low	Restart test. Check for hardware/software failures.
Throat Erosion	Medium	Medium	Adjust mass flow rate to meet requirements. Change chamber in case of severe damage.
Deposit Formation	High	Medium	May affect heat transfer. Analyse deposits,and clean the chamber after every test.
Material Erosion	Medium	Medium	Analyze zones and search for causes. If,suitable, adjust test mixture.

Table C.6: Hazards associated with test campaign.

Hazard	Likelihood	Impact	Damage Control Procedures
Oxygen Explosion	Medium	High	Analyse explosion causes and damages.
Nitrogen Explosion	Medium	High	Analyse explosion causes and damages.
Fire	Medium	Medium	Extinguish fire. If fire source is ammonia,let it burn and protect the material from explosions. Try to extinguish since ammonia fire can cause an explosion [56].
Test Stand Explosion	Low	High	Analyse explosion causes and damages.
Toxic Inhalation	Low	High	Keep people away from test site. If needed, call for medical help.
Skin Burn	Low	High	If the burn is not severe apply water and, if necessary, some drug to relieve the pain. If medical care is required, call it.